CFD Analysis and Optimization of CH_4 Pyrolysis in Commercial Hot Wall Chemical Vapor Deposition Reactor

Thesis submitted in partial fulfillment
for the award of the degree

Doctor of Philosophy

By

Anand Gupta

Department of Chemical Engineering & Technology
Indian Institute of Technology
(Banaras Hindu University)
Varanasi-221005, INDIA

Roll No. 17041502

2024

CERTIFICATE

It is certified that the revised thesis entitled **"CFD Analysis and Optimization of CH_4 Pyrolysis in Commercial Hot Wall Chemical Vapor Deposition Reactor"** is being submitted by **Anand Gupta (Roll No. 17041502)** in partial fulfilment for the award of Ph.D in Department of Chemical Engineering IIT(BHU), Varanasi is a record of bonafide work carried out by him.

Date of Submission:

Dr. Vijay M. Shinde
Supervisor
Department of Chemical Engineering
Indian Institute of Technology (BHU)
Varanasi-221005, India

Head
Department of Chemical Engineering & Technology
Indian Institute of Technology (BHU), Varanasi-221005, India

CERTIFICATE

It is certified that the work contained in the thesis titled **"CFD Analysis and Optimization of CH_4 Pyrolysis in Commercial Hot Wall Chemical Vapor Deposition Reactor"** by **Anand Gupta (Roll No. 17041502)** has been carried out under my supervision and that this work has not been submitted elsewhere for a degree.

It is further certified that the student has fulfilled all the requirements of Comprehensive Examination, Candidacy and SOTA for the award of Ph.D. Degree.

Dr. Vijay M. Shinde
Supervisor
Department of Chemical Engineering
Indian Institute of Technology (BHU)
Varanasi-221005, India

DECLARATION BY THE CANDIDATE

I, Anand Gupta, certify that the work embodied in this thesis is my bonafide work and was carried out by me under the supervision of Dr. Vijay M. Shinde for a period of 7 years from December 2017 to September 2024, at the Department of Chemical Engineering & Technology, Indian Institute of Technology (BHU), Varanasi. The matter embodied in this thesis has not been submitted for the award of any other degree. I declare that I have faithfully acknowledged and given credits to the research workers wherever their works have been cited in my work in this thesis. I further declare that I have not wilfully copied any other's work, paragraphs, text, data, results, etc., reported in journals, books, magazines, reports dissertations, theses, etc., or available on websites and have not included them in this thesis and have not cited as my work.

Date: Signature of Student

Place: IIT BHU (Varanasi) **(Anand Gupta)**

CERTIFICATE BY THE SUPERVISOR

It is certified that the above statement made by the student is correct to the best of my Knowledge.

Dr. Vijay M. Shinde
Department of Chemical Engineering & Technology
Indian Institute of Technology (BHU)
Varanasi-221005, India

Head
Department of Chemical Engineering & Technology
Indian Institute of Technology (BHU), Varanasi-221005, India

COPYRIGHT TRANSFER CERTIFICATE

Title of the Thesis: **CFD Analysis and Optimization of CH_4 Pyrolysis in Commercial Hot Wall Chemical Vapor Deposition Reactor.**

Name of the Student: **Anand Gupta**

Copyright Transfer

The undersigned hereby assigns to the Institute of Technology (BHU) Varanasi all rights under copyright that may exist in and for the above thesis submitted for the award of the **"*Doctor of Philosophy*"**.

Date: Signature of Student

Place: IIT BHU (Varanasi) **(Anand Gupta)**

Note: However, the author may reproduce or authorize others to reproduce material extracted verbatim from the thesis or derivative of the thesis for the author's personal use provided that the source and the Institute's copyright notice are indicated.

Acknowledgement

In the grand tapestry of this doctoral journey, I find myself weaving words of gratitude, and at the forefront stands Dr. Vijay M. Shinde, a mentor par excellence. His guidance has been more than academic; it has been a poetic dance of enlightenment. Like a master potter, he molded my academic clay, quoting the verses of Kabir Das, "गुरु कुम्हार शिष कुंभ है, गढ़ि गढ़ि काढ़ै खोट। अन्तर हाथ सहार दै, बाहर बाहै चोट॥," sculpting not just a researcher but a person of integrity and accountability. To him, I owe not only my academic growth but also the lessons of life. I am indebted to Dr. Shinde not only for his scholarly contributions but also for creating an environment that fostered personal and professional growth. His lessons extended beyond the laboratory, teaching me the art of integrity and the importance of surrounding oneself with a supportive community.

I extend my sincere thanks to Dr. S. S. Rao and Dr. Anurag Kamal for their unwavering mental support, helping me remain resilient through difficult times. Their words of encouragement were a source of strength for me.

Heartfelt thanks to the taxpayers of India, whose contribution forms the foundation of the stipend that supported me during this academic pursuit. The financial support from the Ministry of Human Resource Development (MHRD) added wings to my aspirations, and I acknowledge their role in making this research endeavour possible. The Department of Chemical Engineering & Technology at the Indian Institute of Technology BHU, Varanasi, deserves recognition for providing a nurturing ecosystem for academic excellence. A special note of appreciation goes to my RPEC members, Dr. Jyoti Prasad Chakraborty and Dr. Indrajit Sinha, for their valuable insights and constructive feedback that enriched the quality of this research. To my father, Radhe Shyam Gupta, and my family, who stood as unwavering pillars of love, moral support, and encouragement, I owe immeasurable gratitude.

Lastly, I extend my heartiest thanks to all my well-wishers, whose constant motivation and encouragement were the driving forces that propelled me towards the completion of this thesis.

Anand Gupta

Contents

List of Figures

List of Tables

Nomenclature

$\vec{u}$: velocity (m/s)

A: pre-exponential factor in the Arrhenius equation

b: constant

C: hyperparameter

C_p: specific heat (kJ/kg)

D^m: mass diffusivity (m^2/s)

D^T: thermal diffusivity (m^2/s)

E: activation energy (kcal/mol)

F_B: body force (N/kg)

g: acceleration due to gravity (m/s^2)

h: enthalpy (kJ/kg)

h_w: heat transfer coefficient (J/m^2sK)

h_i^0 : Standard heat of formation (kJ/kg)

I: unit matrix

J^h: energy diffusive flux (w/m^2)

J: mass diffusive flux (kg/m^2s)

k_{eff}: effective thermal conductivity (W/m.K)

MAE: mean square error

M: molecular weight (kg/mol)

Min (x_n): minimum value of x_n

Max (x_n): maximum value of x_n

η: outward unit normal

N_r: total number of surface reaction

P: pressure (Pa)

P_0: initial pressure (Pa)

x^{mol}: mole fraction of species

$x_{i,inlet}^{mol}$: inlet mole fraction of i^{th} species

x^{wt}: mass fraction of species

x: independent variable (predictor)

x^{scaled}: the scaled value of the data point

x_B: best vertex

x_{c1}: inside the compression point

Xc2: outside the compression point

X_G: good vertex

x_M: middle point

X_W: worst vertex

X_R: reflection point

y: dependent variable (response)

y_1: local deposition rate (kg/m^2s)

y_2: local uniformity index

y_1^{upper} : upper limit deposition rate (kg/m^2s)

Greek symbols

ρ: density of gas mixture (kg/m^3)

τ: stress tensor (N/m^2)

μ: gas viscosity (Pa.s)

α: weight for deposition rate

β: weight for deposition rate

β_T: exponential temperature factor

ω: model coefficient

ε: acceptable margin of error

$\hat{R}$: total production rate of species by chemical reaction (kg/m^3.s)

R^2: coefficient of regression

R_i: molar rate of production of i^{th} species (mol/m^{3}s)

RMSE: root mean square error

s: total area of the substrate (m^2)

(s): surface sites

t: time (s)

T: temperature (K)

T_a: atmospheric temperature (K)

T_0: initial reactor temperature (K)

T_{ref}: reference temperature (K)

T_s: substrate temperature (K)

T_w: reactor wall temperature (K)

ϵ: emissivity factor

ξ : slack variable

σ: Stefan-Boltzmann constant (W/m^{2}K^4)

Subscripts

i: i^{th} species

j: j^{th} species

k: k^{th} data point

n: total number of data points

r: r^{th} reaction

Superscript

^: estimated value

-: mean value

w: wall surfaces

Description of non-dimensional numbers

The influence of various operational parameters on the flow behaviour in the CVD reactor and the film growth performance was studied using multiple dimensionless numbers. The ratio of inertial force to viscous force is given as the Reynolds number (Re):

$$\mathrm{Re} = \frac{\rho u D}{\mu}$$

Where ρ is the density of the gas,

u is the gas flow velocity,

D is the reactor diameter and

μ is the dynamic viscosity of the gas.

All simulations satisfy the laminar flow condition (Re 2100). The Grashof number (Gr) is defined as the ratio of buoyant force to the viscous force experienced by the fluid particle, which correlates with thermally induced convective fluid heat and mass transport.

$$\mathrm{Gr} = \frac{\rho^2 g h^3 (T_S - T_o)}{T_o \mu^2}$$

Ts and T_0 represent the substrates and the gas mixture's entrance temperature, respectively, while h represents the vertical distance measured from the spinning shaft. Furthermore, the buoyancy-to-inertia ratio, Gr/Re^2, quantifies the relative strength of natural vs forced convection. Natural convection flow would be dominated by a high Gr/Re^2 ratio, resulting in poorer film uniformity due to increased recirculations in the reactor. To obtain a consistent film growth rate, however, the operating conditions and reactor geometry must be carefully chosen. The rotational Reynolds number Rew based on reactor diameter assesses the forced convection effects caused by substrate rotation and is defined as:

$$\mathrm{Re}_\omega = \frac{\rho \omega D^2}{4\mu}$$

w is the rotation of the substrate. The Prandtl number (Pr) is defined as the ratio of momentum to thermal diffusivity.

$$Pr = \frac{C_p \cdot \mu}{k}$$

A low Prandtl number indicates that thermal diffusion has taken precedence over momentum diffusion, resulting in a higher heat transfer rate due to conduction rather than convection. The Peclet number (Pe) is the ratio of heat transfer rate due to convection to heat transfer rate owing to conduction and is stated as:

$$Pe = \mathrm{Pr}.\mathrm{Re} = \frac{\rho u D C_p}{k}$$

Abstract

Pyrocarbon (PyC) is a kind of carbon that forms on heated surfaces exceeding 900°C due to hydrocarbon cracking. It is generally deposited by chemical vapour deposition (CVD), in which light hydrocarbon gases are pyrolysed over the substrate at high temperatures. PyC CVD successfully fabricates advanced carbon compounds. The ability to control the nanotexture of PyC is crucial for the desired application.

The goal of this thesis is to use machine learning models in conjunction with the Nelder-Mead algorithm to mathematically model and optimise a commercial hot wall vertical reactor for high-quality pyrocarbon coating. To begin, a full 3D CFD model was created by including comprehensive transport reaction kinetics models to explore the effect of various process parameters on the hydrodynamics, temperature, and concentration fields within the CVD reactor. Second, the machine learning model was used in conjunction with the Nelder-Mead algorithm to optimise the CVD reactor to produce a high-quality film. The effect of reactor operating conditions such as temperature, pressure, intake flow rate, and mole fraction on film performance was comprehensively examined. The CVD reactor was then optimised using the model validated by the experimental data. The best film performance can be obtained by selecting the best process parameters. CFD simulations were performed on a vertical hot-wall CVD. The precursor gas mixture of methane and hydrogen enters the reactor through the inlets and pyrolyzes. PyC is deposited on numerous substrates that are placed on the spinning shaft in the reactor's core to ensure uniform coating. The CVD process is made up of several physical and chemical phenomena such as mass, momentum, and heat transfer, as well as chemical reactions. The equations regulating the modelling of physical and chemical events are described in terms of mass conservation, momentum conservation, energy conservation, and species transfer. The reactor geometry was created in Ansys Space-claim and meshed with the ANSYS Workbench mesh generator. A comprehensive CFD model for CH4 pyrolysis in a commercial CVD reactor is developed. The model's accuracy is improved by integrating detailed gas and surface chemistry as well as temperature-dependent transport characteristics of the gas mixture. A parametric analysis is then used to determine the deposition rate and film homogeneity.

SVMs are utilised to link numerous process parameters with deposition rate and film homogeneity. SVM regression works by mapping the input data points into an n-dimensional

feature space and then converting them to a linear. SVM has been demonstrated to be more accurate than the linear regression model. In the SVM regression model, the optimum point was determined using the Nelder-Mead technique. This algorithm compares triangle vertices inside the domain of the desired solution and then shifts the simplex in the direction of the optimal value. The worst vertex is replaced with a new vertex with the best function values in an iterative process. As a result, a new simplex emerges that tends to reach the function's extreme. This strategy has the advantages of high precision, computational efficiency, and quick convergence over previous techniques. The findings demonstrated that reactor pressure and temperature have a significant impact on deposition rate and film uniformity. The most dominant carbon-forming species was found as C2H2. The non-uniform distribution of C2H2 has a significant impact on film uniformity at high pressure. The total flow rate has little effect on reactor hydrodynamics. An appropriate choice of input CH4 concentration can considerably improve film performance. The SVM was used to predict the relationship between different process parameters and film quality, which would otherwise be difficult to achieve by linear regression. This methodology has been found to be efficient and rapid, requiring less time to optimise the CVD reactor.

CHAPTER 1

INTRODUCTION

1.1 Background

Pyrocarbon is a carbon-based material that is formed by the pyrolysis of a hydrocarbon gas at high temperatures. It is a hard, wear-resistant, and biocompatible material that is often used in biomedical and aerospace applications (Tan et al., 2016). Because of its outstanding electrochemical characteristics and electrical conductivity, low friction, chemical inertness, and anisotropic dense and controlled microstructure (Bourrat et al., 2006a), it is a potential coating material. It has lately gained popularity due to its ability to substitute silicon in microelectromechanical systems. Moreover, the superior impermeability of isotropic PyC makes it the best candidate for the mechanical sealing devices used extensively in the aerospace and shipping industries (Beigi-Boroujeni et al., 2019).

Methane pyrolysis is a promising process for the production of carbon-based materials such as pyrocarbon, graphene and carbon nanotubes (Sanchez-Bastardo et al., 2021). Chemical vapour deposition (CVD) is a method of depositing thin layers of material onto a substrate. It involves the decomposition and reactivity of volatile precursor gases in a heated chamber to generate a solid coating on the substrate surface. It is widely utilized in various industries, including semiconductor manufacturing, coating technologies, and nanomaterial synthesis, to produce high-quality and controlled thin films with precise thickness and composition. The understanding of CVD reactors is a complex and challenging task, as it involves multiple interacting factors such as reactor geometry, temperature, pressure, gas flow etc. (Komiyama et al., 1999; Ogawa et al., 2023). The film morphology in CVD is also influenced by these parameters. Temperature affects growth rate and surface quality, while pressure impacts gas diffusion and film quality (Hu, 2012). Gas flow rate determines precursor concentration and uniformity, and reactor geometry affects deposition uniformity and nucleation density. These parameters are interrelated and require optimization to achieve the desired film morphology, considering the specific CVD system and precursor materials. Careful control and optimization of these parameters are crucial for successful CVD processes. In addition, the current process suffers from low yield, low quality, and high energy consumption, which limit its commercial viability. Therefore, there is a pressing need to optimize the process parameters to improve its efficiency and environmental impact (Jabar, 2021; Timmerberg et al., 2020). Traditional

optimization techniques based on trial and error can be time-consuming and costly, and may not guarantee the optimal solution (Dong and Huttinger, 2002; Hu and Hüttinger, 2001).

CFD plays a crucial role in understanding CVD processes by simulating the complex fluid dynamics and heat transfer phenomena involved. CFD models help analyze the gas flow patterns, temperature distribution, and species transport within the CVD reactor (Ogawa et al., 2023). By providing insights into gas mixing, reactant concentration, and residence time, CFD allows the optimization of reactor design and process parameters, leading to enhanced film quality and deposition rates. It also aids in predicting and mitigating issues such as gas phase reactions, particle transport, and deposition non-uniformity, contributing to the overall understanding and improvement of CVD processes (Ali and Ürgen, 2011a; Yang et al., 2009).

Traditional optimization algorithms often struggle to solve complex problems with many variables and constraints. Machine learning can overcome these challenges by learning from data to find optimal solutions more efficiently (Weichert et al., 2019). One way machine learning is used for optimization is to train a model to predict the objective function value for a given set of decision variables. This model can then be used to guide the search for an optimal solution. Another approach is to use machine learning to learn a good initialization for a traditional optimization algorithm (Kubat, 2017). This can help the algorithm to converge to a better solution more quickly. Therefore, the motivation for this thesis is to analyze and optimize the pyrolysis of methane in a commercial hot-wall CVD reactor using CFD simulations. The goal is to achieve high-quality pyrocarbon by combining the support vector machine (SVM) and the Nelder-Mead algorithm by simultaneously maximising the average deposition rate and uniformity index.

1.2 Thermal decomposition of methane

The thermal decomposition of methane, also known as methane pyrolysis or methane cracking, is a chemical process in which methane (CH_4) is broken down into its constituent elements, typically hydrogen (H_2) and solid carbon (C). The reaction is endothermic, requiring the input of heat to drive the process. The overall reaction can be represented as follows:

$$CH_4 \rightarrow C + 2H_2 \qquad 1$$

The thermal decomposition of methane is typically carried out at high temperatures, typically in the range of 900 to 1200^0C, and in the presence of a catalyst to enhance the reaction rate. The reaction can occur in both homogeneous and heterogeneous systems. The thermal

decomposition of methane has a variety of applications in industry and is interesting for several reasons, some of which are briefly discussed below:

1. **Hydrogen production:** Methane pyrolysis is a potential method for hydrogen production. Hydrogen is a clean and efficient fuel that can be used in fuel cells and various industrial processes. By decomposing methane, hydrogen can be obtained as a valuable byproduct (Sánchez-Bastardo et al., 2021; Timmerberg et al., 2020).

2. **Carbon materials synthesis**: The solid carbon produced during methane pyrolysis can be utilized for the synthesis of various carbon-based materials (Dadsetan et al., 2023). These include carbon black, carbon nanotubes, graphene, and other forms of carbon with unique properties and applications. It is used in advanced composite materials for improving mechanical strength and thermal conductivity in industries such as automotive and aerospace (Tan et al., 2016).

3. **Decarbonization:** Methane, a potent greenhouse gas, is a major component of natural gas. The thermal decomposition of methane offers a potential pathway for reducing greenhouse gas emissions by converting methane into useful products like hydrogen and carbon, thereby mitigating its impact on climate change (Parkinson et al., 2018).

4. **Chemical industry:** Methane pyrolysis can be used as a precursor for the production of various chemicals like ethylene benzene, toluene, xylene, and other hydrocarbons (Jabar, 2021). By selectively controlling the reaction conditions and catalysts, specific chemical intermediates or end products can be obtained. The specific chemicals that are produced from methane pyrolysis depend on the reaction conditions and catalysts used. For example, high temperatures favour the production of ethylene, while lower temperatures favour the production of benzene (Fau et al., 2013).

However, there are challenges associated with methane pyrolysis, including high energy requirements due to the endothermic nature of the reaction, catalyst deactivation or degradation, and the need for efficient heat transfer and reactor design. The design of a CVD reactor presents engineering challenges such as achieving uniform deposition, maintaining stable gas flow, and controlling temperature distribution. Addressing these issues is crucial for ensuring consistent film growth and properties, as well as for optimizing safety and scalability

in CVD processes (Komiyama et al., 1999; Ogawa et al., 2023). Research efforts are focused on developing optimized process conditions, exploring new catalyst materials, and improving the energy efficiency of methane pyrolysis to make it commercially viable and environmentally sustainable (Becker et al., 2000; Dong and Hüttinger, 2002) Continued research and development in this field hold promise for advancements in CVD process and sustainable materials development.

1.3 Types of pyrolytic carbon and their importance

Pyrolytic carbon is a form of carbon material that is synthesized through the process of pyrolysis, which involves the thermal decomposition of a carbon-containing precursor. Pyrolytic carbon possesses unique properties and finds important applications in various fields. Here are some types of pyrolytic carbon and their significance:

1. **Pyrolytic graphite (PG)**: Pyrolytic graphite is a highly oriented form of pyrolytic carbon with a layered structure similar to graphite (Gulyaev and Shushkov, 2022). It is produced by depositing carbon vapour onto a substrate at high temperatures. It exhibits excellent thermal conductivity, electrical conductivity, and lubricating properties. Padnya et. al. found that the carbon black layer consisted of roundish particles 30-50 nm in size (Padnya et al., 2018). It is used in applications such as thermal management, electrodes, crucibles, and as a lubricant in high-temperature environments.

2. **Pyrolytic carbon fibre (PyCF):** Pyrolytic carbon fibres are produced by the pyrolysis of carbon-rich precursor fibres, such as polyacrylonitrile (PAN) or rayon, in a controlled environment. Tan et al., 2016 showed that PyCF has high-density isotropic pyrocarbon and exhibits fine grains resembling wrinkled sheets, with a significantly smaller average grain size compared to the substrate's graphite grains. Moreover, Figure 1.2 (i) demonstrates a schistose appearance at the specimen's edge, indicating a layer-by-layer deposition mechanism in that region, consistent with the growth of anisotropic pyrocarbon. PyCF possesses high strength, stiffness, and thermal stability. It finds applications in aerospace, automotive, and sporting goods industries for lightweight structural components, reinforcing materials, and conductive composites (Tan et al., 2016).

3. **Pyrolytic carbon coating (PyCC)**: Pyrolytic carbon coatings are thin layers of pyrolytic carbon deposited on various substrates using CVD techniques. Li et al., 2010 discovered that pyrocarbon is made of granular particles with uniform dimensions of about 1.5 μm (Li et al., 2020). These coatings provide a range of desirable properties, like excellent chemical resistance, biocompatibility, low friction, and electrical conductivity (Bourrat et al., 2006a). PyC is used in applications such as biomedical implants, protective coatings, and electrical contacts (Li et al., 2010).

4. **Pyrolytic carbon electrodes (PCE):** Because of its high electrical conductivity and corrosion resistance, pyrolytic carbon electrodes are widely employed in electrochemical applications. They are employed in fuel cells, batteries, sensors, and other electrochemical devices for efficient electron transfer and stable performance. In Fig 1.2 (iv) Rezaei et. al. found that fast pyrolysis leads to non-isotropic shrinkage and distorted mesh holes, while slow pyrolysis retains the cubic shape with gradual degradation and degassing. Pyrolysis conditions affect both the macro-structure and surface topography of carbonized materials (Rezaei et al., 2020).

5. **Pyrolytic carbon foam (PCF)**: is a porous form of pyrolytic carbon with a three-dimensional interconnected network structure. It exhibits a combination of low density, high thermal conductivity, and excellent mechanical strength. Pyrolytic carbon foam is used in heat exchangers, thermal insulation, catalyst supports, and as a substrate for energy storage devices (Rodríguez et al., 2021).

The importance of pyrolytic carbon lies in its unique combination of properties, including high thermal and electrical conductivity, mechanical strength, chemical stability, and biocompatibility. These characteristics make pyrolytic carbon suitable for a wide range of applications, ranging from aerospace and automotive industries to biomedical and energy sectors. The different types of pyrolytic carbon offer tailored properties to meet specific application requirements and contribute to advancements in various fields of technology and engineering.

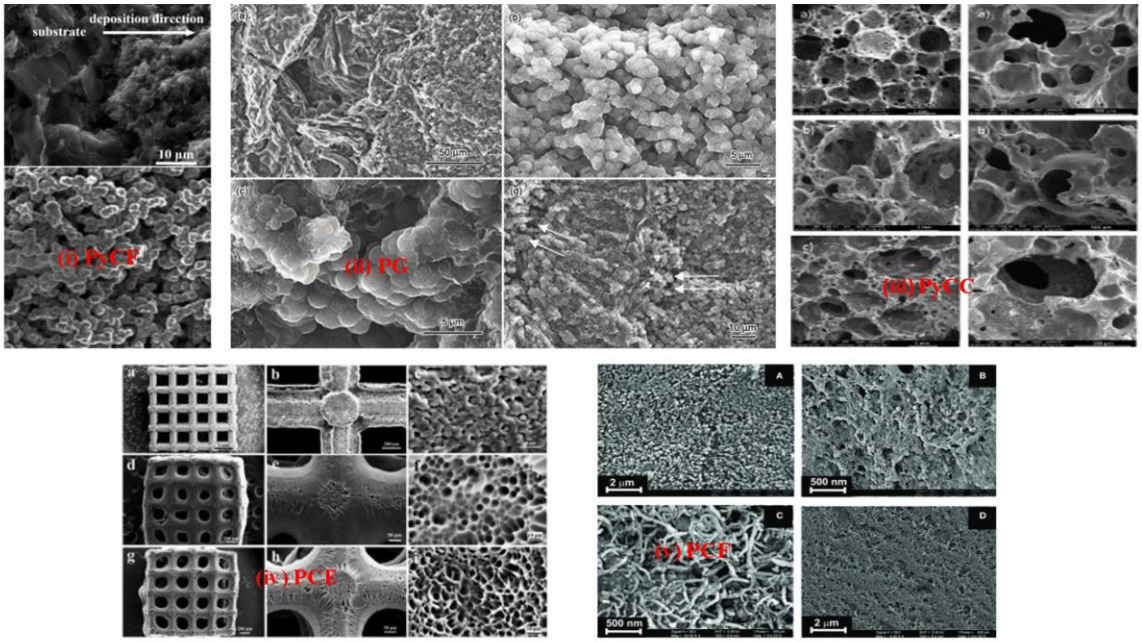

Fig. 1.1 SEM images of different types of PyC
(Li et al., 2020; Padnya et al., 2018; Rezaei et al., 2020; Rodríguez et al., 2021; Tan et al., 2016)

1.4 Various manufacturing processes of pyrocarbon

Pyrocarbon is a high-performance carbon material that finds applications in various industries, including aerospace, automotive, and medical. The manufacturing processes of pyrocarbon involve the deposition of carbon from a gaseous precursor onto a substrate under controlled conditions. The following list of frequently employed pyrocarbon production techniques includes information on each process's benefits and drawbacks:

1. **Chemical Vapor Deposition (CVD)**

   Chemical vapour deposition (CVD) is a process for coating surfaces with a thin film of material from a gas. The type of gas used depends on the application. For example, coating carbon fibres with pyrocarbon can help prevent them from sticking together in carbon fibre-reinforced carbon composites.

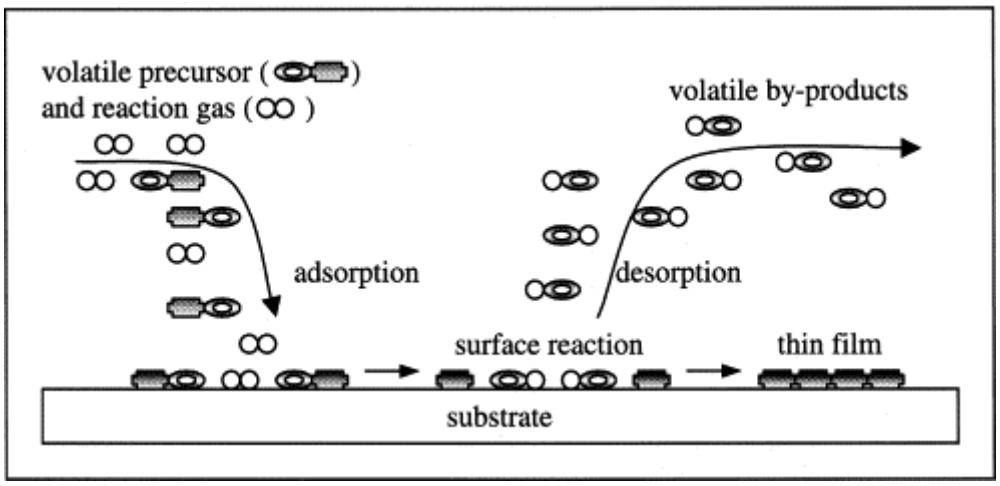

Fig. 1.2 A schematic representation of the CVD reaction (Dahmen, 2003)

Advantages:

i. Allows precise control over deposition parameters such as temperature, pressure, and gas composition, resulting in tailored material properties.
ii. High purity and uniformity of the deposited carbon.
iii. Provides excellent adherence to complex-shaped substrates.
iv. Enables the deposition of thick coatings or bulk materials.

Limitations:

i. Requires specialized equipment and precise process control.
ii. Relatively longer deposition times compared to other processes.
iii. Susceptible to variations in process conditions leading to non-uniform deposition.
iv. Sensitive to impurities in the precursor gases.

2. Polymer Pyrolysis:

Polymer pyrolysis is the thermal decomposition of polymers in the absence of oxygen. It is a complex process that involves a variety of chemical reactions, including chain scission, crosslinking, and cyclization. The products of polymer pyrolysis depend on the type of polymer, the pyrolysis temperature, and the heating rate (Yansaneh and Zein, 2022).

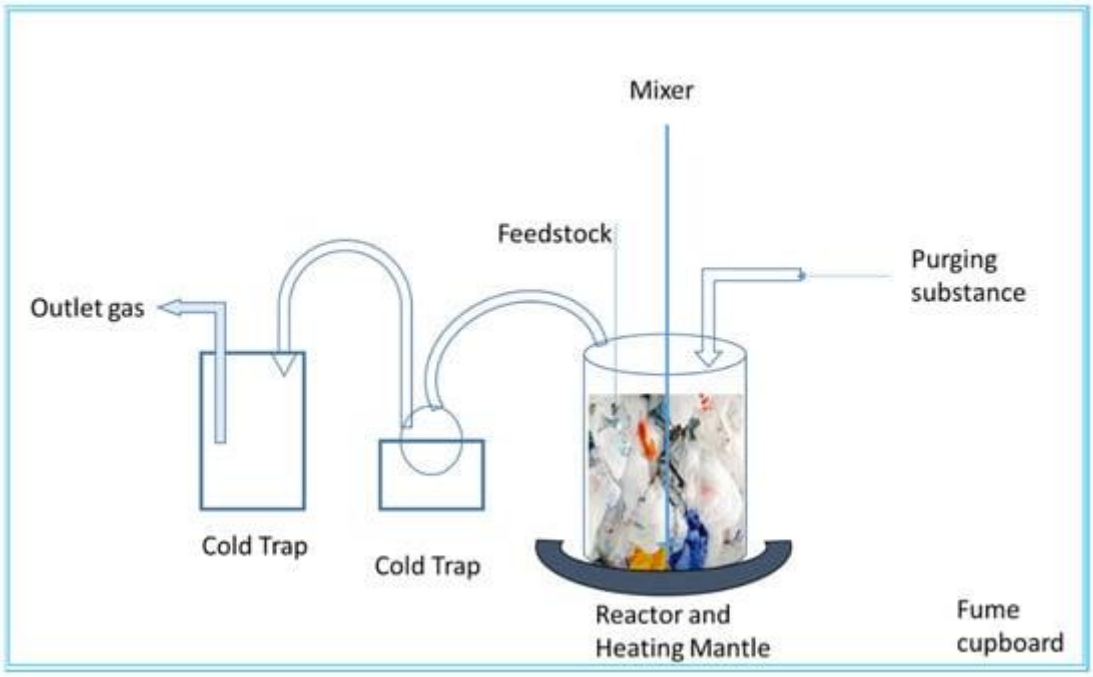

Fig. 1.3 A polymer Pyrolysis setup

(Yansaneh and Zein, 2022)

Advantages:

i. Flexibility in material selection.
ii. Low-temperature operation.
iii. Offers scalability and cost-effectiveness.
iv. Suitable for producing thin coatings and fibres.

Limitations:

i. Generally, produces lower densities compared to CVD.
ii. Limited control over the resulting material properties.
iii. May require additional steps, such as carbonization and graphitization, for enhanced performance.
iv. Polymer precursors may contain impurities that affect the quality of the final pyrocarbon.

3. **Carbonization:** Carbonization involves the formation of C–C bonds and typically occurs in the temperature range of 800°C to 2000°C. When the material undergoes further heating, specifically in the range of 2000°C to 3000°C, this process is termed graphitization (Devi et al., 2020). An illustrative instance of this is observed in the

pyrolysis of coal, leading to the extraction of tars, volatile organic compounds (VOCs), and char (carbon with impurities).

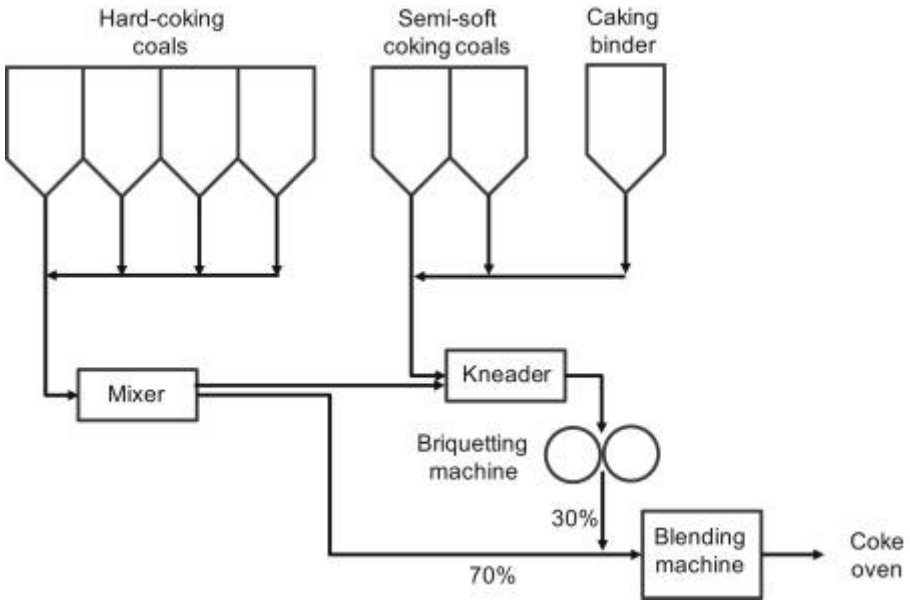

Fig. 1.4 Process flow of briquette blending carbonization process (Nomura, 2019).

Advantages:

i. Involves the heat treatment of carbon-rich materials, such as organic fibres or carbonaceous powders, to convert them into pyrocarbon.
ii. Moderate temperatures and atmospheric pressure.
iii. A relatively simple process requiring minimal equipment.
iv. Suitable for small-scale production or prototyping.

Limitations:

i. Limited control over the resulting material properties.
ii. Formation of amorphous carbon or incomplete conversion to pyrocarbon.
iii. Tends to produce lower densities and mechanical properties compared to other processes.
iv. Require post-treatment steps, such as graphitization, to enhance the performance.

It is important to select the appropriate manufacturing process based on the desired pyrocarbon properties, substrate characteristics, production scale, and cost considerations. Additionally, process optimization and quality control are essential to ensure consistent and reliable pyrocarbon production.

1.5 Advantages of CVD over another manufacturing process

CVD offers several advantages over other manufacturing processes, making it a widely used technique in various industries. Here are some key advantages of CVD:

1. **Conformal deposition:** CVD provides excellent conformal deposition, meaning the thin film uniformly covers the surface of complex three-dimensional structures (Pierson, 1999). This is particularly advantageous for applications where precise and uniform coating on intricate geometries is required, such as microelectronics, MEMS devices, and optical coatings. Other deposition techniques, such as physical vapour deposition (PVD), may struggle to achieve the same level of conformality.

2. **Tailored film composition:** CVD allows for fine control of the deposited film's composition. By selecting appropriate precursor gases and adjusting process parameters, the film's elemental composition, stoichiometry, and doping levels can be precisely tailored (Seo et al., 2016). This flexibility is highly advantageous for applications where specific material properties, such as electrical conductivity, optical transparency, or chemical reactivity, are required (Bourrat et al., 2006b).

3. **A wide range of materials:** Metals, semiconductors, ceramics, oxides, nitrides, and polymers can all be deposited using CVD. This versatility allows for the deposition of various functional coatings and thin films with tailored properties (Beigi-Boroujeni et al., 2019; Bérard et al., 2016; Seo et al., 2016). In contrast, some other deposition methods may be limited to specific material types or have restrictions on the range of materials that can be deposited.

4. **High purity and density:** CVD processes can produce films with high purity and density. The chemical reactions occurring during CVD allow for the formation of dense and highly crystalline films, resulting in improved physical and mechanical properties.

Additionally, CVD can achieve low levels of impurities and contaminants, making it suitable for applications where material purity is crucial, such as semiconductor manufacturing and high-performance coatings (Beigi-Boroujeni et al., 2019; Tan et al., 2016).

5. **Scalability and production efficiency:** CVD can be easily scaled up for large-scale production. CVD reactors can be designed with multiple deposition chambers, enabling high throughput and efficient manufacturing (Chen et al., 2018). Continuous CVD processes allow for the deposition of films over large areas, making them well-suited for industrial-scale production. This scalability and production efficiency make CVD an attractive choice for commercial applications (Lin et al., 2009a).

6. **Film customization and complexity:** CVD allows for the deposition of films with complicated architectures and customised characteristics. By manipulating process parameters, multiple precursor gases, and deposition conditions, it is possible to create multi-layered films, graded compositions, nanostructured coatings, and other advanced structures (Pierson, 1999). This level of customization and complexity is often difficult to achieve with other deposition methods.

7. **Compatibility with substrate materials:** CVD is compatible with a wide range of substrate materials, including metals, ceramics, glass, and polymers. This versatility allows for the deposition of thin films on diverse substrates, expanding the range of applications (Pierson, 1999). Other techniques, such as sputtering or evaporation, may have limitations in terms of substrate compatibility.

1.6 CVD of pyrocarbon (PyC)

PyC can be deposited on a substrate using a variety of methods, including CVD and PVD. CVD is considered better than PVD in certain applications where precise and uniform coatings are required on complex shapes or structures, such as semiconductor fabrication, optical coatings, and thin film deposition for electronic devices due to its ability to create conformal coatings with excellent step coverage and uniform thickness (Sharma et al., 2020; Sun et al., 2021). CVD also allows for the deposition of a wider range of materials, including complex

compounds and alloys. Additionally, CVD can produce coatings with superior adhesion and can be performed at lower temperatures, reducing the risk of substrate damage.

In CVD, a hydrocarbon gas is introduced into a reactor and is heated to a high temperature, where it decomposes to form a solid film of pyrocarbon on the substrate. PyC is generally deposited by CVD, in which light hydrocarbon gases are pyrolysed over the substrate at high temperatures (ca.1050-1450°C) (Sharma et al., 2020). It is generally operated at low pressure to increase the molecular mean free path and diffusion of gases. As a result, more gas molecules collide with a substrate than with other gas molecules.

1.6.1. A sequence of events during CVD of PyC

The gas mixture undergoes intricate flow patterns as it passes through pipes, valves, and chambers, experiencing significant temperature variations and, to a lesser extent, pressure changes. Finally, the gas makes contact with the substrate, when the heterogeneous deposition reaction takes place, converting the gas to a solid. Additionally, in certain cases, the reaction may occur before reaching the substrate, known as gas-phase precipitation. The CVD reaction sequence, represented in Fig. 1.5, is as follows: reactant gases enter the reactor by forced flow and subsequently diffuse through the boundary layer. Upon reaching the substrate surface, the gases come into contact and undergo a deposition reaction. After the reaction, the gaseous byproducts diffuse away from the surface and go through the boundary layer (Sun et al., 2021).

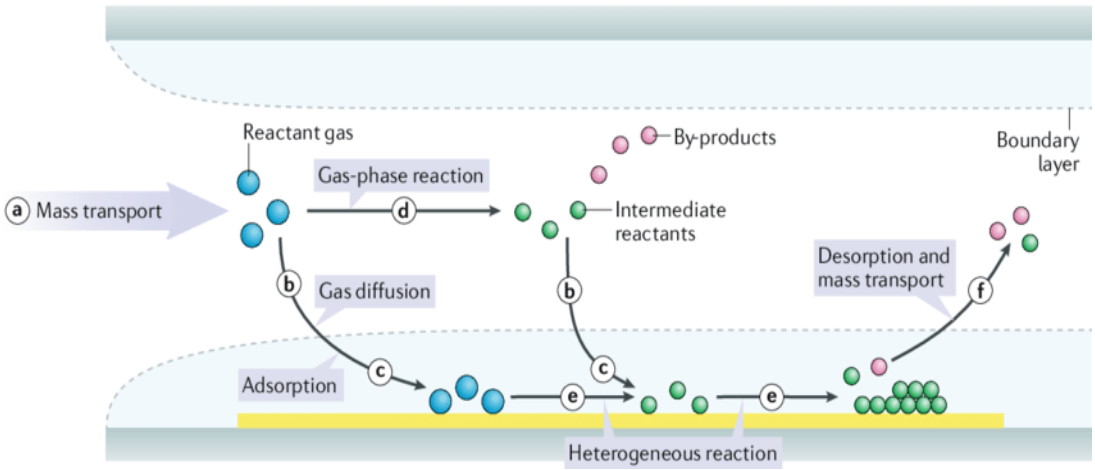

Fig. 1.5 Sequence of events during the CVD process (Sun et al., 2021)

i. Gas-phase transport of reagents (e.g., CH_4, BCl_3, H_2) to the reaction zone (frequently with carrier gas). Diffusion (or convection) through the boundary layer.
ii. Precursor adsorption on the substrate.
iii. Precursor surface diffusion to growth sites. Reaction without diffusion is undesirable because it may result in a rough growth surface.
iv. Surface chemical reaction, solid film formation, and byproduct generation.
v. By-product desorption.
vi. Removal of gaseous byproducts from the reactor.

1.6.2. Types of CVD

CVD is a flexible process for depositing thin films of different materials onto substrates. There are several types of CVD methods, each with its specific characteristics and applications. Here are some common types of CVD:

1. **Thermal CVD**: It is also known as conventional or atmospheric pressure CVD; thermal CVD involves the deposition of films by introducing precursor gases into a reactor at elevated temperatures. The thermal energy initiates chemical reactions that lead to the deposition of the desired material onto the substrate (Pierson, 1999).

Advantages:

i. Simple and cost-effective process.
ii. Suitable for large-area deposition.
iii. Can be performed at atmospheric pressure, eliminating the need for vacuum systems.

Limitations:

i. Limited control over film thickness and uniformity.
ii. High-temperature process, which may restrict the use of temperature-sensitive substrates.
iii. Lower deposition rates compared to other CVD methods.

2. **Low-pressure CVD (LPCVD):** LPCVD operates at reduced pressures compared to atmospheric pressure CVD. To optimise the deposition process, the precursor gases are

delivered into a vacuum chamber and the pressure is adjusted. Materials such as silicon nitride (Si_3N_4), polysilicon, and silicon dioxide (SiO_2) are typically deposited using LPCVD. Microelectronics, MEMS devices, and thin film coatings benefit from LPCVD's ability to provide fine control, homogeneous film deposition, and enough step coverage at lower temperatures (Pierson, 1999; Wang et al., 2013).

Advantages:

i. Allows for better control over film thickness, uniformity, and composition.
ii. Low temperatures compared to other CVD methods.
iii. Offers higher deposition rates compared to APCVD.

Limitations:

i. Requires a vacuum system, increasing equipment complexity and cost.
ii. Limited scalability for large-area deposition.
iii. Poorer step coverage on complex substrate topographies.

3. **Plasma-enhanced CVD (PECVD):** Plasma is used to improve chemical reactions and deposition processes in PECVD. Plasma is generated by applying a high-frequency electric field to a precursor gas or gas mixture. The plasma provides energy to break down the precursor molecules, creating reactive species that contribute to film deposition. PECVD is suitable for depositing various materials, including silicon-based compounds, amorphous silicon and carbon-based films (Mankelevich and May 2008a, 2008b).

Advantages:

i. Lower process temperatures, enabling the use of temperature-sensitive substrates.
ii. Better control over film aspects like composition and structure.
iii. Can deposit films with high conformality on complex geometries.

Limitations:

i. Requires a plasma source, which adds complexity and cost to the system.
ii. Higher susceptibility to plasma damage, which may affect film quality.
iii. Limited scalability for large-area deposition.

4. **Metal-organic CVD (MOCVD):** MOCVD, also known as organometallic CVD, is specifically used for depositing thin films of metal compounds, such as oxides, nitrides, and semiconductors. It involves the use of metal-organic precursors, which are vaporized and decomposed to deposit the desired material onto the substrate. MOCVD is widely used in the production of compound semiconductors for electronic and optoelectronic devices (Chuang and Chen, 2014; Kadinski et al., 2004; Liu et al., 2007).

Advantages:

i. Enables the deposition of compound semiconductor materials.
ii. Offers precise control over film composition and doping.
iii. Suitable for growing thin films for electronic and optoelectronic devices.

Limitations:

i. Requires highly reactive and expensive precursor materials.
ii. Complex gas handling and safety considerations.
iii. Limited to specific materials and applications.

5. **Atomic layer deposition (ALD):** ALD is a form of CVD that allows for atomic-level control of layer thickness and composition. It is accomplished by sequentially exposing the substrate to two or more precursor gases. Each precursor reacts with the surface in a self-limiting manner, allowing for the controlled growth of ultra-thin films with excellent conformality. ALD is commonly used in nanotechnology, semiconductor manufacturing, and advanced materials research (Pierson, 1999).

Advantages:

i. Allows for atomic-level control over film thickness.
ii. Excellent conformal deposition on complex geometries.
iii. Enables high-uniformity deposition of ultra-thin films.

Limitations:

i. Slow deposition rates, resulting in longer processing times.
ii. Requires alternating exposure of precursors, increasing process complexity.
iii. Limited scalability for large-area deposition.

6. **Hot Wall CVD:** The hot wall CVD is a CVD procedure in which the substrate is directly heated, often by placing it on a hot susceptor or heater. The reaction chamber is often cooler than the substrate in this process, and heat is transmitted from the substrate to the reactant gases. When the reactant gases are delivered into the chamber, chemical reactions take place on the heated substrate surface, resulting in the deposition of the desired material (Creighton and Ho, 2001).

Advantages

i. **Higher temperature capability:** Hot wall CVD allows for higher temperature operation compared to cold wall CVD. This enables the deposition of materials that require high temperatures for their growth or for achieving desired properties.
ii. **Enhanced reaction rates:** The elevated substrate temperature in hot wall CVD promotes faster reaction rates, leading to improved deposition kinetics. This can result in higher growth rates and improved film quality.
iii. **Reduced parasitic deposition**: With hot wall CVD, the chamber walls are typically cooler than the substrate. This temperature gradient helps to minimize undesired deposition on the chamber walls, reducing contamination and improving process efficiency (Li et al., 2010).

Limitations

i. **Limited control over temperature distribution**: In hot wall CVD, controlling the temperature distribution across the substrate can be challenging. Variations in temperature across the substrate surface may lead to non-uniform film deposition, impacting the film's quality and thickness uniformity.
ii. **Higher thermal stress:** The direct heating of the substrate in hot wall CVD can result in higher thermal stress on the substrate and deposited films. This can potentially cause cracking, delamination, or other defects in the deposited layers.

7. **Cold wall CVD:** Cold wall CVD is a type of CVD process where the reactor walls are maintained at a lower temperature compared to the substrate. In this method, the reactant gases are introduced into the chamber, and the deposition occurs on the

substrate surface without direct heating from the walls (Creighton and Ho, 2001; Pierson, 1999)

Advantages

Better temperature control: Cold wall CVD provides better control over the temperature distribution across the substrate. Maintaining a temperature gradient allows for more uniform deposition and more exact control of the growth parameters.

i. **Reduced thermal stress:** Compared to hot wall CVD, cold wall CVD imposes lower thermal stress on the substrate and the deposited films. This can lead to improved film quality and reduced likelihood of cracking or delamination.
ii. **Compatibility with sensitive substrates:** Cold wall CVD is often preferred for substrates that are sensitive to high temperatures. By avoiding direct heating, the temperature of the substrate can be kept within a safe range without causing damage or undesirable consequences.

Limitations

Lower temperature capability: Cold wall CVD typically operates at lower temperatures compared to hot wall CVD. This can limit the growth of materials that require higher temperatures for their deposition or for achieving specific properties.

i. **Slower reaction rates:** The lower substrate temperature in cold wall CVD can result in slower reaction rates compared to hot wall CVD. This may lead to slower growth rates and longer deposition times.
ii. **Potential for parasitic deposition:** In cold wall CVD, the chamber walls are generally colder than the substrate. This temperature gradient can sometimes lead to parasitic deposition on the walls, which can cause contamination and reduce the efficiency of the process.

These are just a few examples of the types of CVD methods commonly used in various industries and research fields. Each process has distinct advantages and is best suited to certain applications, allowing for the deposition of a diverse spectrum of materials with customised features. The suitable CVD process is determined by the desired material, film properties, deposition parameters, and unique application needs. The selection of a CVD method depends

on the desired film properties, substrate compatibility, process scalability, and cost considerations. Each approach has advantages and disadvantages, and the choice should be based on the unique deposition process requirements and desired film properties.

1.6.3. Critical components in CVD

CVD critical components are required for the successful fabrication and deposition of high-quality thin films or coatings. These elements are critical in managing deposition parameters, guaranteeing uniformity, and achieving the desired film characteristics (Pierson, 1999). Some of the most important components of CVD systems are:

1. **Reactor chamber:** The reactor chamber provides a controlled environment for the CVD process. It typically consists of a heated chamber where the precursor gases are introduced and the deposition occurs. The chamber design and materials used should be compatible with the process conditions and the desired film characteristics.

2. **Gas delivery system**: The gas delivery system is in charge of bringing the precursor gases into the reactor chamber exactly. To obtain the appropriate gas composition and flow rates, it often incorporates mass flow controls, gas lines, and gas mixing capabilities. Controlling film thickness, composition, and uniformity requires precise control of precursor gas flow.

3. **Substrate holder**: The substrate holder or stage holds the substrate on which the film is deposited. It should provide proper mechanical support, thermal stability, and temperature control during the deposition process. The substrate holder may also have rotation or translation capabilities to ensure uniform deposition across the substrate surface.

4. **Heating system:** Temperature control is vital in CVD processes to promote the desired chemical reactions and achieve the desired film properties. A heating system, such as resistive heaters or induction coils, is used to heat the substrate and/or reactor chamber to the required temperature. Precise temperature control is essential to maintain process stability and repeatability.

5. **Vacuum system**: A vacuum system is employed to evacuate the reactor chamber and maintain the desired process pressure. It typically consists of vacuum pumps, pressure gauges, and valves. Proper control of the process pressure is critical for gas flow, precursor decomposition, and the prevention of unwanted reactions or contaminations.

6. **Exhaust system**: The exhaust system removes the byproducts and unreacted gases from the reactor chamber. It helps maintain a clean environment and prevents the accumulation of unwanted species that can affect film quality. It usually includes a vacuum pump and appropriate gas scrubbing or filtration systems.

7. **Gas exhaust analysis**: Analytical tools, such as mass spectrometers or gas analyzers, may be integrated into the CVD system to monitor and analyze the exhaust gases. These tools provide valuable information about the process chemistry, gas consumption, reaction kinetics, and the presence of impurities.

8. **Safety and process monitoring systems**: CVD systems often include safety features and monitoring systems to ensure operator safety and process control. These may include temperature and pressure sensors, gas leak detectors, interlocks, and alarms.

1.6.4. Advantage of vertical over horizontal CVD reactor

A vertical CVD reactor can have several advantages over a horizontal one. Some of these advantages include:

- **Greater surface area to volume ratio**: A vertical reactor can have a larger surface area for a given volume, which can lead to better heat and mass transfer.
- **Easier to scale up**: A vertical reactor can be scaled up more easily than a horizontal one, as the reactor can simply be made taller rather than wider.
- **Reduced risk of contamination:** A vertical reactor can have a reduced risk of contamination, as the reactants can be fed into the reactor from the top and the products can be removed from the bottom, minimizing the chance of cross-contamination.
- **More efficient use of space:** A vertical reactor can be more space efficient than a horizontal one, as it can be placed in a smaller footprint.

1.7 Importance of CFD in designing CVD reactor:

Computational Fluid Dynamics (CFD) is a valuable tool for developing CVD reactors. CFD can assist in optimising reactor design and operation, increasing process efficiency, and lowering costs. Some of the primary advantages of employing CFD in CVD reactor design are as follows:

1. **Understanding the flow patterns and heat transfer mechanisms**: CFD models can provide precise information on reactor flow patterns and heat transfer mechanisms (Cheng and Hsiao, 2008). This data can be utilised to optimise the reactor's design and increase the process's efficiency.

2. **Optimizing reactor geometry and operating conditions**: CFD simulations can be used to evaluate the performance of different reactor geometries and operating conditions and identify the optimal design that maximizes the production rate and quality of the target material. Jia et al studied the optimal design for dividing wall columns using SVM and PSO. They learn several parameters on their own by fitting the data. In addition, they are also computationally efficient and can be used in real-time prediction (Jia et al., 2017a).

3. **Reducing experimental costs and time**: CFD simulations can provide a cost-effective and time-efficient alternative to experimental testing. By simulating different scenarios and analyzing the results, engineers can reduce the number of experiments needed and optimize the process parameters more quickly and efficiently (Haddadi et al., 2017).

4. **Improving process safety**: CFD simulations can help to identify potential safety hazards, such as high temperatures, pressure drops, and flow instabilities, and design the reactor to mitigate these risks (Szpicer et al., 2023).

5. **Enhancing product quality and consistency**: CFD simulations can aid in the improvement of product quality and consistency by detecting and addressing probable sources of non-uniformity in the reactor.

1.8 Optimisation of CVD

The optimization of CVD processes is of paramount importance to ensure the successful fabrication of high-quality films and coatings. Failure to optimize the CVD process can lead to various undesirable outcomes. Without optimization, the deposition may result in inconsistent film quality, with variations in thickness, composition, and properties from batch to batch or across the substrate surface. This lack of control over film properties can severely limit the range of applications and compromise the performance of the deposited films. Inefficient material utilization is another consequence of poor optimization, leading to the wastage of expensive precursor gases and higher production costs. Additionally, non-uniform film growth, defects, or incomplete coverage can reduce the production yield and increase rejection rates. This not only impacts overall efficiency but also leads to increased costs and time consumption. Inadequate optimization may also result in films that do not adhere to the required specifications and fail to meet the desired performance criteria. Such deficiencies can lead to customer dissatisfaction, rejection of films, and potential loss of business opportunities. Therefore, optimization of the CVD process is essential to achieve consistent film quality, maximize material utilization, reduce costs, improve production yield, and ensure compliance with specifications and performance requirements (George et al., 2006; Lin et al., 2009b; Ramadan and Im, 2019a; Wissmann and Grover, 2010).

1.8 Techniques used for optimisation of CVD

There are several techniques and methods available for CVD processes (Chen, 2007; Creighton and Ho, 2001; del Coso et al., 2008; Hwang et al., 2021a; Jia et al., 2017a; Myers, 2018, 1999; Pierson, 1999; Teixeira et al., 2020; Wissmann and Grover, 2010). Here are some commonly used approaches:

1. **Response surface methodology (RSM):** Response Surface Methodology (RSM) in the Design of Experiments (DoE) is a statistical approach that systematically varies process parameters to analyze their impact on the deposition process. This method efficiently explores a broad parameter space, facilitating the identification of optimal conditions. Through statistical analysis, DoE assists in pinpointing key process variables and their interactions, leading to the development of predictive mathematical models for film properties and informed optimization strategies (Kober et al., 2022). RSM, as a statistical technique, utilizes mathematical models to optimize process parameters. It entails the design of a series of experiments based on a predefined set of input variables,

with the measurement of the response of interest. By fitting a mathematical model to the experimental data, RSM enables the prediction of optimal process conditions for desired film properties. This approach aids in determining the optimal combination of parameters that maximizes both film quality and process efficiency.

2. **Genetic Algorithms (GA):** The GA modelling technique is made up of two steps: computing the predicted outcomes from the reaction model candidates and updating the candidates based on the difference between experimental and anticipated results (Takahashi et al., 2005). Takahiro and colleagues demonstrated the efficacy of this methodology by successfully identifying suitable reaction models using both synthetic and authentic experimental data obtained during the thermal chemical vapour deposition (CVD) of tetraethylorthosilicate (Takahashi et al., 2005).

3. **Machine learning (ML) based techniques:** To model and optimise CVD processes, ML approaches like support vector machines, random forests and neural networks can be used. ML algorithms learn from historical data and develop predictive models to guide the optimization process. These models can help in understanding the complex relationships between process parameters and film properties, enabling efficient optimization of the CVD process (Hwang et al., 2021a; Jia et al., 2017a; Kadinski et al., 2004).

4. **Sequential Optimization and Response Surface Optimization (SORO):** SORO is a method that combines the principles of sequential optimization and response surface methodology. It involves multiple stages of optimization, where the output from one stage serves as the input for the next stage. By iteratively refining the process parameters based on response surface models, SORO helps in achieving progressively better results (Ramadan and Im, 2019b).

It is important to note that the selection of the optimization technique depends on various factors, including the complexity of the CVD process, available resources, and desired objectives. The combination of multiple techniques may also be employed for a comprehensive optimization approach (Chuang and Chen, 2014; Gupta et al., 2022a; Jia et al., 2017b; Ramadan and Im, 2019b). In summary, the use of CFD in the design of CVD reactors can provide a

powerful tool for optimizing the reactor design and operation, improving process efficiency, reducing costs, and enhancing product quality and consistency.

1.9 Machine learning

Machine learning (ML) is a subset of artificial intelligence that enables computers to learn from data without being explicitly taught (Hwang et al., 2021a, 2021b; Kubat, 2017). ML algorithms have recently attracted significant attention in process modelling. They learn several parameters on their own by fitting the data. In addition, they are also computationally efficient and can be used in real-time prediction (Jia et al., 2017a). Several applications of ML are reported in the area of chemical and material process engineering. For example, the optical properties of the materials were predicted using ML and the relationship among various process parameters that were hard to establish using physics-based models (Wu et al., 2020a). Masoumi et al. integrated the wavelet neural network (WNN) and an experimental design to optimise the 2-litre bioreactor (Fard Masoumi et al., 2014). Recently, Chuang et al. proposed a data-driven optimisation technique that coupled a uniform design method, an artificial neural network, and a genetic algorithm to improve the GaAs growth. They observed that the proposed correlated the experimental data reasonably well and improved the performance of the film. In addition, the advantage of using ML, particularly the support vector machine (SVM) for optimising chemical processes, is high speed, accuracy, and robustness, and requires no or fewer human interventions (Chuang and Chen, 2014). Therefore, the rigorous model-based strategy can be framed using the ML method. It can then be coupled with an efficient optimisation technique to explore the optimal solution of the exceptionally complex process. There are several different types of machine learning, including:

1. **Supervised learning**: This is the most common sort of machine learning, in which a model is trained on labelled data and then used to predict unlabeled data.
2. **Unsupervised learning**: The model does not provide labelled data in this sort of machine learning, but rather is used to detect patterns or relationships within the data.
3. **Reinforcement learning:** This sort of machine learning is used to train models to make decisions or execute actions in a given environment to maximise a reward or achieve a goal.
4. **Deep learning:** This is a branch of machine learning in which neural networks are used to represent the structure of the human brain. Deep learning models are particularly

beneficial for applications such as image recognition, audio recognition, and natural language processing.

1.9.1 Advantages of Machine Learning

1. **Data-driven insights:** ML algorithms can extract valuable insights and patterns from large and complex datasets that may be difficult for humans to discern. They can uncover hidden relationships and correlations, leading to a deeper understanding of the data and enabling data-driven decision-making.

2. **Automation and efficiency**: ML automates repetitive and time-consuming tasks, reducing manual effort and increasing efficiency. Once trained, ML models can process and analyze large amounts of data quickly, allowing for faster decision-making and enhanced productivity.

3. **Predictive capabilities**: Based on historical data trends, ML models may make accurate predictions and forecasts. These predictive capabilities can be used to forecast sales patterns, predict equipment faults, or estimate client behaviour, allowing for proactive decision-making and enhanced planning.

4. **Adaptability and generalization:** ML algorithms can adapt to new data and changing conditions, allowing for continuous improvement and adaptation to evolving environments. They can generalize from training data to make predictions on unseen data, providing valuable insights beyond the available training set.

5. **Handling complex and large-scale data:** ML techniques excel in handling complex and large-scale data. They can handle diverse data types, including structured, unstructured, and multi-modal data, and effectively extract meaningful information from them.

1.10 Support vector machines (SVM)

The advantage of SVM for optimising chemical processes is its high speed, accuracy, and robustness, and it requires no or fewer human interventions saving considerable time and cost

of performing actual experiments. The accuracy of SVM is better than the linear regression model. Some more advantages are given below:

1. **Effective in High-Dimensional Spaces:** Even in high-dimensional feature spaces, SVM works effectively. It is capable of handling datasets with a large number of features, making it appropriate for situations involving complicated and diverse data.
2. **Robust to Overfitting**: SVM employs a regularisation parameter (C) to help reduce overfitting, which is a prevalent issue in machine learning. SVM can generalise well to unknown data by regulating the trade-off between the model's complexity and its ability to fit the input.
3. **Versatility in Kernel Functions:** SVM is compatible with a wide range of kernel functions, including linear, polynomial, radial basis function (RBF), and sigmoid. SVM can capture nonlinear relationships in data and manage difficult decision limitations as a result of its adaptability.
4. **Global Optimization:** SVM aims to find the global optimum solution by minimizing the empirical risk, which helps in avoiding local minima. This property contributes to the model's stability and robustness.
5. **Ability to Handle Outliers:** In comparison to other algorithms, SVM is less sensitive to outliers. SVM's usage of the margin notion allows it to focus on support vectors, which are the data points closest to the decision border, rather than all data points.
6. **Memory Efficiency:** SVM uses a subset of training data called support vectors, which reduces memory requirements. Only the support vectors are used to define the decision boundary, making SVM memory-efficient, especially when dealing with large datasets.

1.11 Objectives of the thesis

The detailed research objectives are as follows:

1. To identify the most efficient and effective process parameters for producing high-quality pyrocarbon. This would involve analyzing the effects of various process variables, such as temperature, pressure, and reactant flow rate.
2. To achieve high-quality pyrocarbon by combined support vector machine (SVM) and Nelder-Mead algorithm by simultaneously maximising the average deposition rate and the uniformity index.

1.12 Thesis organisation

This thesis is organised into four sections, each of which focuses on optimising methane pyrolysis in a commercial CVD reactor using support vector machines and the Nelder-Mead algorithm. (a) process modelling and simulation; (b) assimilation of detailed gas and surface chemistry; (c) effect of process parameters; (d) machine learning-based optimization;
This thesis contains five chapters.

- Chapter 1 discusses the introduction, motivation, different types of CVD, the importance of CFD in designing the CVD reactor, the basics of machine learning technique and its types.
- Chapter 2 explains the history of CVD and its modelling and optimization technique, and discusses the pyrolysis of methane in CVD reactors using various machine learning methods.
- Chapter 3 shows the equations governing the modelling of physical and chemical phenomena for the CVD reactor, the gas and surface reaction model and the solution procedure. Subsequently, the optimization technique of NMA and SVM is explained.
- Chapter 4 examines the impact of reactor operating variables such as temperature, pressure, flow rate, and reactant concentration. And how these variables influence thickness and film uniformity.
- Chapter 5 presents the key observations and conclusions derived from the current research, highlighting the significance of SVM and Nelder-Mead Algorithm (NMA) in optimizing methane pyrolysis in a CVD reactor. Furthermore, it outlines the potential for future research in the field, aiming to further enhance the understanding and application of these techniques.

References

1. Ali, M., Ürgen, M., 2011. Surface morphology, growth rate and quality of diamond films synthesised in hot filament CVD system under various methane concentrations. Appl. Sur. Sci. 257, 8420-8426. https://doi.org/10.1016/j.apsusc.2011.04.097
2. Andrew Ng 2018. Machine Learning Yearning. https://info.deeplearning.ai/machine-learning-yearning-book

3. Becker, A., Hu, Z., Hüttinger, K.J., 2000. Hydrogen inhibition model of carbon deposition from light hydrocarbons. Fuel 79, 1573–1580. https://doi.org/10.1016/S0016-2361(00)00030-2

4. Beigi-Boroujeni, S., Katagiri-Tanaka, O., Cardenas-Benitez, B., Martinez-Chapa, S. O., Aguirre-Soto, A., 2020. Pyrolytic carbon from Novolac epoxy resin compressed before photocrosslinking and pyrolysis. Mater. Today: Proc. https://doi.org/10.1016/j.matpr.2020.10.014

5. Bérard, A., Patience, G.S., Chouinard, G., Tavares, J.R., 2016. Photo-initiated chemical vapour deposition to increase polymer hydrophobicity. Sci. Rep. 6, 1–10.

6. Bourrat, X., Langlais, F., Chollon, G., Vignoles, G. L., 2006. Low-temperature pyrocarbons: a review. J. Braz. Chem. Soc, 17, 1090-1095. https://doi.org/10.1590/S0103-50532006000600005

7. Chen, K. Y., 2007. Forecasting systems reliability based on support vector regression with genetic algorithms. Reliab. Eng. Syst. 92, 423-432. https://doi.org/10.1016/j.ress.2005.12.014

8. Chen, K., Shi, L., Zhang, Y., Liu, Z., 2018. Scalable chemical-vapour-deposition growth of three-dimensional graphene materials towards energy-related applications. Chem. Soc. Rev. 47, 3018-3036. https://doi.org/10.1039/C7CS00852J

9. Cheng, T. S., Hsiao, M. C., 2008. Numerical investigations of geometric effects on flow and thermal fields in a horizontal CVD reactor. J. Cryst. Growth. 310, 3097-3106. https://doi.org/10.1016/j.jcrysgro.2008.03.007

10. Chuang, Y.-C., Chen, C.-T., 2014. Mathematical modelling and optimal design of an MOCVD reactor for gas film growth. J. Taiwan Inst. Chem. Eng. 1, 254-267. https://doi.org/10.1016/j.jtice.2013.05.022

11. Creighton, J.R., Ho, P., 2001. Introduction to Chemical Vapor Deposition (CVD).

12. Dadsetan, M., Latham, K.G., Kumral, B., Khan, M.F., Scott, M., Mitra, T., Naseri, A., Manzoor, S., Bobicki, E.R., Filleter, T., Titirici, M., Thomson, M.J., 2023. Carbon film produced from microwave-driven methane pyrolysis. Carbon Trends 12, 100283. https://doi.org/10.1016/j.cartre.2023.100283

13. Dahmen, K.-H., 2003. Chemical Vapor Deposition, in: Encyclopedia of Physical Science and Technology. Elsevier, 787–808. https://doi.org/10.1016/B0-12-227410-5/00102-2

14. del Coso, G., del Cañizo, C., Luque, A., 2008. Chemical Vapor Deposition Model of Polysilicon in a Trichlorosilane and Hydrogen System. J. Electrochem. Soc. 155, D485. https://doi.org/10.1149/1.2902338

15. Devi, M., Rawat, S., Sharma, S., 2020. A comprehensive review of the pyrolysis process: from carbon nanomaterial synthesis to waste treatment. Oxford Open Mater. Sci.1, 1-30. https://doi.org/10.1093/oxfmat/itab014

16. Dong, G.L., Hüttinger, K.J., 2002. Consideration of reaction mechanisms leading to pyrolytic carbon of different textures. Carbon 40, 2515–2528. https://doi.org/10.1016/S0008-6223(02)00174-4

17. Dong, G.L., Hüttinger, K.J., 2002. Consideration of reaction mechanisms leading to pyrolytic carbon of different textures. Carbon 40, 2515–2528. https://doi.org/10.1016/S0008-6223(02)00174-4

18. Fau, G., Gascoin, N., Gillard, P., Steelant, J., 2013. Methane pyrolysis: Literature survey and comparisons of available data for use in numerical simulations. J. Anal. Appl. Pyrolysis. https://doi.org/10.1016/j.jaap.2013.04.006

19. George, P., Gea, H.C., Jaluria, Y., 2006. Optimization of Chemical Vapor Deposition Process, in: Volume 1: 32nd Design Automation Conference, Parts A and B. ASMEDC, 309–316. https://doi.org/10.1115/DETC2006-99748

20. Gulyaev, P. V., Shushkov, A.A., 2022. A Technology for Creating Reference Marks on the Surface of Pyrolytic Graphite. Tech. Phys. Lett. 48, 287–291. https://doi.org/10.1134/S1063785022100030

21. Gulyaev, P. V., Shushkov, A.A., 2022. A Technology for Creating Reference Marks on the Surface of Pyrolytic Graphite. Tech. Phys. Lett. 48, 287–291. https://doi.org/10.1134/S1063785022100030

22. Gupta, A., Mudgal, A., Shinde, V.M., Kumar, H., Prasad, N.E., 2022. Optimal design of CH_4 pyrolysis in a commercial CVD reactor using support vector machines and Nelder-Mead algorithm. Chemical Engineering Research and Design 178. https://doi.org/10.1016/j.cherd.2021.12.015

23. Haddadi, B., Jordan, C., Harasek, M., 2017. Cost efficient CFD simulations: Proper selection of domain partitioning strategies. Comput. Phys. Commun. 219, 121–134. https://doi.org/10.1016/j.cpc.2017.05.014

24. Hu, H.H., 2012. Computational Fluid Dynamics, in: Fluid Mechanics. Elsevier, 421–472. https://doi.org/10.1016/B978-0-12-382100-3.10010-1

25. Hu, Z., Hüttinger, K.J., 2001. Chemistry and kinetics of chemical vapor deposition of pyrocarbon: VIII. Carbon deposition from methane at low pressures. Carbon 39, 433–441. https://doi.org/10.1016/S0008-6223(00)00143-3

26. Hwang, G., Kim, T., Shin, J., Shin, N., Hwang, S., 2021. Machine learnings for CVD graphene analysis: from measurement to simulation of SEM images. J. Ind. Eng. Chem. 101, 430-444. https://doi.org/10.1016/j.jiec.2021.05.031

27. Jabar, J.M., 2021. Pyrolysis: a convenient route for production of eco-friendly fuels and precursors for chemical and allied industries, in: Recent Perspectives in Pyrolysis Research. IntechOpen. http://dx.doi.org/10.5772/intechopen.101068

28. Jia, S., Qian, X., Yuan, X., 2017. Optimal design for dividing wall columns using support vector machine and particle swarm optimisation. Chem. Eng. Res. Des. 125, 422-432. https://doi.org/10.1016/j.cherd.2017.07.028

29. Kadinski, L., Merai, V., Parekh, A., Ramer, J., et al., 2004. Computational analysis of GaN/InGaN deposition in MOCVD vertical rotating disk reactors. J. Cryst. Growth. 261, 175-181. https://doi.org/10.1016/j.jcrysgro.2003.11.083

30. Komiyama, H., Shimogaki, Y., Egashira, Y., 1999. Chemical reaction engineering in the design of CVD reactors. Chem Eng Sci 54, 1941–1957. https://doi.org/10.1016/S0009-2509(98)00443-6

31. Kubat, M., 2017. An Introduction to Machine Learning, An Introduction to Machine Learning. Springer International Publishing. https://doi.org/10.1007/978-3-319-63913-0

32. Leong Choy, K., 2019. Chemical Vapour Deposition (CVD): Advances, Technology, and Applications CRC Press https://doi.org/10.1201/9780429342363

33. Li, F., Huang, X., Liu, J.-X., Zhang, G.-J., 2020. Sol-gel derived porous ultra-high temperature ceramics. J. Adv. Ceram. 9, 1–16. https://doi.org/10.1007/s40145-019-0332-6

34. Li, K., Zhang, D., Guo, L., Li, H., 2010. Micro- and Nano-structure Characterization of Isotropic Pyrocarbon Obtained via Chemical Vapor Deposition in Hot Wall Reactor. J. Mater. Sci. Technol. 26, 1133–1138. https://doi.org/10.1016/S1005-0302(11)60013-3

35. Lin, P. T., Jaluria, Y., Gea, H. C., 2009. Parametric modelling and optimisation of chemical vapour deposition process. J. Manuf. Sci. Eng. 131, 011011. https://doi.org/10.1115/1.3063689

36. Lin, P. T., Jaluria, Y., Gea, H. C., 2009. Parametric modelling and optimisation of the chemical vapour deposition process. J. Manuf. Sci. Eng. 131, 011011. https://doi.org/10.1115/1.3063689

37. Liu, S. M., Gu, S. L., Zhu, S. M., Ye, J. D., et al., 2007. Modelling analysis of the MOCVD growth of ZnO film. J. Cryst. Growth. 299, 303-308. https://doi.org/10.1016/j.jcrysgro.2006.12.011

38. Mankelevich, Y.A., May, P.W., 2008a. New insights into the mechanism of CVD diamond growth: Single crystal diamond in MW PECVD reactors. Diam. Relat. Mater. 17, 1021–1028. https://doi.org/10.1016/j.diamond.2008.03.022

39. Masoumi, H. R. F., Basri, M., Kassim, A., Abdullah, D. K., et al., 2014. Optimisation of process parameters for the lipase-catalysed synthesis of esteramines-based esterquats using wavelet neural network (WNN) in the 2-liter bioreactor. J. Ind. Eng. Chem. 20, 1973-1976. https://doi.org/10.1016/j.jiec.2013.09.019

40. Myers, R.H., 1999. Response surface methodology - Current status and future directions. J. Qual. Technol. 31, 30–44. https://doi.org/10.1080/00224065.1999.11979891

41. Nomura, S., 2019. The development of coke-making technology based on the utilization of semisoft coking coals, in: New Trends in Coal Conversion. Elsevier, 335–365. https://doi.org/10.1016/B978-0-08-102201-6.00012-1

42. Ogawa, T., Fukumoto, K., Machida, H., Norinaga, K., 2023. CFD simulation of CVD reactors in the CH_3SiCl_3(MTS)/H_2 system using a two-step MTS decomposition and one-step SiC growth models. Heliyon 9, e15061. https://doi.org/10.1016/j.heliyon.2023.e15061

43. Padnya, P.L., Porfireva, A. V., Evtugyn, G.A., Stoikov, I.I., 2018. Solid Contact Potentiometric Sensors Based on a New Class of Ionic Liquids on Thiacalixarene Platform. Front Chem 6. https://doi.org/10.3389/fchem.2018.00594

44. Parkinson, B., Tabatabaei, M., Upham, D.C., Ballinger, B., Greig, C., Smart, S., McFarland, E., 2018. Hydrogen production using methane: Techno-economics of decarbonizing fuels and chemicals. Int. J. Hydrogen Energy 43, 2540–2555. https://doi.org/10.1016/j.ijhydene.2017.12.081

45. Pierson, H.O., 1999. Handbook of chemical vapour deposition : principles, technology, and applications. Noyes Publications.

46. Ramadan, Z., Im, I. T., 2019. Optimisation of operating parameters in a planetary CVD reactor using response surface methodology. Silicon. 11, 2067-2074. https://doi.org/10.1007/s12633-018-0026-7

47. Rezaei, B., Pan, J.Y., Gundlach, C., Keller, S.S., 2020. Highly structured 3D pyrolytic carbon electrodes derived from additive manufacturing technology. Mater. Des. 193, 108834. https://doi.org/10.1016/j.matdes.2020.108834

48. Rodríguez, E., Diez, M.A., Antuña-Nieto, C., López-Antón, M.A., García, R., Martínez-Tarazona, M.R., 2021. An insight into the role of biomass, biocompounds and synthetic polymers as additives to coal for the synthesis of carbon foams. J. Anal. Appl. Pyrolysis 160, 105359. https://doi.org/10.1016/j.jaap.2021.105359

49. Sánchez-Bastardo, N., Schlögl, R., Ruland, H., 2021. Methane Pyrolysis for Zero-Emission Hydrogen Production: A Potential Bridge Technology from Fossil Fuels to a Renewable and Sustainable Hydrogen Economy. Ind Eng Chem Res 60, 11855–11881. https://doi.org/10.1021/acs.iecr.1c01679

50. Seo, T.H., Lee, S., Cho, H., Chandramohan, S., Suh, E.-K., Lee, H.S., Bae, S.K., Kim, S.M., Park, M., Lee, J.K., Kim, M.J., 2016. Tailored CVD graphene coating as a transparent and flexible gas barrier. Sci. Rep. 6, 24143. https://doi.org/10.1038/srep24143

51. Sharma, S.P., Ting, J.M., Vilar, R., 2020. Electron microscopy study of surface-treated carbon fiber for interface modification in composites. Diam. Relat. Mater. 109. https://doi.org/10.1016/j.diamond.2020.108021

52. Sun, L., Yuan, G., Gao, L., Yang, J., Chhowalla, M., Gharahcheshmeh, M.H., Gleason, K.K., Choi, Y.S., Hong, B.H., Liu, Z., 2021. Chemical vapour deposition. Nature Reviews Methods Primers 1, 5. https://doi.org/10.1038/s43586-020-00005-y

53. Szpicer, A., Bińkowska, W., Wojtasik-Kalinowska, I., Salih, S.M., Półtorak, A., 2023. Application of computational fluid dynamics simulations in the food industry. Eur. Food Res. Technol. 249, 1411–1430. https://doi.org/10.1007/s00217-023-04231-y

54. Takahashi, T., Funatsu, K., Ema, Y., 2005. Automatic modelling of reaction systems using genetic algorithms and its application to chemical vapour deposition processes: advanced utilization of simulators for chemical systems. Meas. Sci. Technol. 16, 278–284. https://doi.org/10.1088/0957-0233/16/1/036

55. Tan, R., Fan, Z., Xie, Z., Zhang, M., He, K., Huang, Q., 2016. Fabrication of large-sized high-density bulk isotropic pyrocarbon materials of a special composite microstructure

by fixed-bed chemical vapour deposition. Carbon. 101, 439-448. https://doi.org/10.1016/j.carbon.2016.02.019

56. Teixeira, C., Silva, A. F., Rocha, L. A., 2020. A computational fluid dynamics-based sensitivity analysis of the chemical vapour analysis process to synthesise carbon nanotubes. J. Thermal Sci. Eng. Appl. 12, 011010. https://doi.org/10.1115/1.4044424

57. Timmerberg, S., Kaltschmitt, M., Finkbeiner, M., 2020. Hydrogen and hydrogen-derived fuels through methane decomposition of natural gas – GHG emissions and costs. Energy Convers. Manage. X 7, 100043. https://doi.org/10.1016/j.ecmx.2020.100043

58. Wang, Y., Xiong, X., Li, G., Zhao, X., Chen, Z., Sun, W., Wang, Z., 2013. Effect of gas composition on the microstructure and growth behaviour of HfC coatings prepared by LPCVD. Solid State Sci. 20, 86–91. https://doi.org/10.3390/coatings13010188

59. Weichert, D., Link, P., Stoll, A., Rüping, S., Ihlenfeldt, S., Wrobel, S., 2019. A review of machine learning for the optimization of production processes. Int. J. Adv. Manuf. Technol. 104, 1889–1902. https://doi.org/10.1007/s00170-019-03988-5

60. Wissmann, P.J., Grover, M.A., 2010. Optimization of a Chemical Vapor Deposition Process Using Sequential Experimental Design. Ind. Eng. Chem. Res. 49, 5694–5701. https://doi.org/10.1021/ie901055e

61. Wu, S., Lambard, G., Liu, C., Yamada, H., Yoshida, R., 2020. IQSPR in XenonPy: a Bayesian molecular design algorithm. Mol. Inf. 39, 1900107. https://doi.org/10.1002/minf.201900107

62. Yang, Y., Weaver, M.N., Merz Jr, K.M., 2009. Assessment of the "6-31+ G**+ LANL2DZ" mixed basis set coupled with density functional theory methods and the effective core potential: prediction of heats of formation and ionization potentials for first-row-transition-metal complexes. J. Phys. Chem. A 113, 9843–9851.

63. Yansaneh, O.Y., Zein, S.H., 2022. Recent Advances on Waste Plastic Thermal Pyrolysis: A Critical Overview. Processes 10, 332. https://doi.org/10.3390/pr10020332

CHAPTER 2

LITERATURE REVIEW

2.1 History of the CVD processes

CVD reactors have been around since the early twentieth century, with the earliest patents for CVD processes being filed in the 1920s and 1930s. However, the early CVD processes were not very efficient and were mainly used for the production of speciality chemicals (Pierson, 1999). In the 1950s and 1960s, advances in the understanding of the chemistry of CVD reactions and the development of new reactor designs led to the commercialization of CVD for the production of thin films, such as silicon dioxide and silicon nitride, for use in the semiconductor industry. During the 1970s and 1980s, CVD reactors became increasingly sophisticated, with the development of new reactor designs such as horizontal and vertical tube reactors, and the use of computer control systems to optimize process conditions. In the 1990s and 2000s, CVD was used for the growth of a wide range of thin films, including those made of oxide, nitride, and carbide materials for use in the semiconductor, optical, and biomedical industries (Sun et al., 2021). Furthermore, new reactor designs, such as atomic layer deposition (ALD) and molecular beam epitaxy (MBE), have been developed to enable the development of high-quality thin films with precise control over film thickness and composition (Oke and Jen, 2022). Today, CVD is a well-established technique and is used in the production of a wide range of products, including electronic devices, solar cells, and biomedical implants.

2.2 Modelling approaches in CVD

Parametric modelling approaches refer to the methods used to develop mathematical models that describe the relationships between process parameters and the desired outcomes. These models help in understanding and predicting the behaviour of the CVD process, enabling optimization and control. Here are some commonly used parametric modelling approaches in CVD (W Benzinger et al., 1996; Gupta et al., 2022b; Hu and Hüttinger, 2001; Lacroix et al., 2010; Lin et al., 2009a; Meshot et al., 2020; Shinde and Pradeep, 2021)

1. **Empirical models:** Experimental data and statistical analysis are used to build empirical models. They entail using data-driven methodologies to find patterns and

connections between process parameters and outcomes. To represent the correlations between variables, empirical models may employ regression analysis, response surface technique, or artificial neural networks (Chen, 2007; Kober et al., 2022).

2. **Semi-empirical models:** Semi-empirical models combine empirical observations with some underlying physical principles. These models incorporate a mix of empirical data and simplified mathematical representations of the physical and chemical processes involved in CVD. Semi-empirical models are useful when the underlying mechanisms are partially understood but may still require some empirical adjustments (Chuang and Chen, 2014; Filho et al., 2020).

3. **Kinetic models:** Kinetic models focus on the chemical reactions and kinetics occurring during the CVD process. They entail quantitatively characterising the rates of specific reactions and their relationships to variables like as temperature, pressure, and reactant concentrations. Kinetic models can be used to simulate chemical reactions on the surface and in the gas phase using reaction rate equations, mass transfer equations, and thermodynamic principles (Benzinger et al., 1996; Gupta et al., 2022b).

4. **Computational fluid dynamics (CFD) models:** CFD models solve the governing equations of fluid flow, heat transfer, and species movement within the CVD reactor using numerical methods. CFD models simulate the fluid dynamics, temperature distribution, and concentration profiles within the reactor, providing detailed information about the process. These models can incorporate complex geometries, boundary conditions, and reaction kinetics to accurately predict deposition behaviour (Haddadi et al., 2017; Yu et al., 2016).

5. **Multiscale models:** Multiscale models combine different modelling approaches to capture the various length and time scales involved in CVD. They integrate macroscopic models, such as CFD models, with microscopic or atomistic models to bridge the gap between the reactor-scale phenomena and the molecular-scale processes occurring at the surface. Multiscale modelling allows for a more comprehensive understanding of the CVD process and its underlying mechanisms (Kalisch et al., 2023; Ogawa et al., 2023; Yu et al., 2016).

The choice of parametric modelling approach depends on the specific objectives of the study, available data, level of understanding of the process, and computational resources. Often, a combination of different modelling approaches is used to gain a more complete understanding of the CVD process and optimize the desired outcomes. However, the development of chemical kinetics in CVD has been a crucial aspect of understanding and optimizing thin film deposition processes. CVD is a complex process that involves chemical reactions occurring at the gas-solid interface. The development of chemical kinetics in CVD is essential for understanding and controlling the deposition process, as it provides insights into the reaction mechanisms, rate-limiting steps, and the influence of process parameters on the growth of thin films or coatings. Chemical kinetics in CVD may be traced back to the mid-twentieth century when researchers began examining the gas phase and surface reactions involved in film deposition. Initially, basic empirical models based on experimental data were employed to represent the overall deposition rate (Pierson, 1999; Sun et al., 2021). However, as CVD technology advanced, more sophisticated approaches were developed to model the reaction kinetics and provide mechanistic insights. The development of chemical kinetics in CVD can be summarized as follows:

1. **Gas-phase reactions**: The initial step in developing chemical kinetics in CVD is to investigate precursor gas-phase processes. Understanding the breakdown, dissociation, and generation of reactive species from precursor molecules is part of this. Temperature, pressure, and gas composition all have an impact on gas-phase processes.

2. **Surface reactions:** Once the reactive species are formed in the gas phase, they adsorb onto the substrate surface and undergo surface reactions. These reactions involve the breaking of chemical bonds and the rearrangement of atoms on the substrate surface. Surface reactions are critical in determining the growth rate and properties of the deposited film

   Developing detailed reaction mechanisms is essential to gain a comprehensive understanding of the CVD process. This involves identifying the elementary steps involved in both gas-phase and surface reactions and determining their kinetics. Obtaining accurate rate constants for the elementary reactions is crucial for predicting the deposition rate and optimizing the CVD process. Experimental techniques, such as temperature-programmed reaction (TPR) and isothermal reaction studies, are used to measure rate constants. With the advancement of computational tools, quantum

chemical calculations and molecular dynamics simulations are employed to gain insights into the reaction mechanisms and kinetics (Benzinger et al., 1996; Hu and Hüttinger, 2001). These computational methods complement experimental studies and provide a deeper understanding of complex reactions. As CVD processes become more complex, multi-scale modelling approaches, such as Kinetic Monte Carlo simulations and continuum models, are used to bridge the gap between atomistic and macroscopic scales (Raciti et al., 2023). These models help predict film growth under various process conditions. The development of chemical kinetics in CVD continues to evolve as new materials and advanced deposition techniques are introduced. Understanding the underlying chemistry is crucial for tailoring material properties, enhancing film uniformity, and minimizing defects. It also enables the rational design and optimization of CVD processes for a wide range of applications, including semiconductor manufacturing, coating technologies, and the production of advanced materials.

2.3 Literature based on pyrolysis of methane in CVD reactor

Bourrat et al., 2006 provide a review of the current state of research on pyrocarbons produced at low temperatures (Bourrat et al., 2006b). Pyrocarbons are carbon-based materials that are produced by the pyrolysis of hydrocarbons or other organic materials. They discuss the different methods for producing pyrocarbons at low temperatures, as well as their properties and potential applications. The authors concluded that low-temperature pyrocarbons have the potential to be used in a wide range of applications, including as adsorbents, catalysts, and energy storage and conversion (Bourrat et al., 2006b).

Beigi-Boroujeni et al. (2020) describe a method for producing pyrolytic carbon from Novolac epoxy resin (Beigi-Boroujeni et al., 2019) The method involves compressing the resin before undergoing photocrosslinking and pyrolysis. They found that the compression of the resin before the pyrolysis process led to a higher yield of pyrolytic carbon, as well as improved mechanical properties. The pyrolytic carbon produced has a high specific surface area, strong electrical conductivity, and mechanical characteristics. According to their findings, this approach can be utilised to generate high-quality pyrolytic carbon from Novolac epoxy resin (Beigi-Boroujeni et al., 2020).

Tan et al. (2016) describe a method for producing large-sized, high-density, bulk isotropic pyrocarbon materials using fixed-bed CVD (Tan et al., 2016). They found that by using a

special composite microstructure, they were able to produce pyrocarbon materials with high density, good isotropy, and large size. The resulting pyrocarbon materials were found to have excellent mechanical and electrical properties, including high hardness and high electrical conductivity. The study suggests that this method is a promising approach for the large-scale production of high-quality pyrocarbon materials (Tan et al., 2016).

Chen et al. (2018) explain the use of CVD to create three-dimensional graphene materials for energy-related applications (Chen et al., 2018). The authors discuss recent advances in the CVD growth of 3D graphene materials, including distinct CVD growth methods, the synthesis of various 3D graphene structures, and the characteristics of the resulting materials. They also examine the potential applications of 3D graphene materials in energy-related disciplines such as energy storage and conversion, as well as their scalability and constraints. According to their findings, the CVD development of 3D graphene materials is a potential strategy for generating high-quality graphene materials for energy-related applications that can be scaled up for industrial production (Chen et al., 2018).

Kadinski et al. (2004) offer a computational investigation of the formation of GaN/InGaN layers in a vertical rotating disc reactor employing metal-organic chemical vapour deposition (MOCVD). The authors studied the gas flow and temperature distribution in the reactor, as well as the impact of reactor design and operating parameters on the formation of the GaN/InGaN layers, using CFD models. They discovered that the reactor design and operating circumstances have a substantial impact on the formation of the GaN/InGaN layers and that a high disc rotation rate resulted in better growth uniformity and fewer flaws. According to the findings, computational analysis can be utilised to optimise the growth of GaN/InGaN layers in MOCVD vertical rotating disc reactors, resulting in high-quality and uniform layers.

Liu et al. (2007) offer a study on the development of zinc oxide (ZnO) films using MOCVD. The authors explore the influence of growth parameters such as temperature, pressure, and precursor flow rate on the characteristics of ZnO films using a kinetic model. They discover that the film's growth rate is sensitive to these factors and that the films have good crystalline quality. According to the paper, the MOCVD method is a promising technology for the growth of ZnO films, and the kinetic model created in the study can be utilised to optimise the growth parameters for high-quality ZnO films (Liu et al., 2007).

Cheng and Hsiao (2008) report on numerical studies of the influence of geometric factors on the flow and temperature fields in a horizontal CVD reactor. CFD simulations were utilised in the study to examine the impact of various geometric characteristics, such as the reactor's aspect ratio and the position of the inlet, on the flow and temperature fields within the reactor. The

simulation findings revealed that the reactor's aspect ratio had a substantial effect on the flow and thermal fields, with larger aspect ratios resulting in more uniform flow and thermal fields. Furthermore, the position of the inlet had a considerable effect on the flow and thermal fields, with inlets situated closer to the centre of the reactor resulting in more uniform flow and thermal fields.

Wang et al. (2016) provide a study on the simulation optimisation of filament parameters for uniform diamond film deposition on surfaces of ultra-large circular holes using a CVD technique (Wang et al., 2016). The researchers performed numerical simulations to investigate the effects of various filament parameters on the uniformity of diamond film deposition, such as the distance between the filament and the hole surface, the filament diameter, and the filament shape. Based on the simulation results, the authors also offered an optimisation technique. The simulation findings revealed that the filament distance, diameter, and shape all had a substantial impact on the regularity of diamond film deposition. Overall, the work demonstrates that utilising simulation to optimise filament parameters might improve the uniformity of diamond film depositions on ultra-large circular holes using a CVD technique (Wang et al., 2016).

Barbosa et al. (2009) studied the effect of substrate temperature on the generation of ultra-nanocrystalline diamond (UNCD) films deposited using a hot filament CVD technique with an argon-rich gas mixture. The findings revealed that increasing the substrate temperature reduced the average grain size of the UNCD films while improving their crystallinity. The ideal substrate temperature for generating high-quality UNCD films, according to the authors, was around 800°C. Furthermore, Barbosa et al. (2009) discovered that UNCD films generated at higher substrate temperatures exhibited superior mechanical characteristics and increased surface roughness.

Barua and Povitsky 2020 presented a computational model for carbon CVD at internal surfaces. The model is built around a set of differential equations that characterise the mass and energy balance of the CVD process while accounting for mass transfer, heat transfer, and chemical reactions (Barua and Povitsky, 2020). The authors utilised the model to simulate the formation of carbon films on interior surfaces under various conditions and discovered that it can predict the rate of growth as well as the microstructure of the films. The work also demonstrates that the model may be used to optimise CVD process parameters like as temperature, reactant gas flow rate, and pressure to obtain desired film qualities. According to the findings, the model can be used to better understand and manage the CVD process on internal surfaces (Barua and Povitsky, 2020).

Teixeira et al., 2020 propose a CFD-based sensitivity study of the CVD process for the synthesis of carbon nanotubes (CNTs). The scientists conducted CFD simulations to study the effects of numerous process parameters on CNT growth, including temperature, reactant gas flow rate, and pressure. The temperature and flow rate of the reactant gases were shown to have a substantial influence on the formation of CNTs, while pressure had a comparatively modest effect. The results also showed that the rate of CNTs growth increased with increasing temperature and decreasing flow rate of reactant gases. According to the study, CFD simulation can be a useful tool for understanding and optimising the CVD process for CNT synthesis (Teixeira et al., 2020).

Coso et al. (2008) offer a CVD model for polysilicon development in trichlorosilane (TCS) and hydrogen environments. The authors created a set of mathematical equations to represent the mass and energy balance of the CVD process while accounting for mass transfer, heat transfer, and chemical interactions. They discovered that the rate of polysilicon growth is affected by TCS and hydrogen flow rates, substrate temperature, and pressure. They also discovered that the TCS/H_2 ratio affects polysilicon film quality and that the ideal ratio is around 1.5. Del Coso et al. (2008) found that the model can be used to estimate the growth rate and quality of polysilicon films, as well as to optimise CVD process parameters.

Lin et al., 2009 offer a parametric model for the CVD process. The model predicts the growth rate of the deposited film by taking into account several process parameters such as pressure, temperature, and reactant flow rate. This model is then used by the authors to optimise the CVD procedure for maximum growth rate (Lin et al., 2009a).

An et al. (2018) provide research on the use of response surface methodology (RSM) to optimise operating parameters in a polysilicon CVD reactor. The authors look into how process parameters like pressure, temperature, and flow rate affect the growth rate and quality of the deposited polysilicon film. RSM is used to identify the optimal operating conditions for the CVD process by analysing the relationship between process parameters and responses. The optimal working conditions for the maximum growth rate and best quality of the polysilicon film were discovered to be at a pressure of 600 Pa, a temperature of 673 K, and a flow rate of 100 sccm (An et al., 2018).

Ramadan and Im (2019b) report research on the optimisation of operational parameters in a planetary CVD reactor using response surface methodology (RSM). The authors look at how process parameters like rotation speed, substrate temperature, and flow rate affect the growth rate of the formed silicon layer. RSM is used to identify the optimal operating conditions for the CVD process by analysing the relationship between process parameters and responses. The

study discovered that the ideal working conditions for the maximum growth rate are 30 rpm rotation, 953 K substrate temperature, and 800 sccm flow rate (Ramadan and Im, 2019b).

Cheng and Hasiao (2008) study the effect of various geometric designs on the flow and temperature fields in a horizontal CVD reactor. The study uses numerical simulations to evaluate how changes in the geometric parameters of the reactor, such as its width and height, affect the distribution of reactants and the temperature within the reactor. The width and height of the reactor were discovered to have a substantial impact on the flow and temperature fields within the reactor. The study discovered that increasing the width of the reactor increases flow velocity while decreasing the height of the reactor decreases the temperature gradient. The study also discovered that the flow and thermal fields are not symmetric about the reactor's centre and that the thermal field is more sensitive to changes in the geometric parameters of the reactor than the flow field.

2.4 Use of machine learning (ML) in chemical processes

Jia et al. (2017) offer a study that combines the usage of a Support Vector Machine (SVM) and Particle Swarm Optimisation (PSO) to optimise the design of a dividing wall column (DWC) for binary mixture separation (Jia et al., 2017a). SVM was used to predict the link between the DWC design parameters and separation performance, and PSO was used to find the ideal set of design parameters that maximised separation efficiency. The study's findings revealed that the SVM-PSO strategy was capable of effectively optimising the DWC design and improving separation efficiency (Jia et al., 2017a).

Wu et al., 2020 present the development of a new computational algorithm called Inverse Quantitative Structure-Property Relationship (IQSPR) implemented in the open-source platform XenonPy (Wu et al., 2020b). The IQSPR algorithm uses Bayesian Machine Learning to predict the structural and electronic properties of a molecule from its experimental thermodynamic data, such as boiling point, melting point and heat of vaporization. The authors tested the performance of IQSPR using a dataset of organic compounds and reported a high accuracy in the predictions (Wu et al., 2020b)**.**

Masoumi et al. (2014) propose a study that used a wavelet neural network (WNN) to optimise the process parameters for the lipase-catalyzed production of ester amines-based esterquats in a 2-liter bioreactor. WNN was utilised by the authors to simulate the link between process factors (such as temperature, pH, and substrate concentration) and the esterquat conversion

rate. The WNN model was then utilised to optimise the process parameters to get the highest conversion rate possible. The study's findings revealed that the WNN model could properly forecast the esterquat conversion rate and that optimising the process parameters increased the conversion rate (Fard Masoumi et al., 2014).

Chuang and Chen (2014) offer a mathematical model of a MOCVD reactor for gas film growth. They use this model to improve the growth of the films by optimising the reactor architecture. They also present a method for adjusting the reactor's temperature to achieve optimal growth conditions. According to the findings of the study, the proposed model and design can improve the efficiency of the MOCVD process for gas film growth (Chuang and Chen, 2014).

Azarpour et al. (2017) provide a generic hybrid model for the analysis of industrial fixed-bed catalytic reactors. To anticipate reactor performance, the approach integrates mathematical modelling, artificial neural networks, and experimental data. The model was applied to a variety of fixed-bed catalytic reactors, including those used to produce hydrogen, methanol, and ethylene. The model was found to be capable of properly predicting reactor performance, including conversion and selectivity of the catalytic reaction. The authors also discovered that the model might be used to optimise the reactor's operating settings to increase its performance (Azarpour et al., 2017).

Yang et al. 2020 describe a hybrid model for predicting fluid catalytic cracking performance that incorporates deep learning and mechanistic kinetics. The scientists used experimental data to develop a deep learning model, which they then used to predict the performance of a fluid catalytic cracking reactor. They combined the deep learning network's predictions with a mechanistic kinetics model to boost prediction accuracy. The hybrid model effectively predicted the performance of the fluid catalytic cracking reactor, including conversion and product distribution, according to the scientists. They also discovered that the hybrid model outperformed other models based only on deep learning or mechanistic kinetics (Yang et al., 2020).

References

1. An, L-s, Liu, C-j, Liu, Y-w., 2018. Optimisation of operating parameters in polysilicon chemical vapour deposition reactor with response surface methodology. J. Cryst. Growth. 489, 11–19. https://doi.org/10.1016/j.jcrysgro.2018.02.030
2. Azarpour, A., N.G. Borhani, T., R. Wan Alwi, S., A. Manan, Z., I. Abdul Mutalib, M., 2017. A generic hybrid model development for process analysis of industrial fixed-bed

catalytic reactors. Chem. Eng. Res. Des. 117, 149–167. https://doi.org/10.1016/j.cherd.2016.10.024

3. Barbosa, D. C., Almeida, F. A., Silva, R. F., Ferreira, N. G., et al., 2009. Influence of substrate temperature on the formation of ultra nanocrystalline diamond films deposited by HFCVD argon-rich gas mixture. Diam. Relat. Mater. 18, 1283-1288. https://doi.org/10.1016/j.diamond.2009.05.002

4. Barua, H., Povitsky, A., 2020. Numerical model of carbon chemical vapour deposition at internal surfaces. Vacuum. 175, 109234. https://doi.org/10.1016/j.vacuum.2020.109234

5. Beigi-Boroujeni, S., Katagiri-Tanaka, O., Cardenas-Benitez, B., Martinez-Chapa, S. O., Aguirre-Soto, A., 2020. Pyrolytic carbon from Novolac epoxy resin compressed before photocrosslinking and pyrolysis. Mater. Today: Proc. https://doi.org/10.1016/j.matpr.2020.10.014

6. Benzinger, W., Becker, A., Hüttinger, K.J., 1996. Chemistry and kinetics of chemical vapour deposition of pyrocarbon: I. Fundamentals of kinetics and chemical reaction engineering. Carbon 34, 957–966. https://doi.org/10.1016/0008-6223(96)00010-3

7. Bourrat, X., Langlais, F., Chollon, G., Vignoles, G. L., 2006. Low-temperature pyrocarbons: a review. J. Braz. Chem. Soc, 17, 1090-1095. https://doi.org/10.1590/S0103-50532006000600005

8. Chen, K. Y., 2007. Forecasting systems reliability based on support vector regression with genetic algorithms. Reliab. Eng. Syst. 92, 423-432. https://doi.org/10.1016/j.ress.2005.12.014

9. Chen, K., Shi, L., Zhang, Y., Liu, Z., 2018. Scalable chemical-vapour-deposition growth of three-dimensional graphene materials towards energy-related applications. Chem. Soc. Rev. 47, 3018-3036. https://doi.org/10.1039/C7CS00852J

10. Cheng, T. S., Hsiao, M. C., 2008. Numerical investigations of geometric effects on flow and thermal fields in a horizontal CVD reactor. J. Cryst. Growth. 310, 3097-3106. https://doi.org/10.1016/j.jcrysgro.2008.03.007

11. Chuang, Y.-C., Chen, C.-T., 2014. Mathematical modelling and optimal design of an MOCVD reactor for gas film growth. J. Taiwan Inst. Chem. Eng. 1, 254-267. https://doi.org/10.1016/j.jtice.2013.05.022

12. Coso, G. D., Canizo, D. C., Luque, A., 2008. Chemical vapour deposition model of polysilicon in a trichlorosilane and hydrogen system. J. Electrochem. Soc.m. 155, 485-491. https://doi.org/10.1149/1.2902338

13. Filho, P.I.O., Carmalt, C.J., Angeli, P., Fraga, E.S., 2020. Mathematical Modeling for the Design and Scale-Up of a Large Industrial Aerosol-Assisted Chemical Vapor Deposition Process under Uncertainty. Ind. Eng. Chem. Res. 59, 1249–1260. https://doi.org/10.1021/acs.iecr.9b05869

14. Gupta, A., Mudgal, A., Shinde, V.M., Kumar, H., Prasad, N.E., 2022. Optimal design of CH_4 pyrolysis in a commercial CVD reactor using support vector machines and Nelder-Mead algorithm. Chem. Eng. Res. Des. 178. https://doi.org/10.1016/j.cherd.2021.12.015

15. Haddadi, B., Jordan, C., Harasek, M., 2017. Cost efficient CFD simulations: Proper selection of domain partitioning strategies. Comput. Phys. Commun. 219, 121–134. https://doi.org/10.1016/j.cpc.2017.05.014

16. Hu, Z., Hüttinger, K.J., 2001. Chemistry and kinetics of chemical vapor deposition of pyrocarbon: VIII. Carbon deposition from methane at low pressures. Carbon 39, 433–441. https://doi.org/10.1016/S0008-6223(00)00143-3

17. Jia, S., Qian, X., Yuan, X., 2017. Optimal design for dividing wall columns using support vector machine and particle swarm optimisation. Chem. Eng. Res. Des. 125, 422-432. https://doi.org/10.1016/j.cherd.2017.07.028

18. Kadinski, L., Merai, V., Parekh, A., Ramer, J., et al., 2004. Computational analysis of GaN/InGaN deposition in MOCVD vertical rotating disk reactors. J. Cryst. Growth. 261, 175-181. https://doi.org/10.1016/j.jcrysgro.2003.11.083

19. Kalisch, M., Friedrich, B., Reuter, M.A., 2023. Development and Design of the First Industrial Magnetohydrodynamic Slag-Cleaning Reactor From Execution and Analysis of Pilot Plant Tests Through Coupled CFD Simulations. Metall. Mater. Trans. B 54, 1017–1042. https://doi.org/10.1007/s11663-023-02758-9

20. Kober, R., Schwaab, M., Barbosa-Coutinho, E., Pinto, J.C., 2022. Are Empirical Models Based on the Response Surface Methodology Suitable for Biodiesel Production Optimization? Ind. Eng. Chem. Res. 61, 12458–12472. https://doi.org/10.1021/acs.iecr.2c01848

21. Lacroix, R., Fournet, R., Ziegler-Devin, I., Marquaire, P.M., 2010. Kinetic modelling of surface reactions involved in CVI of pyrocarbon obtained by propane pyrolysis. Carbon 48, 132–144. https://doi.org/10.1016/j.carbon.2009.08.041

22. Lin, P. T., Jaluria, Y., Gea, H. C., 2009. Parametric modelling and optimisation of the chemical vapour deposition process. J. Manuf. Sci. Eng. 131, 011011. https://doi.org/10.1115/1.3063689

23. Lin, P. T., Jaluria, Y., Gea, H. C., 2009. Parametric modelling and optimisation of chemical vapour deposition process. J. Manuf. Sci. Eng. 131, 011011. https://doi.org/10.1115/1.3063689

24. Liu, S. M., Gu, S. L., Zhu, S. M., Ye, J. D., et al., 2007. Modelling analysis of the MOCVD growth of ZnO film. J. Cryst. Growth. 299, 303-308. https://doi.org/10.1016/j.jcrysgro.2006.12.011

25. Masoumi, H. R. F., Basri, M., Kassim, A., Abdullah, D. K., et al., 2014. Optimisation of process parameters for lipase-catalysed synthesis of esteramines-based esterquats using wavelet neural network (WNN) in a 2-litre bioreactor. J. Ind. Eng. Chem. 20, 1973-1976. https://doi.org/10.1016/j.jiec.2013.09.019

26. Meshot, E.R., Park, S.J., Buchsbaum, S.F., et al., 2020. High-yield growth kinetics and spatial mapping of single-walled carbon nanotube forests at wafer scale. Carbon 59, 236–246. https://doi.org/10.1016/j.carbon.2019.12.023

27. Ogawa, T., Fukumoto, K., Machida, H., Norinaga, K., 2023. CFD simulation of CVD reactors in the CH_3SiCl_3(MTS)/H_2 system using a two-step MTS decomposition and one-step SiC growth models. Heliyon 9, e15061. https://doi.org/10.1016/j.heliyon.2023.e15061

28. Oke, J.A., Jen, T.-C., 2022. Atomic layer deposition and other thin film deposition techniques: from principles to film properties. J. Mater. Res. Technol. 21, 2481–2514. https://doi.org/10.1016/j.jmrt.2022.10.064

29. Pierson, H.O., 1999. Handbook of chemical vapour deposition : principles, technology, and applications. Noyes Publications.

30. Raciti, D., Calogero, G., Ricciarelli, D., et al., 2023. Multiscale atomistic modelling of CVD: From gas-phase reactions to lattice defects. Mater. Sci. Semicond. Process 167, 107792. https://doi.org/10.1016/j.mssp.2023.107792

31. Ramadan, Z., Im, I. T., 2019. Optimisation of operating parameters in a planetary CVD reactor using response surface methodology. Silicon. 11, 2067-2074. https://doi.org/10.1007/s12633-018-0026-7

32. Shinde, V.M., Pradeep, P., 2021. Detailed gas-phase kinetics and reduced reaction mechanism for methane pyrolysis involved in CVD/CVI processes. J. Anal. Appl. Pyrolysis 154. https://doi.org/10.1016/j.jaap.2020.104998

33. Sun, L., Yuan, G., Gao, L., Yang, J., Chhowalla, M., Gharahcheshmeh, M.H., Gleason, K.K., Choi, Y.S., Hong, B.H., Liu, Z., 2021. Chemical vapour deposition. Nature Reviews Methods Primers 1, 5. https://doi.org/10.1038/s43586-020-00005-y

34. Tan, R., Fan, Z., Xie, Z., Zhang, M., He, K., Huang, Q., 2016. Fabrication of large-sized high-density bulk isotropic pyrocarbon materials of a special composite microstructure by fixed-bed chemical vapour deposition. Carbon. 101, 439-448. https://doi.org/10.1016/j.carbon.2016.02.019

35. Teixeira, C., Silva, A. F., Rocha, L. A., 2020. A computational fluid dynamics-based sensitivity analysis of the chemical vapour analysis process to synthesise carbon nanotubes. J. Thermal Sci. Eng. Appl. 12, 011010. https://doi.org/10.1115/1.4044424

36. Wang, X., Shen, X., Sun, F., Shen, B., 2016. Simulation optimisation of filament parameters for uniform depositions of diamond films on surfaces of ultra-large circular holes. Appl. Surf. Sci. 388, 593-603. https://doi.org/10.1016/j.apsusc.2015.09.139

37. Wu, S., Lambard, G., Liu, C., Yamada, H., Yoshida, R., 2020. IQSPR in XenonPy: a Bayesian molecular design algorithm. Mol. Inf. 39, 1900107. https://doi.org/10.1002/minf.201900107

38. Yang, Y., Weaver, M.N., Merz Jr, K.M., 2009. Assessment of the "6-31+ G**+ LANL2DZ" mixed basis set coupled with density functional theory methods and the effective core potential: prediction of heats of formation and ionization potentials for first-row-transition-metal complexes. J. Phys. Chem. A 113, 9843–9851.

39. Yu, K., Hayman, C.C., Manjunath, S., Fan, W., Martin, I.T., Martin, H.B., Sankaran, R.M., 2016a. A combined CFD modelling and experimental study of pyrolytic carbon deposition. Diam. Relat. Mater. 70, 173–178. https://doi.org/10.1016/j.diamond.2016.10.010

CHAPTER 3

CFD MODEL AND OPTIMISATION METHODOLOGY

3.1 Basic equation, assumptions, and properties estimation

The simulations were carried out on a vertical hot-wall CVD reactor located at the DMSRDE (DRDO), Kanpur. The schematic diagram of the CVD reactor employed in this work is shown in Fig. 3.1. The reactor height is 1.4 m with a diameter of 0.5 m. Four inlets are provided at the base; three are located at the periphery, while one is positioned at the centre. The precursor gas mixture consisting of methane and hydrogen enters through these inlets and pyrolyses in the reactor. The PyC deposition occurs on multiple substrates, separated by 120 mm apart, and the diameter of each substrate plate is 0.3 m. They are placed on the rotating shaft at the centre of the reactor to ensure a uniform coating. The sufficient residence time of the reactants was achieved by placing the baffles at the reactor outlet. The reactor is non-axisymmetric; therefore, it is necessary to simulate the entire reactor volume.

Using twelve circumferential heating rods, the reactor wall was initially heated from ambient temperature (27^0C) to the appropriate temperature. It was then allowed to stabilise at the desired temperature. Four temperature sensors were strategically placed within the reactor to maintain temperature uniformity. Although the reactor hardware only allowed temperatures up to 1100^0C, simulations were run up to 2500^0C to find the limiting stage during deposition. When the temperature was reached, the CH_4 vapour was delivered into the reactor with the help of an H_2 and Ar mixture. Before entering the input nozzles, the whole gas flow rate was dispersed uniformly. The mixture's interaction with the buoyancy-driven flow resulted in cracking, which was followed by deposition on the substrate. The revolving shaft's centrifugal force disseminated the reactant towards the reactor wall, and maintaining an ideal rotation speed provided homogeneous deposition.

The amount of deposition was calculated by comparing the sample before and after the reaction. All tests used the same reaction time of 12 h. The reactor was purged with Ar after the reaction and allowed to cool to ambient temperature.

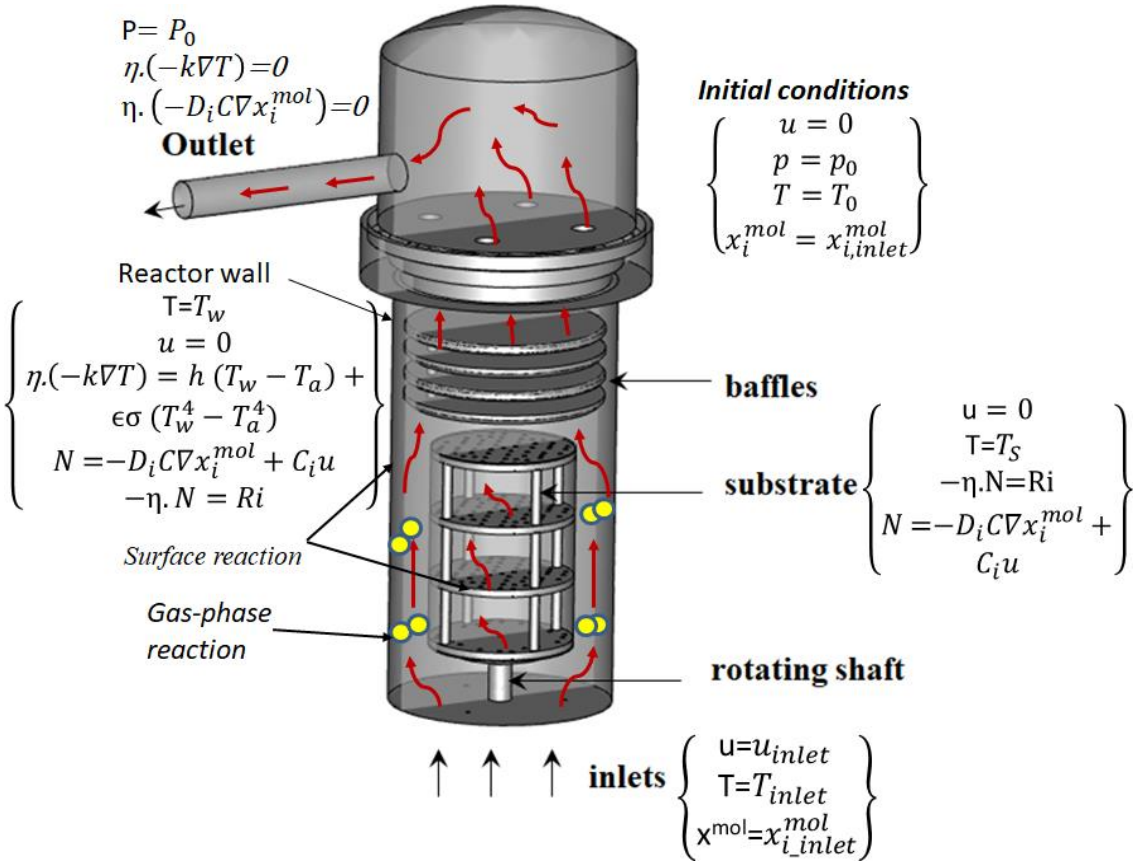

Fig. 3.1 The cross-sectional view of the commercial CVD reactor with boundary conditions used in the simulation

Several physical and chemical phenomena, such as mass, momentum, and heat transfer, along with chemical reactions, constitute the CVD process. These partial differential equations (PDEs) were numerically evaluated utilising the finite volume method assuming a continuum approach. As discussed in the subsequent section, the deposition process was simulated with well-defined gas and surface reaction kinetics. The equations governing the modelling of physical and chemical phenomena are expressed in the conservation of mass, momentum, energy, and species transport.

$$\frac{\partial \rho}{\partial t} + \nabla.\left(\rho\vec{u}\right) = 0 \tag{1}$$

$$\frac{\partial}{\partial t}\left(\rho\vec{u}\right) + \nabla.\left(\rho\vec{u}\vec{u}\right) = -\nabla P + \nabla.\tau + \rho\vec{g} + \vec{F}_B \tag{2}$$

Where $\tau = \mu\left[\nabla\vec{u} + \left(\nabla\vec{u}\right)^T - \frac{2}{3}\left(\nabla.\vec{u}\right)I\right]$ and

$$\frac{\partial}{\partial}\left(\rho x_i^{mol}\right)+\nabla.\left(\rho x_i^{mol}\vec{u}\right)=-\nabla.\vec{J}_i+M_i\sum_{i=1}^{N_r}\hat{R}_i^r \tag{3}$$

$$\frac{\partial}{\partial}\left(\rho h\right)+\nabla.\left(\rho h\vec{u}\right)=\nabla.\left[k_{eff}\nabla T-\sum_i h_i\vec{J}_i^h+\left(\tau.\vec{J}\right)\right] \tag{4}$$

The effect of thermal diffusion was taken into account in the species conservation equation. Due to this effect, large molecules diffuse less rapidly towards the heated surface compared to small ones. The combined flux due to molecular and thermal diffusion of species *i*, is presented as:

$$J_i=-\frac{\rho D_i^m}{M_i}\nabla x_i^{wt}-D_i^T\frac{\nabla T}{T} \tag{5}$$

The transport properties such as viscosity, diffusivity, and thermal conductivity of the gas mixture were estimated using the kinetic theory of gases. The mixture enthalpy was calculated as

$$h_i=h_i^0+\int_{T_{ref}}^{T}C_p dT \tag{6}$$

The specific heat capacity of species, *i*, at constant pressure was expressed in the NASA polynomials. The coefficients of these polynomials were obtained from the literature (Reinisch et al., 2011). The mass diffusivity for species, *i*, in the mixture D_i^m was estimated using Eq. (7).

$$D_i^m=\frac{1-x_i^{mol}}{\sum_{j,j\neq i}x_j^{mol}/D_{ij}^m} \tag{7}$$

The thermal diffusivity was estimated using the empirical expression given by Eq. (8) (Kuo et al., 2005).

$$D_i^T=-2.59\times10^{-7}T^{0.659}\left(\frac{M_i^{0.511}x_i^{mol}}{\sum_{i=1}M_i^{0.511}x_i^{mol}}-x_i^{wt}\right)\left(\frac{\sum_{i=1}M_i^{0.511}x_i^{mol}}{\sum_{i=1}M_i^{0.489}x_i^{mol}}\right) \tag{8}$$

The average rate of deposition (RD) and uniformity index (UI) was calculated as:

$$\overline{RD}=\frac{\int RD dA}{A} \tag{9}$$

$$UI=\frac{\int|\mathrm{RD}-\overline{RD}|\,dA}{A} \tag{10}$$

where A is the total area of the substrate.

3.2 Gas and surface reaction models

A detailed gas-phase kinetic modelling for light hydrocarbon pyrolysis in the CVD reactor was accomplished by many researchers. Norinaga et al. reported a kinetic study of PyC deposition from various precursors (Norinaga et al., 2006). They proposed a lumped parameter model with the assumption that PyC deposits directly from ethylene and acetylene. Later, a qualitative model was developed by Descamps et al. for propane pyrolysis and explained kinetic and microstructure transitions using two parallel reaction pathways (Descamps et al., 2001). These models provided a good foundation for further investigation. However, the limitation of these models is that they work in a narrow operating parameter window and do not render a fundamental understanding of the process. Consequently, a comprehensive gas-phase reaction mechanism with hundreds of elementary steps has been proposed. Recently, Hu et al. presented a model that consists of 241 species and 909 reactions for CH_4 pyrolysis, which predicts mole fractions of dominant species without adjusting kinetic parameters (Hu et al., 2016). However, solving a large number of CFD solver reactions is computationally expensive and not possible in many cases. Therefore, a reduced reaction mechanism was developed by Birakayala et al (Birakayala and Evans, 2002). Though this model is often used to depict the gas phase CH_4 pyrolysis, it underestimates the mole fractions of the dominant species in the present case. Our research group recently modelled the gas phase of CH_4 pyrolysis, and a relatively small model with 13 species and 29 reactions was proposed for CH_4 pyrolysis (Shinde and Pradeep, 2021). It was found that this model is more accurate compared to the models reported earlier in the literature. The reduced model used in the present study is given in Table 3.1 (Shinde and Pradeep, 2021).

Compared to the gas phase, the surface reaction mechanism is more complex due to the dynamic events on the depositing surface. Several speculative theories that have assumed the immediate decomposition of adsorbed species have been proposed to describe the PyC formation (Benzinger et al., 1996). The pre-exponential factor and apparent activation energy were estimated by assuming the whole process as the first-order reaction. However, precise knowledge of the rate-limiting step is still missing in the literature (Yu et al., 2016a). The boundary layer diffusion, nucleation, and crystal growth make understanding the surface reactions more complex (Ali and Ürgen, 2017, 2011b). It has been concluded that the concentration of intermediates depends on the identity of the carbon precursor, its initial mole fraction, flow rate, residence time, and temperature (Hu and Hüttinger, 2001). Dong et al.

modelled the multi-step reactions and correlated the formation of a distinct PyC structure considering C_2H_2, C_2H_4, and C_6H_6 as dominating growth species (Dong and Hüttinger, 2002). They investigated hydrogen inhibition on the carbon deposition for the mixture of CH_4/H_2, and the rate constants of the surface reaction were obtained by fitting the experimental results. The surface reaction model developed by Li et al. was adopted in the present study and given in Table 3.1 (Li et al., 2008). The surface site density was evaluated to be 6.3102×10^{-8} kmol/m^2 from geometrical considerations (Lacroix et al., 2010), and PyC bulk density was assumed to be 2.20 g/cm^3.

Table 3.1 Gas-phase and surface reactions along with kinetic parameters of methane pyrolysis (Norinaga et al., 2006; Shinde and Pradeep, 2021).

No.	Reaction	A	β_T	E (kJ/mol)
Gas-phase reactions				
G1	$C_2H_4 \leftrightarrow C_2H_3 + H$	3.98×10^{17}	0.0	410.86
G2	$H + C_2H_4 \leftrightarrow C_2H_3 + H_2$	1.32×10^{06}	2.5	46.86
G3	$H + H \leftrightarrow H_2$	1.00×10^{00}	0.0	0.0
G4	$CH_4 \leftrightarrow H + CH_3$	1.00×10^{17}	0.0	358.98
G5	$CH_3 + C_2H_4 \leftrightarrow C_2H_3 + CH_4$	5.00×10^{12}	0.0	54.39
G6	$CH_3 + H_2 \leftrightarrow CH_4 + H$	2.75×10^{04}	2.5	39.32
G7	$2CH_3 \leftrightarrow C_2H_6$	3.18×10^{41}	-7.0	11.29
G8	$CH_3 + CH_4 \leftrightarrow C_2H_6 + H$	8.00×10^{13}	2.0	167.36
G9	$C_2H_5 \leftrightarrow C_2H_4 + H$	2.04×10^{15}	0.0	31.0
G10	$C_2H_6 \leftrightarrow C_2H_5 + H$	2.08×10^{38}	-7.1	129.7
G11	$2CH_3 \leftrightarrow C_2H_5 + H$	3.01×10^{13}	0.0	56.48
G12	$CH_3 + CH_4 \leftrightarrow C_2H_5 + H_2$	1.00×10^{13}	0.0	96.23
G13	$C_2H_5 + H \leftrightarrow C_2H_4 + H_2$	2.00×10^{12}	0.0	0.0
G14	$2C_2H_4 \leftrightarrow C_2H_5 + C_2H_3$	1.82×10^{14}	0.0	269.86
G15	$C_2H_6 + C_2H_3 \leftrightarrow C_2H_5 + C_2H_4$	1.08×10^{-03}	4.5	14.64
G16	$C_2H_6 + H \leftrightarrow C_2H_5 + H_2$	5.40×10^{02}	3.5	21.75
G17	$CH_3 + C_2H_6 \leftrightarrow CH_4 + C_2H_5$	5.50×10^{-01}	4.0	37.65
G18	$C_3H_6 + H \leftrightarrow C_2H_4 + CH_3$	3.40×10^{13}	0.0	14.64
G19	$C_3H_6 \leftrightarrow C_2H_3 + CH_3$	2.50×10^{14}	0.0	368.19

G20	$C_3H_6 + C_2H_3 \leftrightarrow C_4H_6 + CH_3$	1.00×10^{00}	0.0	0.0
G21	$C_4H_6 \leftrightarrow 2C_2H_3$	4.07×10^{16}	0.0	390.78
G22	$C_4H_6 + C_2H_3 \leftrightarrow C_6H_6 + H + H_2$	3.98×10^{10}	0.0	0.0
G23	$C_4H_6 + H \leftrightarrow C_2H_4 + C_2H_3$	5.01×10^{11}	0.0	0.0
G24	$C_2H_4 \leftrightarrow C_2H_2 + H_2$	8.00×10^{12}	0.4	371.12
G25	$C_2H_3 + H \leftrightarrow C_2H_2 + H_2$	3.00×10^{13}	0.0	0.0
G26	$C_3H_6 \leftrightarrow C_2H_2 + CH_4$	1.80×10^{12}	0.0	292.88
G27	$C_2H_3 \leftrightarrow C_2H_2 + H$	7.94×10^{14}	0.0	129.70
G28	$C_4H_6 + H \leftrightarrow C_2H_3 + C_2H_2 + H_2$	3.16×10^{14}	0.0	60.66
G29	$C_4H_6 \leftrightarrow C_2H_2 + C_2H_4$	8.40×10^{14}	0.0	355.64
Surface reactions				
S1	$C_2H_4 \rightarrow 2C(s) + 2H_2$	7.24×10^{01}	0.0	154.39
S2	$C_2H_2 \rightarrow 2C(s) + H_2$	1.35×10^{01}	0.0	125.52
S3	$C_6H_6 \rightarrow 6C(s) + 3H_2$	4.71×10^{05}	0.0	215.89

3.3 Boundary condition and solution procedure

The following assumptions were made to solve the above-mentioned governing equations: the flow was assumed to be a continuum, laminar, and ideal compressible gas. No-slip, impermeable boundary conditions were imposed on the solid surfaces, and zero species gradients were employed in the case of non-reacting walls. The reactor outlet flow was supposed to be fully developed. The thermal radiation effects are neglected because the reactor is operated at low pressure (50-500 mbar). It has been observed that the absorption coefficients of light hydrocarbons are very low under such operating pressure. In addition, the temperature inside the reactor is almost homogeneous. Therefore, the absorption of thermal radiation was ignored in the present work (Minakov et al., 2019). However, the heat loss due to radiation is accounted for in the boundary condition. The various operating conditions employed in the simulation are depicted in Fig. 3.1.

Table 3.2 The range of operating parameters used in the CFD simulation.

Parameter	**Value**	**Unit**
Reactor temperature	900-1100	^{0}C
Operating Pressure	100-1000	mbar
Speed of rotation	1	rpm

Inlet mole CH_4	0.2-1	--
Inlet mole H_2	0-0.8	--
Inlet mole C_2H_4 and C_2H_2	0	--
Total flow rate	10-30	lpm
Inlet gas temperature	80	^0C

Fig. 3.2 Schematic representation of unstructured tetrahedral mesh used for the computational domain

The reactor geometry was built in Ansys SpaceClaim, and the meshing was done using the ANSYS Workbench mesh generator. The high-quality unstructured tetrahedral mesh (skewness < 0.7) was used for the computational domain as depicted in Fig. 3.2. ANSYS Fluent, a commercial package, was used to perform simulations. The grid independence study was conducted by systematically increasing the number of elements from 2,012,374 to

2,952,435. Several key variables, including velocity, temperature, C_2H_2 concentration, and deposition rate, were closely monitored to assess convergence. The convergence of these variables was evaluated at various critical points within the domain, including near the inlet, outlet, and regions with high gradients, to ensure an accurate representation of the flow field. Steady-state numerical simulations were performed on various grid sets under identical boundary conditions. The resulting inlet Reynolds number was compared, revealing a continuous increase with the grid number up to 3.5 million, as shown in Fig. 3.3. Beyond this point, the Reynolds number stabilized. Considering available computational resources, a grid number of 3,660,910 million was selected for subsequent simulations where the relative increase of less than 1% in the cell values of the aforementioned variables

The simulations were conducted using Ansys, a commercial finite volume element software. Numerical grids with quadrilateral elements were generated based on the reactor geometry, resulting in a total mesh of 3,660,910 elements for this study. The convective-diffusive transport equations were discretized using a second-order upwind scheme. The discretized equations, along with the boundary conditions, were solved using the pressure-based COUPLED algorithm. The time step was taken to be 0.001 s for all the simulations. Appropriate relaxation factors were applied to pressure, velocity, temperature, and concentration to ensure a stable solution. Convergence was achieved when the residuals in the governing equations were less than 10^{-3}. The time step for all simulations was set to 0.001 seconds. A grid independence study was also performed by varying the number of elements from 1,012,374 to 4,952,435. It was observed that the relative increase in the cell Reynolds number was less than 1% after 3,660,910 elements, confirming the adequacy of the chosen grid size. The following points summarize the approach and criteria used to ensure computational convergence in our study: i) Residual Monitoring: The residuals of the governing equations (continuity, momentum, energy, and species transport) were closely monitored. Convergence was deemed achieved when all residuals fell below 10^{-3}. ii) Key Variable Monitoring: Specific variables such as velocity, temperature, C_2H_2 concentration, and deposition rate were tracked to ensure they reached steady-state values. iii) Mass and Energy Conservation: The overall mass and energy entering and leaving the system were checked to ensure they balanced within an acceptable tolerance, preventing unphysical accumulation or depletion. By adhering to these criteria, we ensured the accuracy and reliability of our computational results.

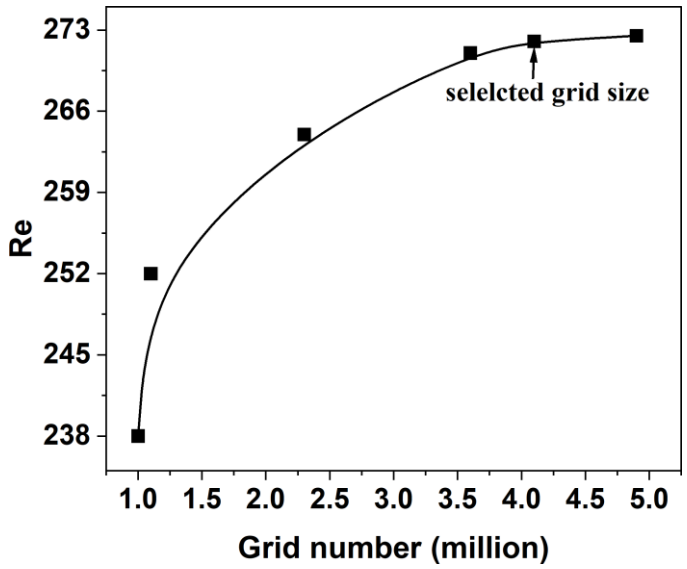

Fig. 3.3 Grid independence test.

3.3 Machine learning model for prediction of PyC deposition

A support vector machine (SVM) algorithm was employed to envisage how process variables such as temperature, pressure, inlet flow rate, and concentration of CH_4 affect the PyC deposition and film uniformity. Thus, there are two dependent variables: deposition rate and film uniformity, while four parameters, including reaction temperature, pressure, the concentration of CH_4, and total flow rate, are used as independent variables. Before training the models, the data were scaled using Eq. (11) to reduce multi-collinearity produced by higher-order terms.

$$x_i^{scaled} = \frac{x_i - \min(x_n)}{\max(x_n)} \tag{11}$$

10-fold cross-validation was availed to optimise the model hyperparameter so that the problems of overfitting and selection bias are minimised. One round of cross-validation was performed by dividing the data into complementary subsets, training the model on one subset, and validating on the other. In this way, several rounds of cross-validations were performed to reduce the variability of the model prediction on new data. The advantage of this procedure compared to the repeated random sub-sampling is that all sample data points are used to train and validate the model, and each data point is used only once for verification.

The SVM, a robust classifier, was used to correlate various process parameters with deposition rate and film uniformity. Support Vector Regression (SVR) is an SVM extension when applied to regression (Chen, 2007). There are many variants of SVR; however, ε-

insensitive regression was implemented in this study. The goal of SVR is not to minimise the error but to ensure it is within an acceptable range and to find an appropriate line (or hyperplane in higher dimensions) that fits the data. For n predictors, the hyperplane consists of n-1 dimensions. The best-fit line is the hyperplane with the maximum number of data points within a distance, sometimes referred to as the margin. Data points with residuals outside the margin contribute to the regression fit and support vectors. SVR achieves the fit by minimising the L2-norm of the coefficient vector while constraining the absolute error within a specified range. The solution to the SVR is reduced to the following optimisation problem (Hwang et al., 2021a).

$$\min \frac{1}{2}||\omega||^2 + C\sum_{k=1}^{n}|\xi_k| \tag{12}$$

Subject to $|y_k - \langle \omega_k, x_k \rangle - b| \leq \varepsilon + |\xi_k|$ (13)

Where ω_k is the coefficient of the model, and x_k and y_k are predictor and response, respectively, and C is a hyperparameter used to penalise large residuals. The value of C was obtained by trial and error (called grid search) over a grid of possible values such that the best value corresponds to the minimum training error. The term $\langle \omega_k, x_k \rangle$ in Eq. (13) denotes the dot product of the two elements w_k and x_k, which was replaced with a Gaussian kernel function while fitting the model. ε is the acceptable margin of error on both sides of the fitted line and the deviation of each data point from the line. The above formulation is based on the assumption that the corresponding convex optimisation problem is feasible. The performance of the model was estimated concerning the correlation coefficient (R^2), root means square error (RMSE) and means absolute error (MAE).

$$R^2 = 1 - \frac{\sum_{k=1}^{n}(y_k - \hat{y}_k)^2}{\sum_{i=1}^{n}(y_k - \bar{y})^2} \tag{14}$$

$$MAE = \sum_{k=1}^{n}\frac{|\hat{y}_k - y_k|}{n} \tag{15}$$

$$RMSE = \sqrt{\frac{\sum_{k=1}^{n}(\hat{y}_k - y_k)^2}{n}} \tag{16}$$

The variables $\bar{y}$, $\hat{y}_k$, y imply the mean, estimated, and observed values of the deposition rate (y1) and uniformity index (y_2), respectively.

3.4 Nelder-Mead algorithm

The Nelder-Mead algorithm, also known as the downhill simplex method, is a multidimensional optimisation process used to find the minimum of an objective function. It is a direct search or derivative-free optimisation approach developed by John Nelder and Roger Mead. It is a heuristic technique to minimise a function using a dynamic simplex (Shevkunov et al., 2019). It considers (n+1) points on the n-dimensional space and ensures better convergence by adjusting the step size based on the loss function. Suppose a new point is better than the previous one in subsequent iterations, the step size increases (expansion) to move to the minima faster. Otherwise, the step size is reduced (contraction) to converge around the minima. The function fitted previously using an SVM algorithm was evaluated at those n+1 points and used to find the optimal condition for the CVD reactor. The methodology framework employed in optimising the CVD reactor is illustrated in Fig. 3.4. x_B, x_w, and x_G in Fig. 3.4 represents the best, worst and good points. The new points required to locate the optimal value can be estimated as $x_M = \frac{x_B + x_G}{2}, x_R = 2x_M - x_W \quad x_{C_1} = \frac{x_R + x_M}{2}, x_{C_2} = \frac{x_W + x_M}{2}$. Detailed steps involved in the NM algorithm can be found elsewhere (Shevkunov et al., 2019).

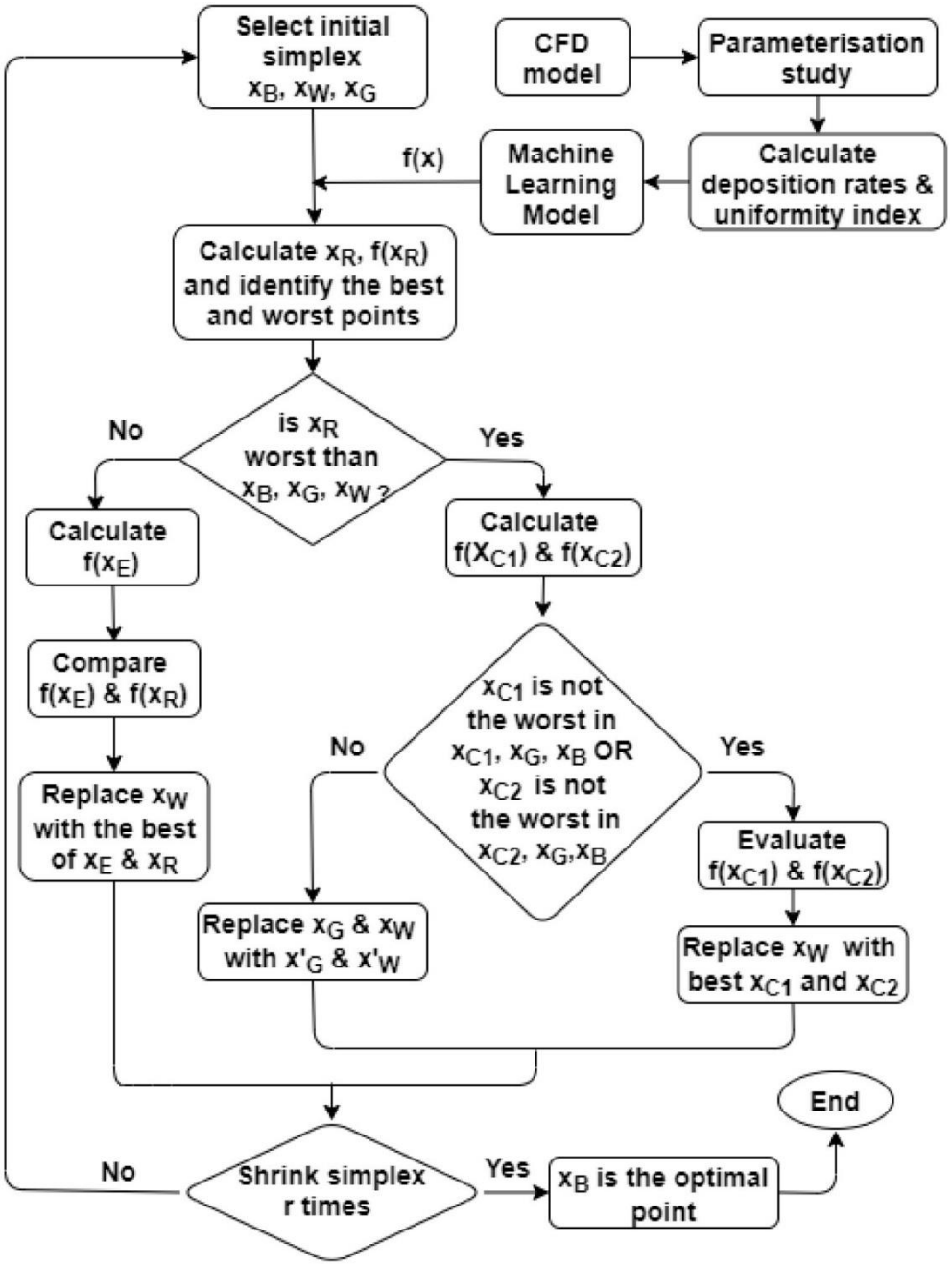

Fig. 3.4 Methodology framework for the optimisation of CVD reactor with the Nelder-Mead algorithm.

Steps involved in the NM algorithm:

1. **Initialization:**
   - Start with a simplex, which is a set of n+1 points in n-dimensional space.
   - Evaluate the objective function at each vertex of the simplex.
2. **Ordering:**

- Order the vertices based on the function values, so the best vertex has the lowest function value, and the worst has the highest.

3. **Reflection:**
   - Reflect the worst point across the centroid of the remaining points.

4. **Expansion, Contraction, or Reduction:**
   - If the reflected point is better than the second-worst, consider expanding farther in that direction.
   - If the reflected point is the new best, try expanding even more.
   - Contract towards the centroid if the reflected point is worse than the second-worst.
   - If the worst point remains the worst after reflection, contract the whole simplex towards the best point.

5. **Termination:**
   - Repeat the process until convergence criteria are met (e.g., a certain level of accuracy is achieved, or a maximum number of iterations is reached).

3.6 Objective function

After fitting the ML model, the function y (as given in Eq. (17)), which combined the PyC deposition and the film uniformity, was maximised by minimising -y. The NM algorithm was used for locating the optimal combination of the process variables. The optimisation algorithm was initialised using randomly selected data points to avoid the problem of local minima. Constraints were imposed on the response variables to avoid searching for values beyond the observation space. Finally, optimisation was performed on the functions fitted using the SVR. The optimisation problem can be stated as follows:

Maximise $y = \alpha \times y_1 + \beta \times y_2$

Where $y = \begin{cases} 0 \ if \ \ \mathrm{y}_1 \geq y_1^{upper} \\ \mathrm{y} \ if \ \ \mathrm{y}_1 < y_1^{upper} \end{cases}$

Subject to:

$900^0 C \leq T \leq 1100^0 C$

$$50\ mbar \le P \le 1000\ mbar \qquad (17)$$
$$10\ \text{slm} \le Q \le 30\ \text{slm}$$
$$0.2 \le mol.frac \le 1$$

Where $y_i(i)$ represents the function evaluated at i[th] iteration. The goal is to simultaneously maximise the average deposition rate (y_1) and the uniformity index (y_2). Besides, searching the acceptable range of each process parameter given in Eq. (17), the average growth rate was restricted to be lower than the upper limit value ($y_1^{upper} = 357 \times 10^{-9}\,\text{kg/m}^2\text{s}$). Our experience suggests thicker film (y_1^{upper}) creates high intrinsic stress and produces cracks or delaminates at elevated temperatures. Therefore, the upper limit for deposition rate was restricted below this value for obtaining an optimal solution. The step-by-step procedure followed for the optimisation of the CVD reactor is described below as:

Step 1: Set the acceptable range of each process parameter (independent variables) and initialise the simplex.
Step 2: Estimate the objective function given in Eq. (17).
Step 3: Perform various actions, including ordering, expansion, contraction, reflection and shrink, to search for the optimal value.
Step 4: Set the obtained values and evaluate the performance of the objective function.
Step 5: Check the convergence criteria. If the termination criterion is satisfied, then end the loop or else return to step 1

References

1. Ali, M., Ürgen, M., 2017. Switching dynamics of morphology-structure in chemically deposited carbon films - a new insight. Carbon. 122, 653-663. https://doi.org/10.1016/j.carbon.2017.07.021
2. Benzinger, W., Becker, A., Hüttinger, K. J., 1996. Chemistry and kinetics of chemical vapour deposition of pyrocarbon: I. fundamentals of kinetics and chemical reaction engineering. Carbon. 34, 957–966. https://doi.org/10.1016/0008-6223(96)00010-3
3. Birakayala, N., Evans, E. A., 2002. A reduced reaction model for carbon CVD/CVI processes. Carbon. 40, 675-683. https://doi.org/10.1016/S0008-6223(01)00184-1

4. Chen, K. Y., 2007. Forecasting systems reliability based on support vector regression with genetic algorithms. Reliab. Eng. Syst. 92, 423-432. https://doi.org/10.1016/j.ress.2005.12.014

5. Deivendran, B., Shinde, V. M., Kumar, H., Prasad, N. E. 2021. 3D modelling and optimisation of sic deposition from CH_3SiCl_3/H_2 in a commercial hot-wall reactor. J. Cryst. Growth. 554, 125944. https://doi.org/10.1016/j.jcrysgro.2020.125944

6. Descamps, C., Vignoles, G. L., Féron, O., Langlais, F., Lavenac, J., 2001. Correlation between homogeneous propane pyrolysis and pyrocarbon deposition. J. Electrochem. Soc. 148, 695-708.

7. Dong, G. L., and Hüttinger, K. J., 2002. Consideration of reaction mechanisms leading to pyrolytic carbon of different textures. Carbon. 40, 2515–2528. https://doi.org/10.1149/1.1402981

8. Hu, C., Li, H., Zhang, S., Li, W., 2016. A molecular-level analysis of gas-phase reactions in chemical vapour deposition of carbon from methane using a detailed kinetic model. J. Mater. Sci., 51, 3897-3906. https://doi.org/10.1007/s10853-015-9709-2

9. Hu, Z., Hüttinger, K. J., 2001. Chemistry and kinetics of chemical vapour deposition of pyrocarbon: VIII. carbon deposition from methane at low pressures. Carbon. 39, 433-441. https://doi.org/10.1016/S0008-6223(00)00143-3

10. Hwang, G., Kim, T., Shin, J., Shin, N., Hwang, S., 2021. Machine learnings for CVD graphene analysis: from measurement to simulation of SEM images. J. Ind. Eng. Chem. 101, 430-444. https://doi.org/10.1016/j.jiec.2021.05.031

11. Kuo, K. K., 1986. Principles of Combustion. John Wiley and Sons, New York.

12. Li, A., Norinaga, K., Zhang, W., Deutschmann, O., 2008. Modeling and simulation of materials synthesis: chemical vapour deposition and infiltration of pyrolytic carbon. Compos. Sci. Technol. 68, 1097-1104. https://doi.org/10.1016/j.compscitech.2007.07.007

13. Li, A., Norinaga, K., Zhang, W., Deutschmann, O., 2008. Modelling and simulation of materials synthesis: chemical vapour deposition and infiltration of pyrolytic carbon. Compos. Sci. Technol. 68, 1097-1104. https://doi.org/10.1016/j.compscitech.2007.07.007

14. Minakov, A. V., Simunin, M. M., Ryzhkov, I. I., 2019. Modelling of ethanol pyrolysis in a commercial CVD reactor for growing carbon layers on alumina substrates. Int. J. Heat Mass Transfer.145, 118764. https://doi.org/10.1016/j.ijheatmasstransfer.2019.118764

15. Reinisch, G., Vignoles, G. L., Leyssale, J.-M., 2011. Reaction mechanism for the thermal decomposition of $BCl_3/CH_4/H_2$ gas mixtures. J. Phys. Chem. A. 115, 11579-11588. https://doi.org/10.1021/jp2039114

16. Shevkunov, N. O., Zhigunova, A. v., Shevkunova, A. V., 2019. Modelling parameters of the production project. IOP Conf. Ser. Mater. Sci. Eng. 560, 012043. https://doi.org/10.1088/1757-899X/560/1/012043

17. Shinde, V. M., Pradeep, P., 2021. Detailed gas-phase kinetics and reduced reaction mechanism for methane pyrolysis involved in CVD/CVI processes. J. Anal. Appl. Pyrol. 154, 104998. https://doi.org/10.1016/j.jaap.2020.104998

18. Yu, K., Hayman, C. C., Manjunath, S., Fan, W., Martin, I. T., Martin, H. B., Sankaran, R. M., 2016. A combined CFD modelling and experimental study of pyrolytic carbon deposition, Diamond Relat. Mater. 70, 173-178. https://doi.org/10.1016/j.diamond.2016.10.010

CHAPTER 4

RESULTS AND DISCUSSION

The simulations were run for a variety of operating parameters, including temperature, pressure, concentration, and gas inlet flow rate. The pyrolysis rate was found to be maximum at high temperatures and low pressures. The effects of Other operating parameters were also studied.

4.1 Validation of simulation results

The deposition rate and outlet CH_4 conversion obtained from the CFD model were validated against the experimental data, as shown in Fig. 4.1. The overall relative error in the deposition rate and CH_4 conversion is less than 12% and 8%, respectively. Thus, this indicates that the present model can predict the experimental trends quite accurately. However, CFD simulations are underpredicted actual performance due to several factors, including oversimplified geometries, inaccurate chemical kinetics, and numerical errors. These errors can arise from discretization limitations, solver algorithm shortcomings, and experimental challenges related to multiphase flows and coupled phenomena. Moreover, the fidelity of the CFD model was accomplished by incorporating highly accurate numerical schemes, temperature-dependent physical properties, thermal diffusion (Soret effect) and radiation effects. As a result, capturing the flow physics of the commercial CVD reactor became very computationally demanding. In this work, the sensitivity analysis of the above parameters was performed in detail. However, the fidelity of the CFD simulation that included the temperature-dependent physical properties was shown in Fig. 4.1. The effect of thermal diffusion on the velocity profile, and concentration of methane is shown in Fig. D1 and D2. It has been observed that the CFD simulation that considers temperature-dependent physical properties is ~10 % more accurate than the simulation with constant temperature-physical properties.

4.2 Effect of reactor temperature

Fig. 4.2 illustrates how the temperature field varies inside the reactor at the different set values. As the gas mixture flows through the reactor, it is rapidly heated due to convection, and a uniform temperature is achieved in the axial direction at low temperatures. The simulation

results show that significant temperature variations exist near the wall surfaces at high temperatures. This implies that the maximum local Nusselt number is near hot surfaces, and it decreases as we move away from the wall due to increased thermal boundary layer thickness. Moreover, the radial temperature distribution shows that the temperature profile is axisymmetric and uniform, except at the bottom plate. The considerable temperature variation is attributed to the entry effect. It can be inferred from the simulation results that if the deposition occurs in a reaction-limited growth regime, then the deposition rate increases with increases in the temperature. However, the non-uniform distribution of precursor/intermediate caused due to non-homogenous temperature distribution considerably affects the film uniformity.

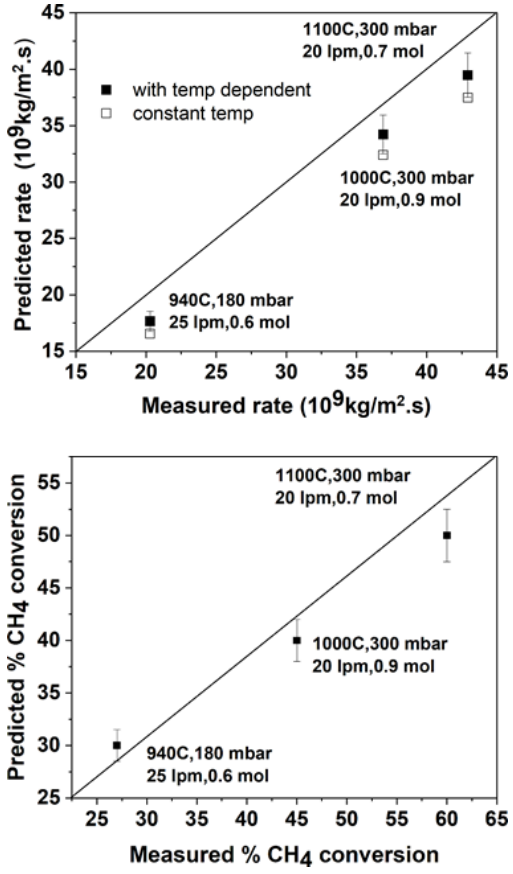

Fig. 4.1 Comparison of the model prediction of the deposition rate and exit CH_4 conversion with experimental data.

Fig. 4.3 shows the simulated cross-sectional average mole fractions of major species as a function of the reactor height at different temperatures. The vertical height mentioned in Fig. 4.3 is normalized by the total height of the four-plate substrate. The concentration (or mole fraction) values were measured as cross-sectional averages at the given horizontal plane, and

only the species with a molar fraction >10^{-4} are plotted. Several different intermediates, C_2H_2, C_2H_4, C_6H_6, and H_2 species, are formed during the pyrolysis of CH_4. A substantial difference in mole fractions was obtained at varying temperatures. Low-temperature (900°C) leads to less conversion of CH_4, and its concentration remained constant up to the middle of the reactor and then decreased slowly. It has been noted that C_2H_2 was the most abundant carbon-forming species, and the concentration of other hydrocarbons (e.g., C_2H_4 and C_6H_6), was minimal. This trend was observed for all studied temperatures. Above 900°C, the mole fractions of CH_4 rapidly diminish with increasing residence time. It is apparent that the mole fraction of C_2H_2 always increases with an increase in temperature, and it begins to be the most dominating carbon-forming species.

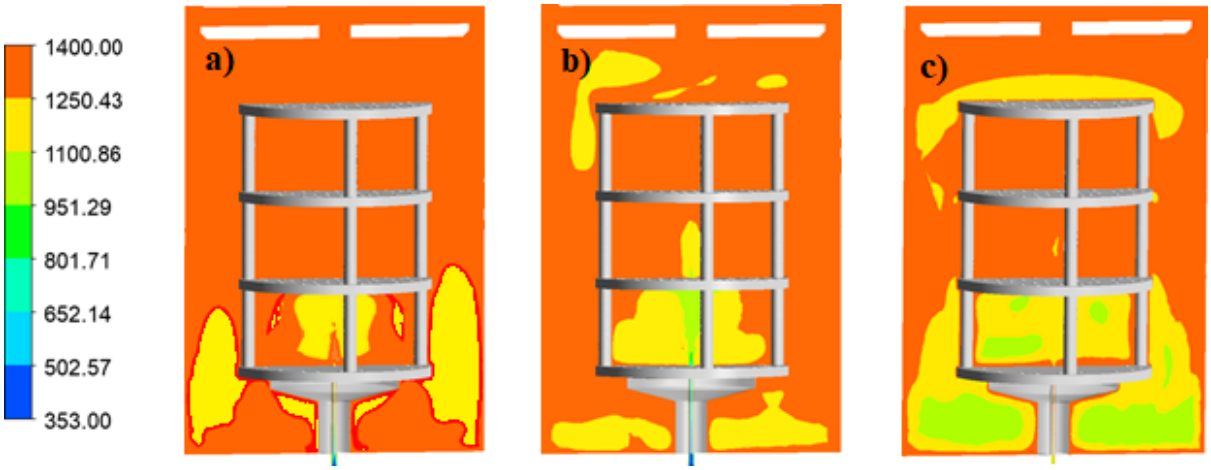

Fig. 4.2 Simulated temperature distribution at a) 900^{0}C, b) 1000^{0}C, and c) 1100^{0}C.

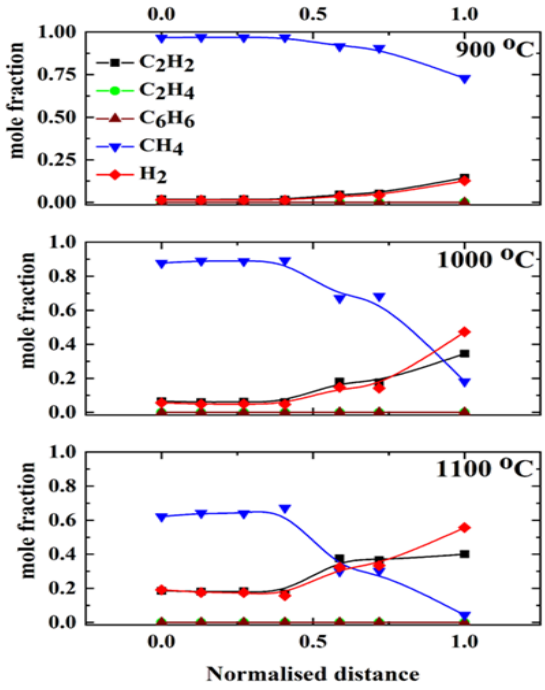

Fig. 4.3 Variation of cross-sectional averaged mole fractions of various species along the reactor length at different temperatures.

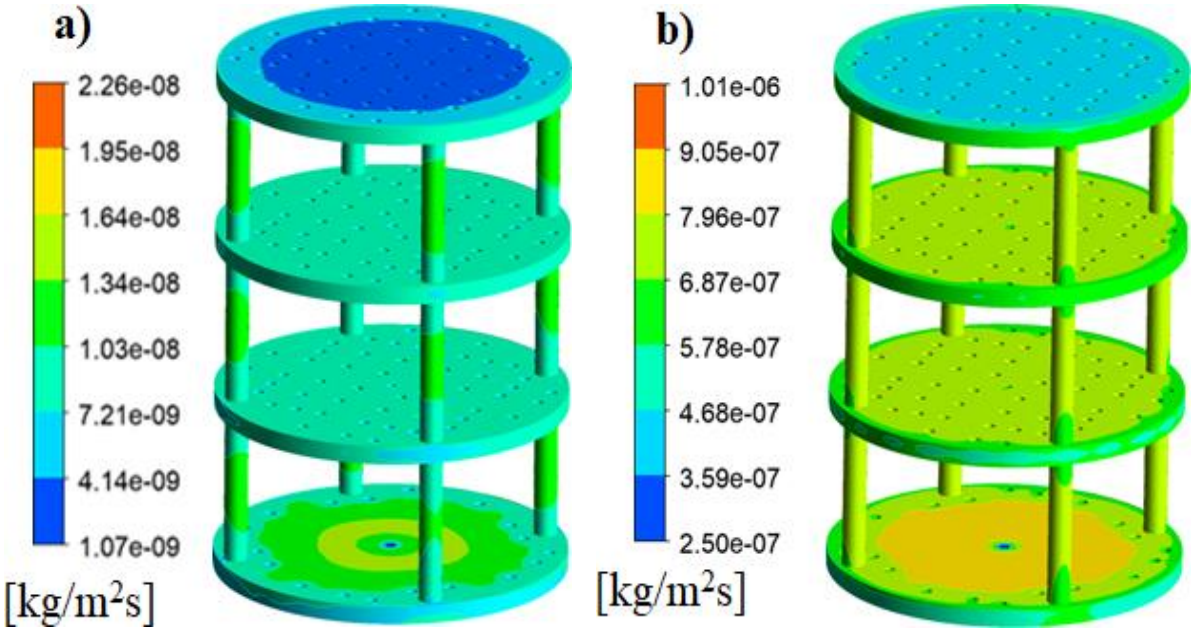

Fig. 4.4 Simulated deposition rate at reactor temperature a) 900^{0}C, and b) 1100^{0}C.

The simulated deposition profiles at 900^{0}C and 1100^{0}C are presented in Fig. 4.4. It was noticed that the film deposition rate increases with an increase in reactor temperature. However, a drastic drop in the deposition at the upper plate can be ascribed to a rise in the hydrogen

concertation at the top, inhibiting the deposition processes. Becker et al. studied carbon deposition from light hydrocarbons and observed that the carbon deposition was hindered due to the inlet H_2 concentration (Becker et al., 2000). Moreover, the species distribution in the present study unveils that C_2H_2 mainly contributes to the PyC deposition, consistent with the literature (Mankelevich and May, 2008a). The average PyC deposition rate increased from $8.75x10^{-9}$ to $7.41x10^{-7}$ kg/m^2.s when the reactor temperature rose from 900^0C to 1100^0C.

4.3 Effect of operating pressure

Fig. 4.6 depicts the distributions of C_2H_2 as a significant intermediate for PyC deposition at various pressures. It can be seen that the distribution of C_2H_2 species is axisymmetric and more homogenous at low pressure (100 mbar). The gas flow inside the reactor is controlled by forced convection. As a result, fewer circulations due to the negligible buoyancy effect were observed in the reactor at low pressure. Besides, Fig. 4.6 also illustrates how the deposition rates vary with pressures. It is evident that the deposition rate is increased with pressure. In general, the gas mixture density increases with an increase in pressure, which ultimately enhances the concentration of the C_2H_2 and decreases the concentration boundary layer thickness near the substrate. This ultimately accelerates the diffusion of C_2H_2 through the boundary layer and reacts readily at the substrate, giving rise to a higher deposition rate. However, the film uniformity is severely affected at high pressure due to the non-uniform distribution of C_2H_2, as seen in Fig. 4.5. Therefore, appropriate pressure may be used to achieve the intended growth rate and film uniformity.

The Reynolds number was calculated based on the reactor diameter, while the Grashof number was calculated using the vertical distance from the first plate. A cross-sectional average of velocity and concentration was used to estimate the various dimensionless numbers. The difference between the inlet temperature and the averaged temperature at a given cross-sectional position was used to calculate the Grashof number. The Gr/Re^2 is used to study the relative strength of natural convection compared to forced convection. It was observed that the deposition rate increased with an increase in operating pressure. However, the uniformity index decreased at higher pressures due to buoyancy-driven flow within the reactor. At high pressures (above 250 mbar), significant circulation between the wall and substrate was observed, leading to non-uniform reactant distribution and a decrease in uniformity index. Fig. 4.6 shows the variation of Gr/Re^2 ratio at different operating pressures. The Gr/Re^2 ratio increased with increasing reactor pressure, confirming the dominance of buoyancy-driven flow at high

pressures. Extensive flow recirculations were noticed around the substrate at high pressure as shown in Fig 4.6. This consequently results in considerable variation in the concentration of C_2H_2, thereby affecting the film uniformity. These findings are consistent with the dimensionless (Gr/Re^2) ratio, implying the relative magnitude of buoyancy force over the inertial force. The low Gr/Re^2 ratio is manifested at low pressure, suggesting less buoyancy-driven flow, and the strength of the flow circulations diminishes. A detailed analysis of buoyancy flow in a hot-wall CVD reactor can be found in our previous study (Deivendran et al., 2020).

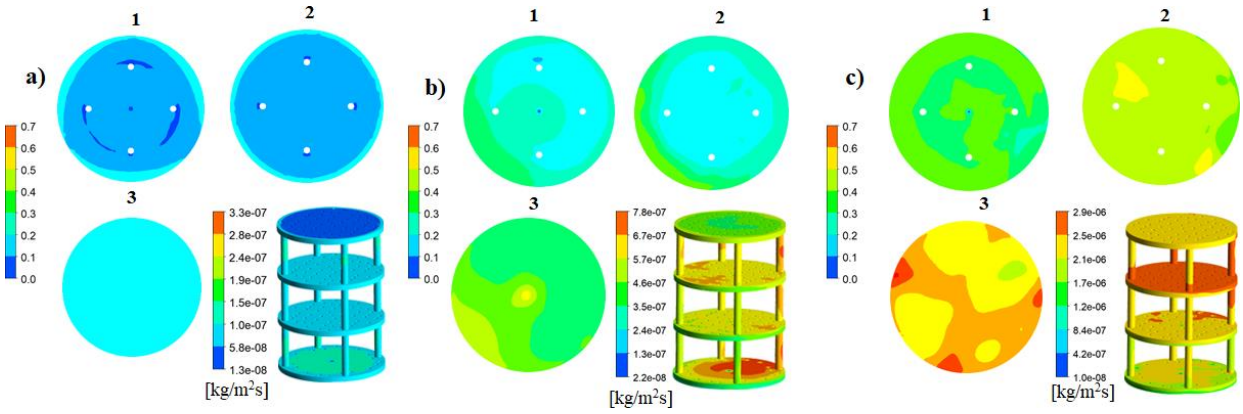

Fig. 4.5 Variation of mole fraction of C_2H_2 at different cross-sections of the reactor and deposition rate on the substrate at a) 100 mbar, b) 250 mbar, and c) 500 mbar.

The effect of pressure on the cross-section average mole fractions of all dominant species is shown in Fig. 4.5. These three cross-sections were taken in the middle of two substrates in a horizontal plane. It is apparent that the operating pressure significantly influences CH_4 conversion, increasing with an increase in reactor operating pressure. C_2H_2 is the dominant carbon forming in the reactor, and the mole fractions of C_2H_4 and C_6H_6 are negligible compared with C_2H_2 for all studied pressures. The CH_4 is immediately pyrolysed at an inlet at high pressure, and its mole fraction drastically decreases in the reactor. On the other hand, the C_2H_2 mole gradually increases from the inlet towards the exit of the reactor.

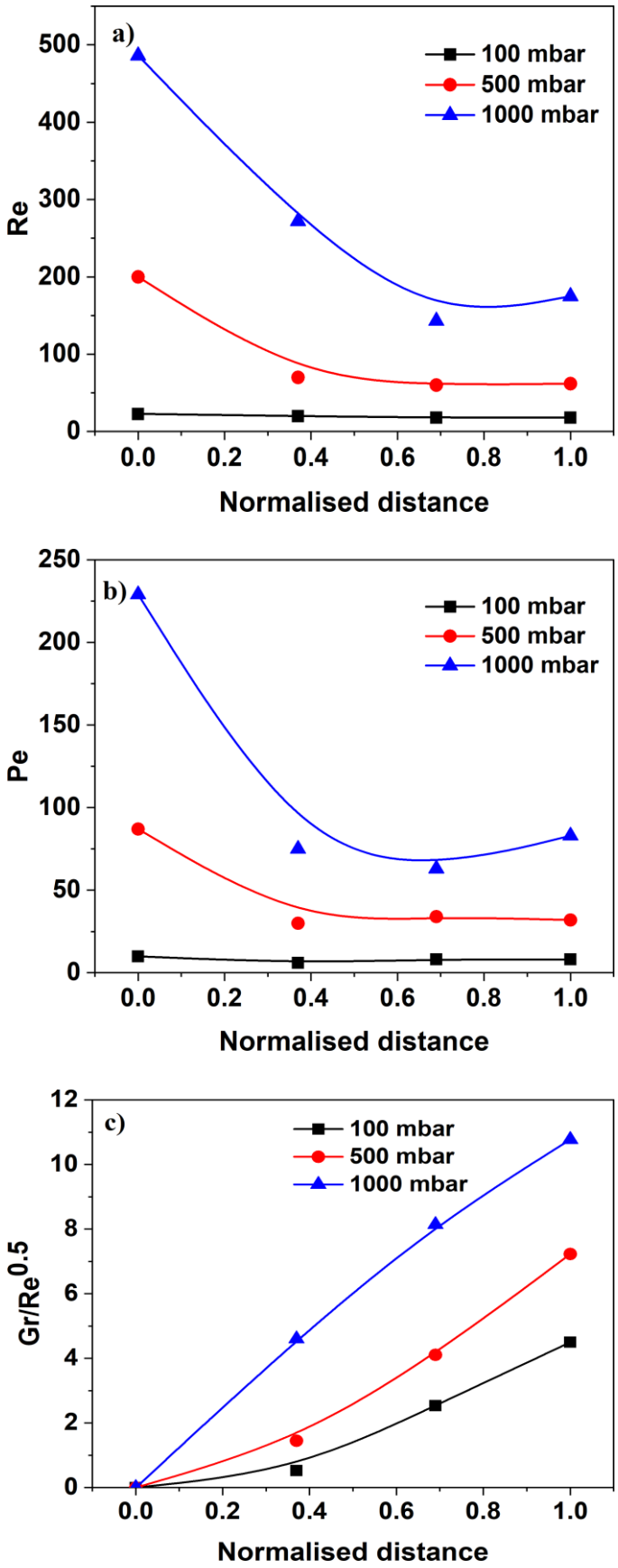

Fig. 4.6 Distribution of various dimensionless numbers at different operating pressures.

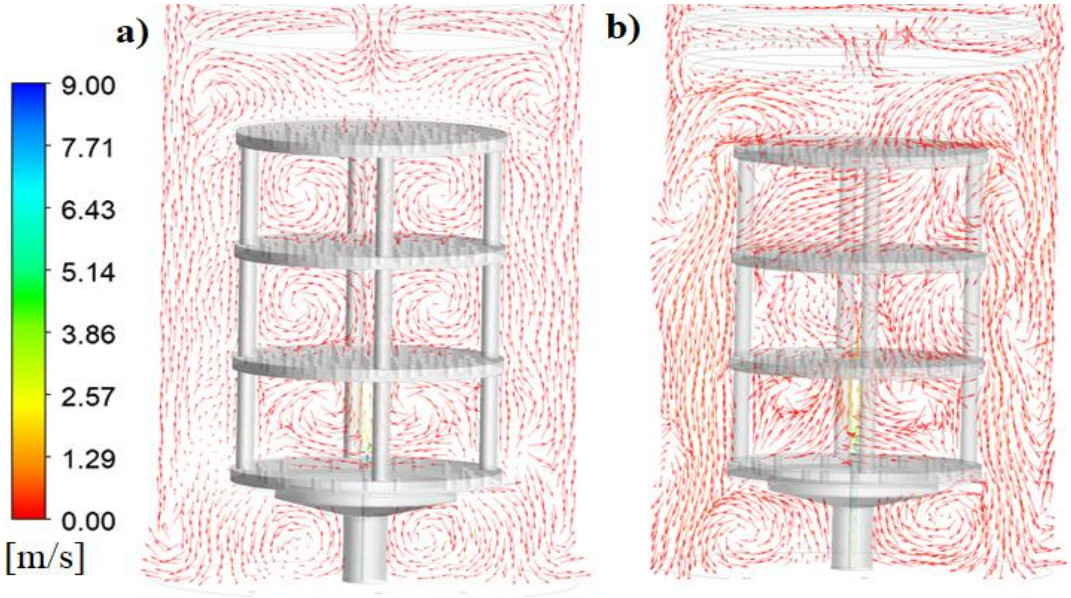

Fig. 4.7 Velocity vectors near the substrate at a) 100 mbar, b) 500 mabr and c) 1000 mbar, respectively.

4.4 Effect of total flow rate

The total flow rate was changed in the range of 10-30 standard litre per minute (slm) (hardware limitation of the reactor) to study its effect on the film quality. With increasing the flow rate, the cold gas flow is penetrated further into the reactor and reduces the temperature of the surrounding areas as shown in Fig.4.8. However, the thermal boundary layers near the substrate are still uniform. The simulation results reveal that the inlet flow rate increase does not significantly affect the reactor hydrodynamics. There are always recirculations present in the reactor, but the size of the recirculation slightly diminishes due to reduced buoyancy force at 30 slm. Fig. 4.10 shows the C_2H_2 concentration and deposition rate profiles at different flow rates. It can be seen that the mole fraction of C_2H_2 remained unchanged in both cases, indicating that the pyrolysis of CH_4 is not affected by flow rate, and similar deposition rates were achieved in both cases. However, a slightly high film uniformity was obtained at 30 slm owing to the uniform concentration of C_2H_2. Therefore, the simulation results disseminate that the effect of flow rate on film performance is feeble.

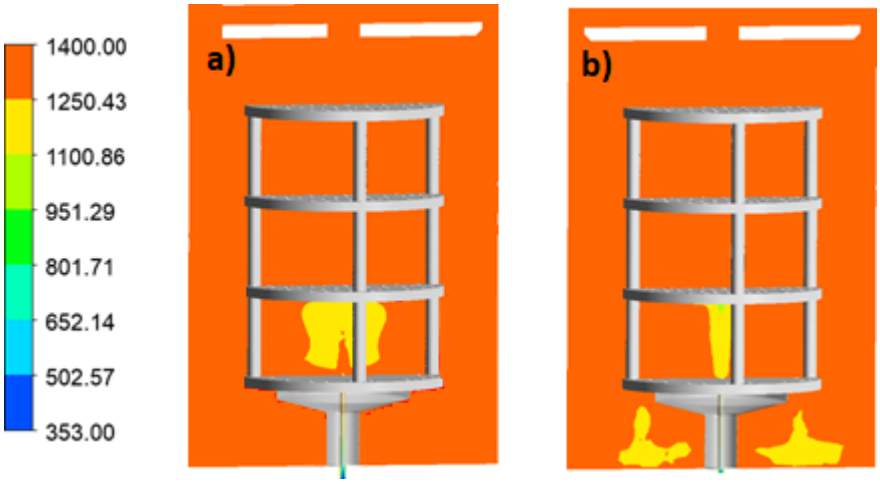

Fig. 4.8 Temperature profile at a) 10 slm, and b) 30 slm, respectively.

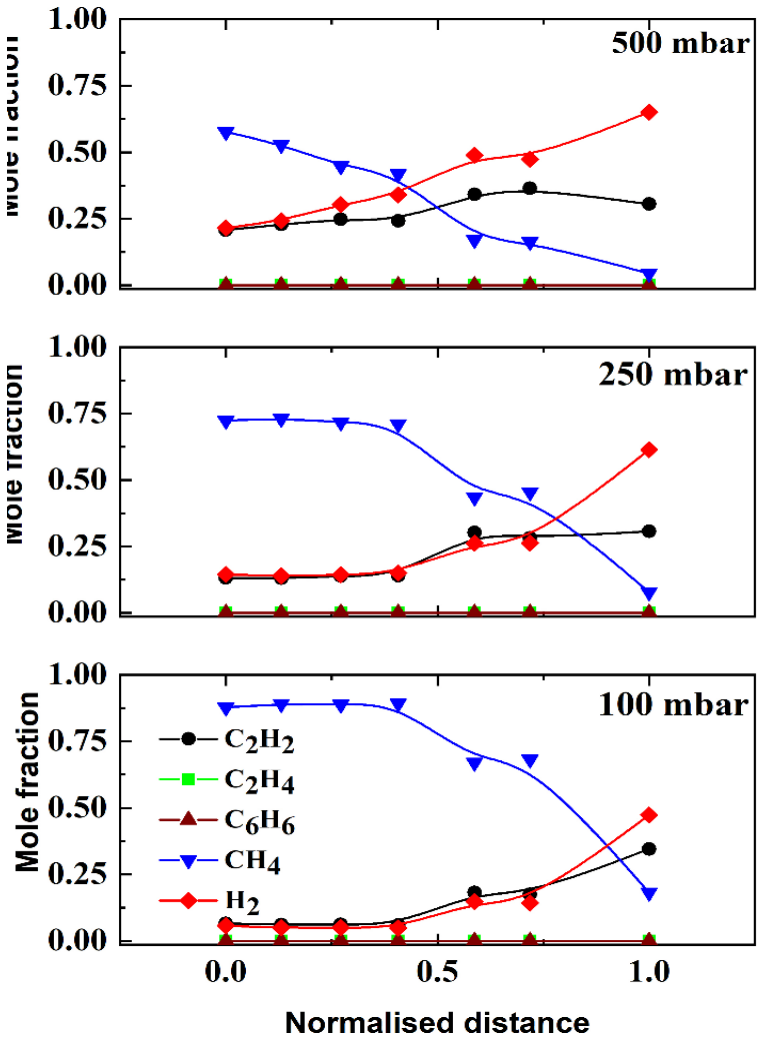

Fig. 4.9 Variation of cross-sectional averaged mole fractions of various species along the reactor length at different temperatures.

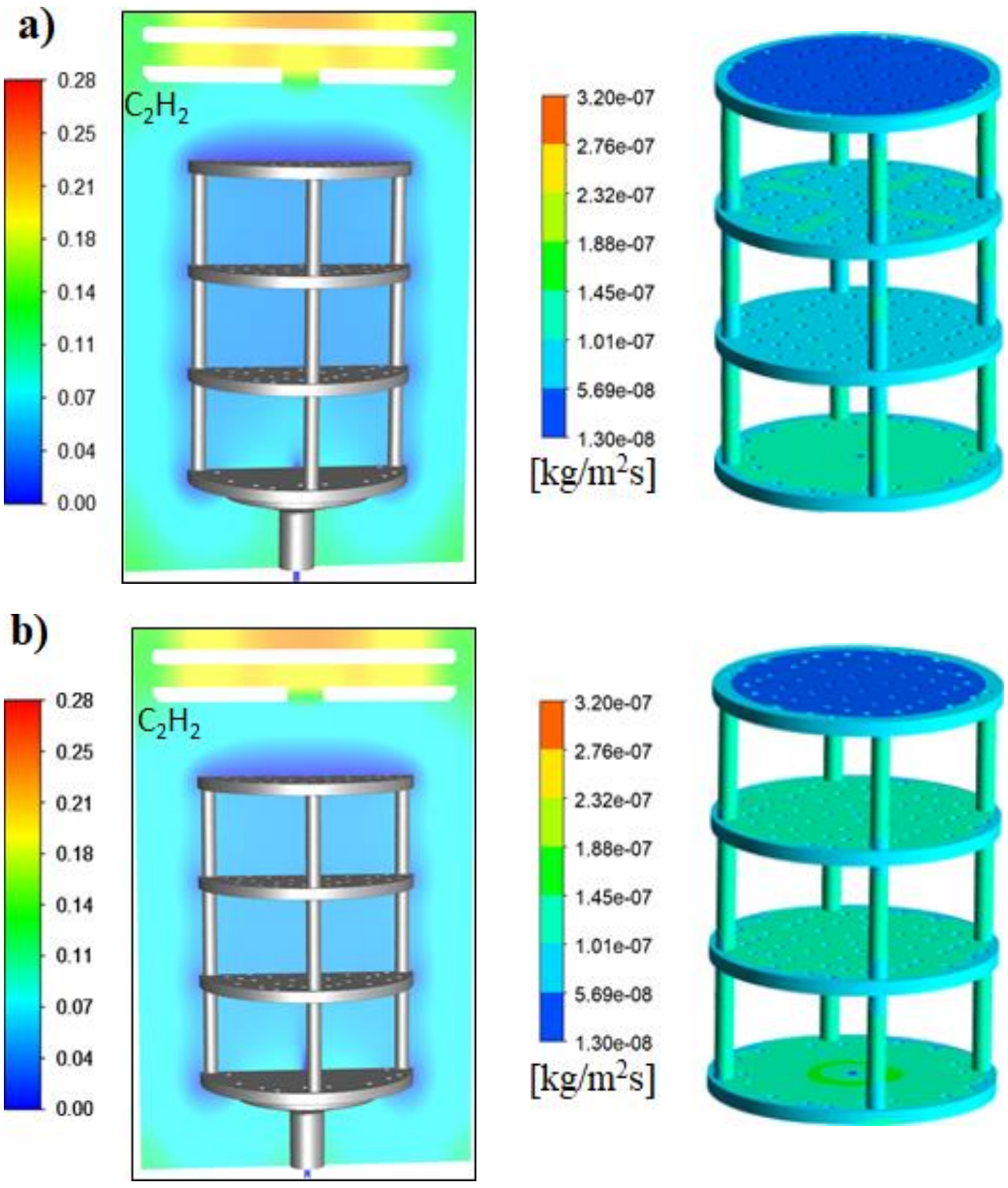

Fig. 4.10 Variation of mole fraction of C_2H_2 species along the reactor length and deposition rate at a) 10 slm, b) 30 slm.

4.5 Effect of CH_4 mole fraction

The effect of the CH_4 mole fraction on the PyC deposition and film uniformity is described in Fig. 4.11. The CH_4 mole fraction was varied from 0.2 to 1, keeping all other parameters constant. Since the thermal conductivity (molecular diffusivity) of H_2 is high, the temperature and concentration distribution inside the reactor significantly improve on the addition of H_2 in the feed. The simulation results manifest that increasing the inlet CH_4 mole

fraction causes an increase in the PyC growth rate up to 0.7, and it decreases on further increasing the inlet CH_4 mole fraction. It can be argued that C_2H_2, being heavy, prefers to stay away from the hot substrate due to the thermophoresis effect at low inlet CH_4 mole fraction. On the other hand, an excess CH_4 prevents C_2H_2 from diffusing homogeneously over the substrate, resulting in a low deposition at a high CH_4 inlet mole fraction. Besides, the CH_4 conversion and concentration of C_2H_2 are almost identical for all CH_4 inlet mole fractions, as seen in Fig. 4.11. However, the distribution of C_2H_2 is mainly dependent on the inlet CH_4 mole fraction. The uniform concentration of C_2H_2 over the substrate was observed at 0.7 CH_4 mole fraction, which resulted in high film uniformity. The summary of the parametric effect on the film performance is depicted in Table 4.1.

Table 4.1 The summary of the parametric effect on the film performance.

Parameters	**Effects**
Pressure	Forced convection dominated gas flow at low pressure (fewer flow recirculations), C_2H_2 is the most abundant carbon forming species, Homogenous distribution of C_2H_2 species at low pressure, increase in the deposition rate with pressure, However, the film uniformity severely affected at high pressure due to the non-uniform distribution of C_2H_2.
Temperature	Significant temperature variations at high temperatures due to entry effect, increase in the C_2H_2 mole fraction with temperature, Reaction-limited growth regime (900-1100 ^{0}C), Increase in the deposition rate with temperature, film uniformity is affected at high temperature due to non-uniform distribution of C_2H_2.
CH_4 mole fraction	Improvement in the C_2H_2 distribution on the addition of H_2 in the feed, Excess CH_4 prevents homogeneous diffusion of C_2H_2, Maxima in the deposition rate, Uniform concentration of C_2H_2 over the substrate at 0.7 CH_4 mole fraction, resulting in high film uniformity.
Total flow rate	Inlet flow rate does not affect the reactor hydrodynamics, slightly low buoyancy force at the high flow rate, pyrolysis of CH_4 is not affected by flow rate, and similar deposition rates, a slightly high film uniformity at a high flow rate.

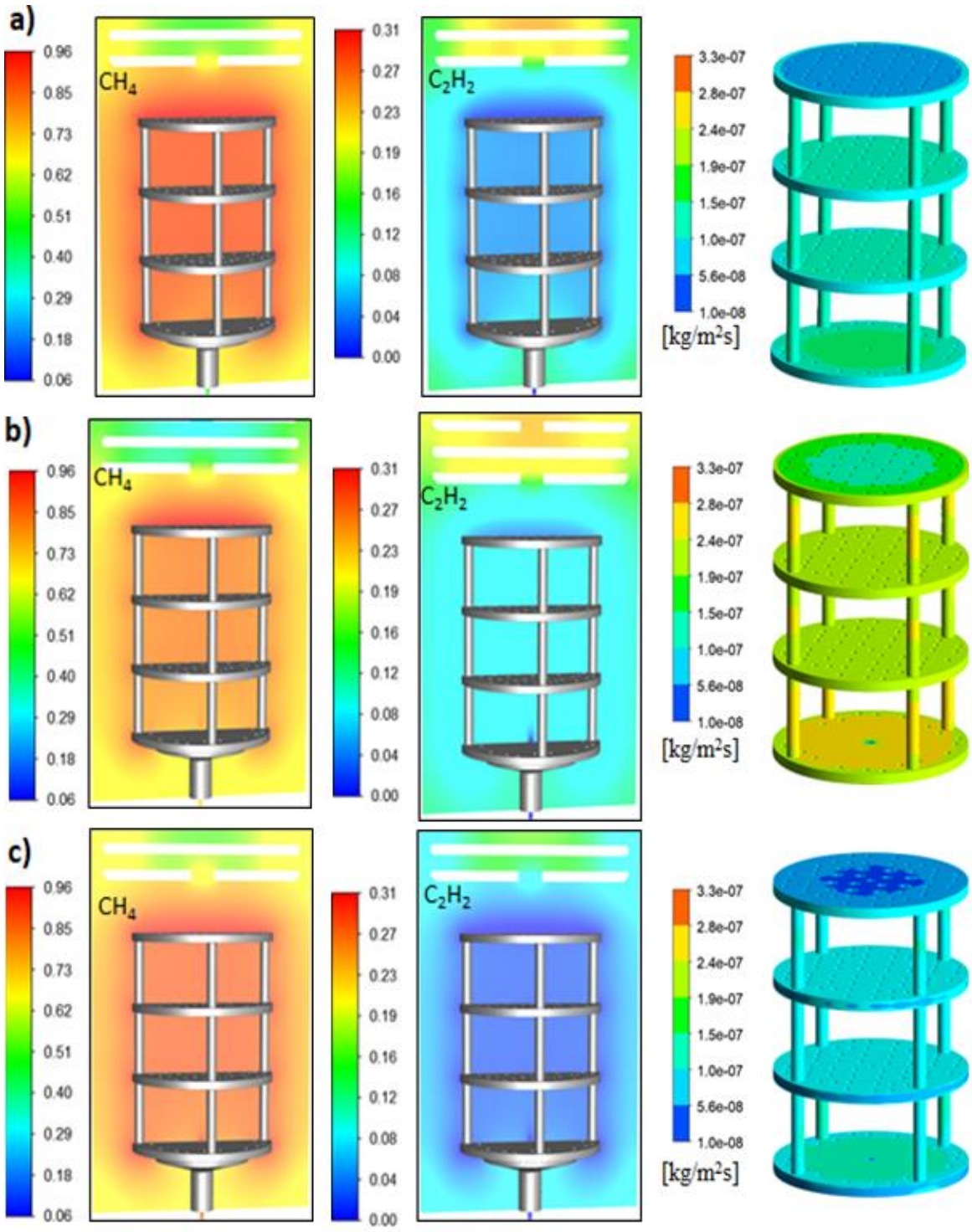

Fig. 4.11 Variation of mole fraction of CH_4 and C_2H_2 species along the reactor length and deposition rate at a) 0.5, b) 0.7, and c) 0.9 inlet mole fraction of CH_4.

4.6 Optimisation of the CVD reactor

Exploratory data analysis revealed that deposition rate was highly correlated with pressure and slightly with temperature. Contrarily, the uniformity index was strongly dependent on temperature and slightly on pressure: the combined deposition rate and uniformity depended on pressure and temperature. Fig. 4.12, 4.13 and 14 presents 2-D contour plots of how the deposition rate uniformity and combined vary with any two parameters involving total flow rate, temperature, pressure, and inlet CH_4 mole fraction. It is apparent that operating parameters have a coupling effect on the PyC deposition and film uniformity. Finally, the PyC deposition rate, uniformity, and combined (y in Eq.17) were modelled as a function of operating parameters.

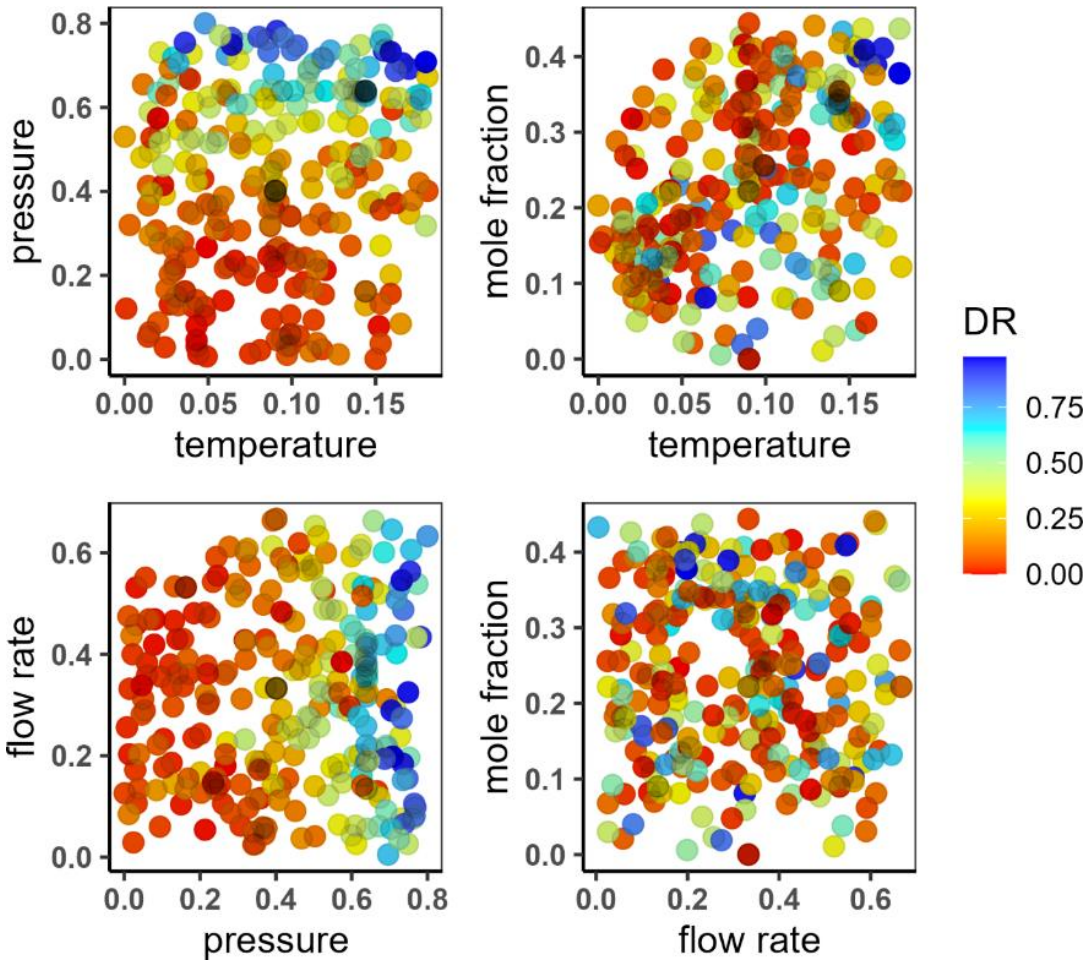

Fig. 4.12 2-D contour plots for deposition rate with two operating parameters.

The SVM algorithm was availed to envisage the deposition rate and uniformity both individually at different operating conditions. The performance of the SVM for each case is presented in Table 4.2. The performance of the SVM model via the parity plots (i.e., predicted vs. observed) for both deposition rate, uniformity index and combination of both are shown in

Fig. 4.13. There are two parity plots, one for deposition rate and one for uniformity index, both predicted using an SVM algorithm. Ideally, the data points would fall on the line y=x, which would indicate that the predicted values are perfectly accurate. However, in both plots, there is some scatter around the line y=x. This indicates that the SVM algorithm is not perfectly accurate, but it is still making relatively good predictions. The scatter is slightly more pronounced in the plot for the uniformity index, which suggests that the SVM algorithm is better at predicting the deposition rate than the uniformity index.

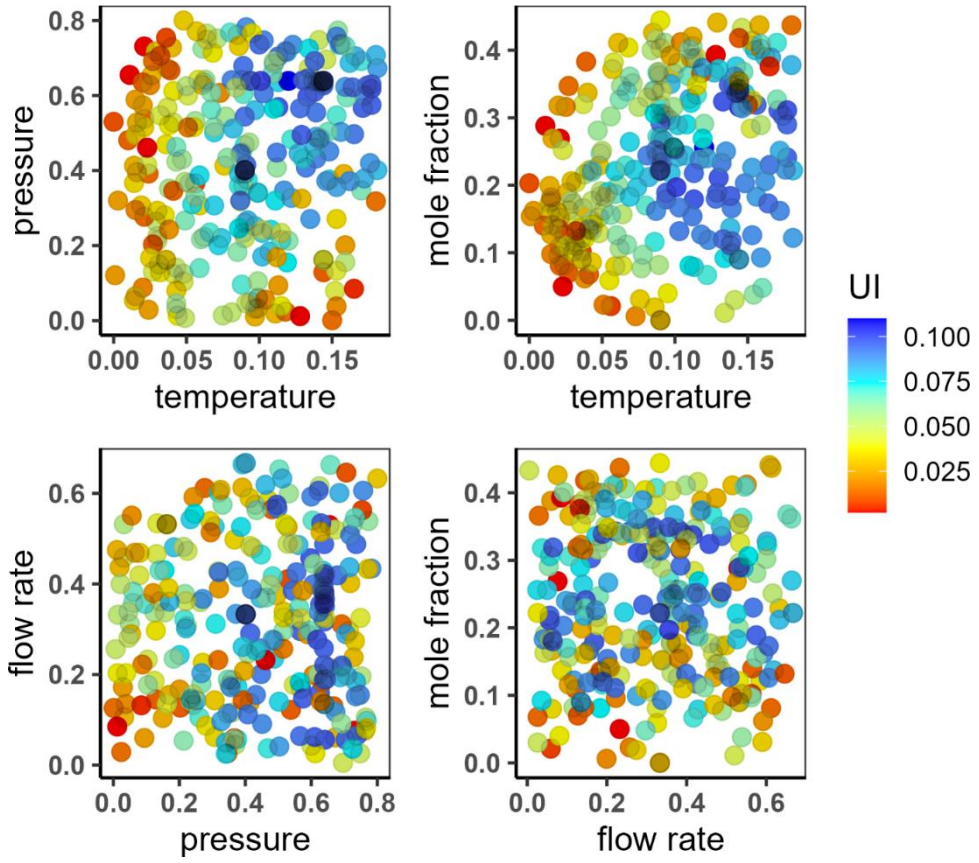

Fig. 4.13 2-D contour plots for uniformity index with a combination of two operating parameters.

Deposition rate: The deposition rate plot shows that the SVM algorithm is generally overestimating the deposition rate. This is because the predicted values tend to fall above the line y=x. However, the overestimation is not very large, and the overall correlation between the actual and predicted values is good.

Uniformity index: The uniformity index plot shows that the SVM algorithm is underestimating the uniformity index at low values and overestimating it at high values. This is because the predicted values tend to fall below the line y=x at low values and above the line

y=x at high values. However, the underestimation and overestimation are not very large, and the overall correlation between the actual and predicted values is still good.

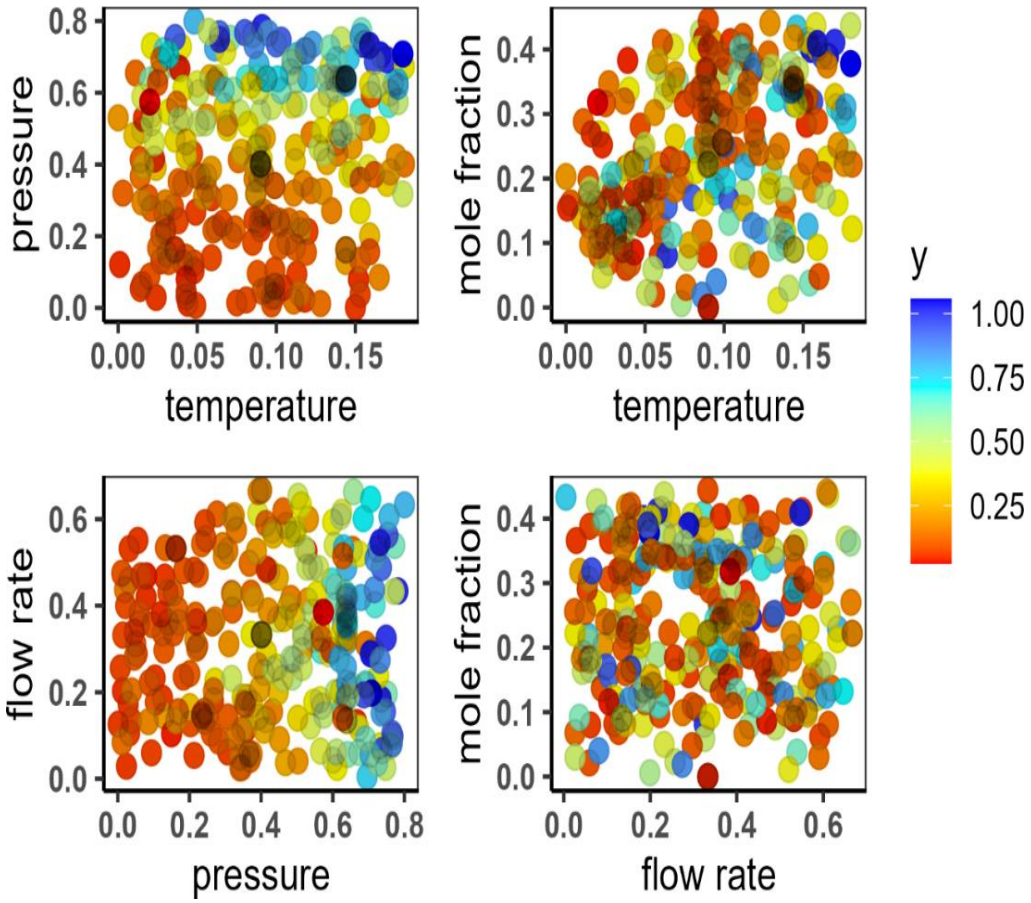

Fig. 4.14 2-D contour plots for combining the deposition rate and uniformity index with a combination of two operating parameters

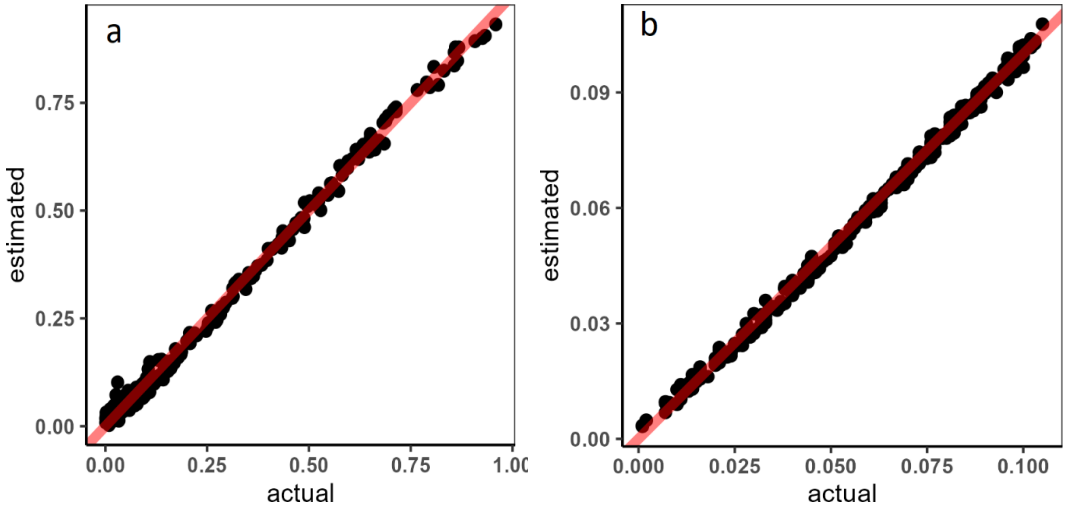

Fig. 4.15 Parity plot of predicted values versus the original values for a) deposition rate and b) uniformity index using SVM algorithm.

Apart from this, the machine learning models listed below were also trained. Before running any model, the data was separated into 'training' and 'testing' sets. A training strategy based on repeated cross-validation was used. Resampling was conducted five times with ten iterations each. The same random seed was used before running each model. It is clear that the SVR envisages the deposition and uniformity index rate with process parameters relatively well. Below is the graphical depiction of the table showing various comparisons. The linear regression model (R^2=0.64) was less accurate as compared to SVM (R^2=0.88). As already discussed in Chapter 3, the proposed strategy integrates the CFD analysis, the SVM model, and NM algorithms into a unified framework to optimise the CVD process. The optimum conditions of the CVD reactor are presented in Table 4.3.

Table 4.2 The comparison of model SVM algorithm performance to predict the simulated data

Model	RMSE	R^2	MAE
Deposition rate (DR)	0.017	0.996	0.0142
Uniformity index (UI)	0.0017	0.997	0.0014

Table 4.3 The performance of various statistical and machine learning models predicting deposition rate.

Model	Type	RMSE	R-squared	MAE
SVM	ML	0.0514	0.8867	0.0375
Boosted Tree	ML	0.0516	0.8832	0.0384
Cubist	ML	0.0516	0.8791	0.0387
Regression Tree	ML	0.0525	0.8771	0.0393
Rpart	ML	0.0548	0.8111	0.0419
Tree Bag	ML	0.0574	0.7906	0.0427
Earth	ST	0.0601	0.6718	0.0461
Neural Networks	ML	0.0617	0.6781	0.0457
PLS	ST	0.0623	0.6578	0.0455
Lasso	ST	0.0627	0.6441	0.0458
Linear Reg	ST	0.0627	0.6441	0.0458

ST = Statistics, ML = Machine Learning.

Table 4.4 The obtained optimal operating conditions for high growth and film uniformity in the CVD reactor.

Case	Temp (^{0}C)	Pressure (mbar)	Flow rate (slm)	% inlet CH_4	Deposition rate (y_1) $\times 10^{-9}$ (kg/m^2.s)	Uniformity Index (y_2)
α=1, β=1	1082	462	27	0.57	262	0.96
α=100, β=1	1082	462	27	0.57	258	0.96
α=10, β=1	1088	500	27	0.5	252	0.93
α=1, β=10	997	415	14	0.78	275	0.97
α=0.1,β=10	1082	462	27	0.57	258	0.96

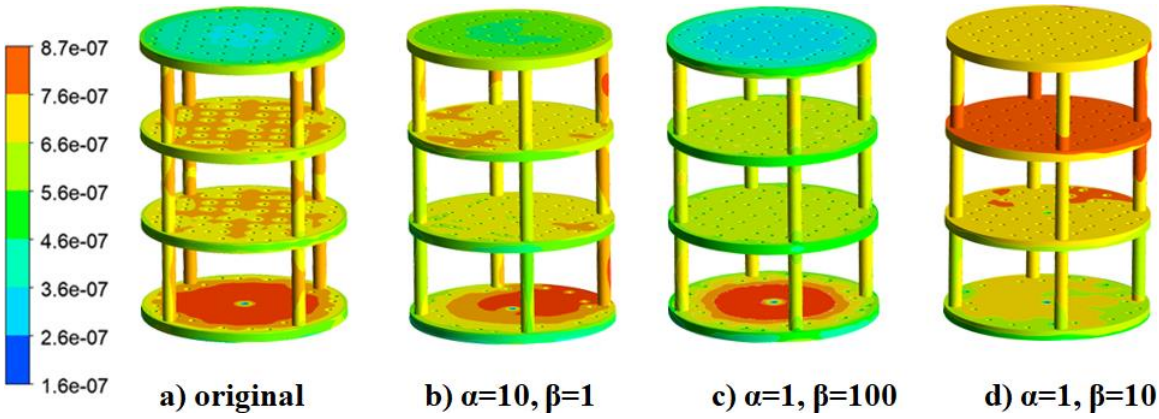

Fig. 4.16 Comparison of the uniformity index to the original operating parameters with optimum conditions from Table 4.3.

No convergence problem was encountered during the optimisation. It was observed that the fitted function (Eq. (17)) increases considerably initially and then grows slowly in the subsequent iterations. Therefore, it is evident that the combined SVM and NM algorithms efficiently locate the maxima. The advantage of the present methodology over the traditional optimisation techniques (e.g., Sequential quadratic programming) is high accuracy, computational efficiency, and easy convergence. Moreover, the CVD process is very complex; as a result, finding the analytical form of the objective function concerning the process

variables needs many trials and tremendous experience. Pareto optimality also indicates that the operating parameters cannot be assigned to make deposition rate more desirable without making film uniformity undeniable. Fig. 4.16 compares the uniformity index under the original operating conditions (Table 4.3) to those proposed in the optimized conditions. The results clearly demonstrate that the deposition uniformity is significantly enhanced by the optimized parameters. Therefore, combining the machine learning algorithm with the robust optimisation technique is advantageous for optimising complex CVD processes.

References

1. Becker, A., Hu, Z., Hüttinger, K. J., 2000. Hydrogen inhibition model of carbon deposition from light hydrocarbons. Fuel. 79, 1573-1580. https://doi.org/10.1016/S0016-2361(00)00030-2
2. Mankelevich, Y. A., May, P. W., 2008. New insights into the mechanism of CVD diamond growth: single crystal diamond in MW PECVD reactors. Diamond Relat. Mater. 17, 1021-1028. https://doi.org/10.1016/j.diamond.2008.03.022
3. Deivendran, B., Shinde, V. M., Kumar, H., Prasad, N. E. 2021. 3D modelling and optimisation of sic deposition from CH_3SiCl_3/H_2 in a commercial hot-wall reactor. J. Cryst. Growth. 554, 125944. https://doi.org/10.1016/j.jcrysgro.2020.125944

CHAPTER 5

CONCLUSIONS AND FUTURE SCOPE

5.1 Conclusions

The use of SVM and the Nelder-Mead algorithm to optimise CH4 pyrolysis in a commercial CVD reactor has important implications for the synthesis of advanced carbon materials. The research presented in this thesis has demonstrated the feasibility of using machine learning techniques to optimize the process parameters and to achieve high-quality pyrocarbon. Two factors, such as average growth rate and uniformity index, were used to define the film quality, acquired by a comprehensive CFD modelling combining accurate gas and surface chemistry. Firstly, the parametric investigation was performed to understand how the deposition and film uniformity vary with the total flow rate, reactor temperature, pressure, and inlet concentration of CH_4. The results revealed that the reactor pressure and temperature remarkably influence the deposition rate and film uniformity. C_2H_2 species was identified as the most dominating carbon-forming species. At high pressure, the film uniformity is severely affected due to the non-uniform distribution of C_2H_2. The total flow rate has a negligible effect on the reactor hydrodynamics. The film performance can be significantly improved using an appropriate choice of the inlet CH_4 concentration. The relationship between various process parameters and film quality was modelled using the SVM otherwise is difficult to obtain through linear regression. The SVM model exhibited high accuracy, saving considerable time and cost of performing actual experiments. Finally, the SVM combined with the Nelder-Mead algorithm was employed to optimise the CVD reactor. It has been found that this methodology is efficient and fast and requires less time to optimise the CVD reactor.

5.2 Future Scope

This research has a broad future reach. This study's CFD model can be used to mimic the pyrolysis of different hydrocarbons, such as C_2H_6 and C_3H_8. It can also be used to investigate the effects on the pyrolysis process of various reactor configurations and operating conditions. Other forms of CVD reactors, such as cold wall reactors and plasma-enhanced CVD reactors, can also benefit from the optimisation process. The optimized design of CH_4 pyrolysis in a commercial CVD reactor has significant future scopes for research and development. These include integration with other technologies, alternative feedstocks, advanced materials

synthesis, scaling up for industrial applications, process optimization for other industrial applications, environmental sustainability, process control and automation, integration with renewable energy sources, and new applications and markets. Continued research and development in these areas can enhance the efficiency, sustainability, and commercial viability of the process, opening up new opportunities for scientific and technological innovation. Some of them are:

- **Integration with other technologies**: The optimization of CH_4 pyrolysis in a CVD reactor can be integrated with other technologies such as artificial intelligence and machine learning algorithms to enhance the efficiency of the process and develop a more robust model.
- **Alternative feedstocks:** Currently, methane is the most widely used feedstock for CVD reactors. However, research can be conducted to explore other sustainable feedstocks such as biomass, waste materials, or other hydrocarbons.
- **Advanced materials synthesis:** The optimized CH_4 pyrolysis process can be applied for the synthesis of other advanced materials such as carbon nanotubes, diamond-like carbon, and other functionalized carbon materials.
- **Scaling up for industrial applications:** The optimized process can be scaled up for industrial applications, and commercialized for large-scale production of graphene and other advanced carbon materials.
- **Process optimization for other industrial applications:** The optimization of the CH4 pyrolysis process can be applied to other industrial applications that require high-temperature and gas-phase reactions, such as chemical manufacturing, solar cell production, and semiconductor processing.
- **Environmental sustainability:** It can be further developed to minimize the environmental impacts of the process. For example, research into strategies to reduce energy use, greenhouse gas emissions, and garbage generation can be conducted.
- **Process control and automation:** The optimized process can be further developed to implement advanced process control and automation technologies. This can help to reduce human error, enhance process efficiency, and increase the consistency and quality of the products.
- **Integration with renewable energy sources:** The integration of the optimised process with renewable energy sources such as solar, wind, and geothermal power

can be studied. This can help to minimise the process's carbon impact and improve its overall sustainability.

- **New applications and markets**: The optimized process can be further developed to explore new applications and markets for advanced carbon materials. For example, research can be conducted to explore the potential use of graphene in energy storage, water purification, and biomedical applications.

Appendix A

Process description

The reactor wall was initially heated using twelve circumferential heating rods to reach the desired temperature from room temperature (27°C). Four temperature sensors placed inside the reactor monitored temperature uniformity. Simulations were conducted up to 2500°C to identify the limiting step during deposition. However, the reactor hardware limited the maximum temperature to 1000°C. After reaching the desired temperature, MTS vapour was introduced into the reactor along with a mixture of H_2 and Ar gases. The total gas flow rate was evenly distributed across the inlet nozzles. The mixture interacted with the buoyancy-driven flow, undergoing cracking and subsequent deposition on the substrate. The centrifugal force generated by the rotating shaft spread the reactants towards the reactor wall, and the optimal rotation speed was maintained to ensure uniform deposition. The amount of deposition was calculated by measuring the difference in sample weight before and after the reaction. A reaction time of 12 h was used consistently in all experiments. Following the reaction, the reactor was purged with Ar and allowed to cool to room temperature.

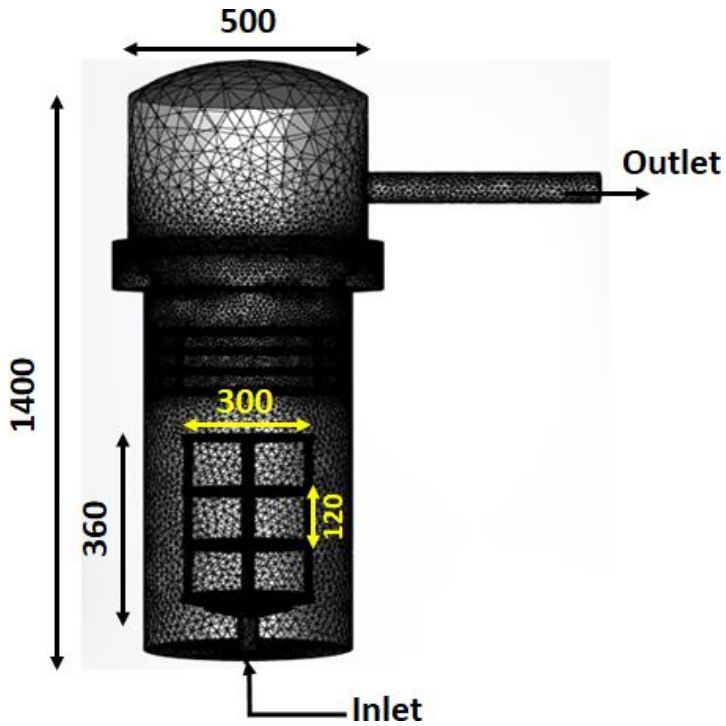

Fig. A1. Schematic of the SiC coating process (All dimensions are in mm).

Mathematical model

The CFD model for the CVD reactor is built on the conservation of mass, momentum, energy, and species and can be expressed as follows.

$$\frac{\partial \rho}{\partial t} + \nabla.(\rho \vec{u}) = 0 \tag{A1}$$

$$\frac{\partial (\rho \vec{u})}{\partial t} + \nabla.(\rho \vec{u}\vec{u}) = -\nabla p + \nabla.\tau + \rho \vec{g}\beta(T - T_a) \tag{A2}$$

Where ρ is the density,$u = (u_r, u_\theta, u_z)$ is the fluid velocity, p is the pressure, g is the gravity vector, τ is the viscous stress tensor. β and T_a is the coefficient of expansion of the gas mixture and the reference temperature, respectively.

$$\tau = \mu\left(\nabla \vec{u} + \nabla \vec{u}^T - \frac{2}{3}\nabla.\vec{u}I\right) \tag{A3}$$

uu and ∇u represent the dyadic products, and I denotes the unit tensor. The ideal gas law was used to calculate the density of the gas, and flow was assumed to be compressible. In the present study, the use of an ideal gas model is accurate because the CVD process is the following conditions are met: i) At low pressures, gas molecules are far apart, and intermolecular forces are minimal. ii) At high temperatures (>1000^0C), the kinetic energy of the gas molecules is significant, overwhelming the effects of intermolecular forces. iii) Gases with small molecules, such as hydrogen and methane, are less likely to deviate from ideal behaviour due to their reduced volume and minimal intermolecular interactions.

$$\rho = \frac{P}{RT\sum_{i=1}^{n}\frac{y_i}{M_i}} \tag{A4}$$

P, R, T, y_i and M_i are the reactor operating pressure, the universal gas constant, temperature, mass fraction, and molar mass of species i, respectively. The kinetic theory of gases was used to estimate the viscosity of gases [1].

$$\mu = 2.6693 \times 10^{-5}\frac{\sqrt{M_{avg}T}}{\sigma_i^2 \Omega} \tag{A5}$$

Where σ_i and Ω are the collision diameter and the collision integral, respectively. In general, Ω is a function of the dimensionless temperature, which can be defined as $T^{\#} = \varepsilon T/k_B$ and is evaluated using the empirical formula given in Eq. (6).

$$T^{\#} = \frac{\varepsilon}{k_B} = 0.77T_c, \text{ and } \sigma_i = 2.44(T_c/P_c)^{\frac{1}{3}} \tag{A6}$$

The critical temperature and pressure were estimated using a group-contribution method [2]. The specific heat capacity of species i at constant pressure C_{p_i} is expressed in the NASA polynomials. The coefficient of these polynomials was obtained from the literature [3].

$$\frac{C_{p_i}}{R} = \alpha_0 + \alpha_1 T + \alpha_2 T^2 + \alpha_3 T^3 + \alpha_4 T^4 \quad \text{(A7)}$$

The energy equation is written as

$$\rho C_p \frac{\partial T}{\partial t} + \nabla.\left(\rho C_p T \vec{u}\right) = \nabla.\left(-k\nabla T\right) - \sum_{i=1}^{n} M_i h_i R_i \quad \text{(A8)}$$

Where k is the thermal conductivity of the gas mixture, h_i is the enthalpy of species i, and R_i the volumetric net rate of production of species i due to the reactions (mol/m^{3}s). The mixture enthalpy is computed as

$$h_i = h_i^0 + \int_{T_0}^{T} C_{p_i} dT \text{ and } h = \sum_{i=1}^{n} y_i h_i \quad \text{(A9)}$$

Here, T_0 is the reference temperature. A simple semi-empirical formula developed by Eucken was used to approximate the thermal conductivity of a polyatomic gas [4].

$$k = \mu\left(C_p + \frac{5R}{4M}\right) \quad \text{(A10)}$$

The species transport of reacting flow is given by

$$\frac{\partial c_i}{\partial t} + \nabla.\left(c_i \vec{u}\right) = \nabla.\left(-D_i \nabla c_i - D_{T_i} \nabla T/T\right) + M_i \sum_{i=1}^{n_r} R_i \quad \text{(A11)}$$

Where D_i and D_{T_i} are the mass and thermal diffusion of species i, respectively. The diffusivity of the binary gas mixture was estimated using the Chapman-Enskog equation [4]:

$$D_{ij} = 1.8583 \times 10^{-3} \frac{\sqrt{T^3\left(1/M_i + 1/M_j\right)}}{P\sigma_{ij}^2 \Omega_{D,ij}} \quad \text{(A12)}$$

Where D_{ij} is the binary diffusivity of the mixture i-j. σ_{ij} is calculated by averaging the individual collision diameters: $\sigma_{ij} = 0.5(\sigma_i + \sigma_j)$.

The Soret diffusion coefficient was estimated using the following empirical equation [5].

$$D_{T,i} = -2.59 \times 10^{-7} T^{0.659} \left[\frac{M_{w,i}^{0.511} x_i}{\sum_{i=1}^{n} M_{w,i}^{0.511} x_i} - y_i\right]\left[\frac{\sum_{i=1}^{n} M_{w,i}^{0.511} x_i}{\sum_{i=1}^{n} M_{w,i}^{0.489} x_i}\right] \quad \text{(A13)}$$

x_i and y_i are mole and mass fractions of species i, respectively. Both the mass diffusivity and thermal diffusion were combined and specified in the simulation using a user-defined function.

The existing models commonly use a constant wall temperature profile or constant heat transfer coefficient to simplify the complexity of heat transfer phenomena. Unlike the conventional approaches, in this work, we consider a more realistic situation and propose detailed heat transfer boundary conditions to illustrate the effective heat transfer between the inner reactor gas and the outer reactor surface. More precisely, we use the well-known convective heat flux as follows:

$$n.\left(-k\nabla T\right) = q_{in} = h_{in}\left(T - T_{inlet}\right) \quad \text{(A14)}$$

In the above context, q refers to the inward convective heat fluxes, which are normal to the inner reactor wall. The term h_{in} (W/m^2/K) represents the heat transfer coefficient of the inner mixture gas. The temperatures of the inner mixture gas are indicated by T. This work proposes an empirical correlation for the heat transfer coefficients, which is based on forced convection across the inner reactor walls.

$$h = C\frac{k}{D_H}\mathrm{Re}^n\,\mathrm{Pr}^m \tag{A15}$$

In this context, k represents the thermal conductivity of the flow, and D_H denotes the characteristic length of the system. The Reynolds number Re and the Prandtl number Pr are dimensionless quantities used to describe the flow dynamics. The constants C, n, and m are dimensionless parameters that depend on the specific geometry of the reactor. These parameters are typically determined by approximating the actual reactor geometry with an equivalent standard configuration, such as a plate or cylinder. For instance, by approximating the inner reactor geometry as a hot plate subjected to forced laminar flow, the correlation parameters can be defined as [C, n, m] = [0.664, 0.5, 0.333]. Similarly, the heat transfer between the outer reactor wall and the surrounding atmosphere is characterized by free convection flux, which can be expressed as follows:

$$n.\left(-k_c\nabla T_c\right) = q_w = h_{iw}\left(T_w - T_a\right) \tag{A16}$$

The heat transfer coefficient under free convection conditions for the outer tube wall is defined as (h_w = 7.5 (W/m^2/K).

Table: The boundary conditions used in the simulation.

Boundary location	**Momentum conservation equation**	**Energy conservation equation**	**Species conservation equation**
Inlet	$u_r = u_\theta = 0,$ $u_z = u_{inlet} = 5\ cm/s$	$T = T_{inlet} = 80^0C$	$y_i = y_{i\_inlet} = 0.02$
Outlet	$p = p_0$ $\left[\mu(\nabla\vec{u} + \nabla\vec{u}^T) - \frac{2}{3}\nabla.\vec{u}\right].n = 0$	$n.(-k\nabla T) = 0$	$\eta.(-D_i c\nabla y_i) = 0$
Substrate	$u = 0$	$T = T_s$	$-n.N = R_i$ $N = -D_i c\nabla y_i + cy_i u$

Reactor wall	$u = 0$	$T = T_s$	$-n.N = R_i$ $N = -D_i c \nabla y_i + c_i u$

n represents the outward unit normal.

References

[1] B. Ning, T. Xia, Z-X. Tong, Y-L. He, Experimental and numerical studies of tungsten line growth in laser chemical vapour deposition, Int. J. Heat. Mass. Transf. 140 (2019) 564-578. https://doi.org/10.1016/j.ijheatmasstransfer.2019.06.001

[2] Y. Nannoolal, J. Rarey, D. Ramjugernath, Estimation of pure component properties: Part 3. Estimation of the vapour pressure of non-electrolyte organic compounds via group contributions and group interactions, Fluid Phase Equilibria, 269 (2008) 117-133. https://doi.org/10.1016/j.fluid.2008.04.020

[3] D. M. Matheu, A. M. Dean, J. M. Grenda, W. H. Green, Mechanism generation with integrated pressure dependence: a new model for methane pyrolysis, J. Phys. Chem. A 107 (2003) 8552-8565. https://doi.org/10.1021/jp0345957

[4] R. B. Bird, W. E. Stewart, E. N. Lightfoot, D. B. Spalding, Transport Phenomena, John Wiley & Sons (1961), pp. 338-359.

[5] K. K. Y. Kuo. Principles of Combustion. John Wiley and Sons, New York, 1986.

Appendix B

SVM and Nelder Mead algorithm code in R

```
# Import Libraries
library(tidyverse)
library(tidymodels)
library(tune)
library(workflows)
library(workflowsets)
library(caret)
library(kableExtra)
library(Rama)
library(glue)
library(flextable)
library(officedown)
library(officer)

ALL_Combinations = tibble(
  α = c(0.1, 1, 1,10, 100),
  β = c(10, 1, 10, 1, 1)
)

for(INDEX in 1:5){

  α = ALL_Combinations$α[INDEX]
  β = ALL_Combinations$β[INDEX]
```

```
# Read data
cone_data <- read_csv('Cone data_ML.xlsx - Sheet1.csv') %>%
  select(temp = Temp,pressure = Press,flow_rate =`flow rate`,mole_frac = molfract,DR,UI) %>%
  mutate(y = α*DR + β*UI)

minmax_cone = make_minmax(cone_data)

set.seed(2021)
spl <- initial_split(cone_data)
cone_train <- training(spl)
cone_test <- testing(spl)
train_5fold <- cone_train %>%  vfold_cv(5)

# Two SVM models were fitted separately for UI and DR. The test level performance measure for those are as follows:

DR_rec <- recipe(DR ~ ., data = cone_train %>% select(temp:mole_frac,DR)) %>%
  step_center(all_numeric(), -all_outcomes()) %>%
  step_scale(all_numeric(), -all_outcomes())

UI_rec <- recipe(UI ~ ., data = cone_train %>% select(temp:mole_frac,UI)) %>%
  step_center(all_numeric(), -all_outcomes()) %>%
  step_scale(all_numeric(), -all_outcomes())

cv <- trainControl(method = 'repeatedcv',number = 10,repeats = 5)
```

```
# Construct grid of hyperparameter values
hyper_grid <- expand.grid(k = 10^seq(-3, -1, by = .1))
# Tune α knn model using grid search
svmRFit_DR <- train(DR ~ ., data = cone_train %>% select(temp:mole_frac,DR),
                    method = "svmRadial",
                    tuneLength = 15,
                    preProc = c("center", "scale"),
                    trControl = cv)
svmRFit_UI <- train(UI ~ ., data = cone_train %>% select(temp:mole_frac,UI),
                    method = "svmRadial",
                    tuneLength = 15,
                    preProc = c("center", "scale"),
                    trControl = cv)
cat('\nDR')
dT_DR = tibble(observed = cone_test$DR,
               predicted = predict(svmRFit_DR,newdata = cone_test %>%
select(temp:mole_frac,DR)))

dT_DR %>% ggplot(aes(x = observed,y = predicted)) + geom_point() + geom_abline(color
= 'steelblue',size=1.2) +
  ggtitle(label = NULL,subtitle = 'Observed/Predicted Deposition Rate')

dT_DR %>% mutate(error = observed  - predicted, SL = row_number()) %>% ggplot() +
  geom_point(aes(SL, error))

dT_DR %>% mutate(error = observed  - predicted, SL = row_number()) %>% gghist(error)
```

```
cat('\nUI')
dT_UI = tibble(observed = cone_test$UI,
               predicted = predict(svmRFit_UI,newdata = cone_test %>% select(temp:mole_frac,UI)))

dT_UI %>%  ggplot(aes(x = observed,y = predicted)) + geom_point() + geom_abline(color = 'steelblue',size=1.2) +
  ggtitle(label = NULL,subtitle = 'Observed/Predicted UI')

dT_UI %>% mutate(error = observed  - predicted, SL = row_number()) %>% ggplot() +
  geom_point(aes(SL, error))

dT_UI %>% mutate(error = observed  - predicted, SL = row_number()) %>% gghist(error)

# Combined Model
y_rec <- recipe(y ~ ., data = cone_train %>% select(-DR,-UI)) %>%
  step_center(all_numeric(), -all_outcomes()) %>%
  step_scale(all_numeric(), -all_outcomes())

cv <- trainControl(method = 'repeatedcv',number = 10,repeats = 5)
# Construct grid of hyperparameter values
# Tune α knn model using grid search
svmRFit_y <- train(y ~ ., data = cone_train %>% select(-UI,-DR),
                   method = "svmRadial",
                   tuneLength = 15,
                   preProc = c("center", "scale"),
                   trControl = cv)
```

```
dT_y = tibble(observed = cone_test$y,
              predicted = predict(svmRFit_y,newdata = cone_test %>% select(temp:mole_frac)))

perform_tbl <- tibble(Measure = c('RMSE','Rsquared','MAE'),
                      DR = postResample(dT_DR$observed, dT_DR$predicted),
                      UI = postResample(dT_UI$observed, dT_UI$predicted),
                      y = postResample(dT_y$observed, dT_y$predicted)) %>%
  mutate_if(is.numeric,.funs = \(x) round(x,4))

# Optimization Setup

# The minimum and maximum values of the predictors and responses
minmax_cone %>% as.data.frame() %>%
  mutate_all(.funs = \(x) round(x,3)) %>% flextable()

## Optimized values
# The following combinations of predictors provide the optimized values of the parameters
# y=`r α`.DR + `r β`.UI

Function_to_Optimize <- function(x, model = svmRFit){
  # x = unlist(cbResults[i,1:4 ] )
  # minmax_scal e d
  if(x[1] < minmax_cone$temp[1]      | x[1] > minmax_cone$temp[2]     ) { return(10^138)}
  if(x[2] < minmax_cone$pressure[1]  | x[2] > minmax_cone$pressure[2] ) {return(10^138)}
  if(x[3] < minmax_cone$flow_rate[1] | x[3] > minmax_cone$flow_rate[2]) {return(10^138)}
```

```
  if(x[4] < minmax_cone$mole_frac[1] | x[4] > minmax_cone$mole_frac[2])
{return(10^138)}


  tmp <- as.data.frame(t(x))
  names(tmp) <- c("temp","pressure","flow_rate","mole_frac")
  y  = round(predict(model, tmp), 3)
  if(any(y > minmax_cone$y[2] , y < minmax_cone$y[1])){
    print(cbind(tmp,y))
    return(10^78)
  } else {
    return(-y)
  }
 }
  # revive_val <- function(x, min_max_i)  x*min_max_i[2] + min_max_i[1]
 set.seed(10-10-10)
 subTrain <- subset(cone_train)#, Age == 28)
 ### Center and scale the data to use dissimilarity sampling
 pp1 <- preProcess(subTrain[, 1:4], method = 'pca')#c("center", "scale"))
 scaledTrain <- predict(pp1, subTrain[, 1:4])


 ### Randomly select α few mixtures as α starting pool
 set.seed(91)
 set.seed(00)
 startMixture <- sample(1:nrow(subTrain), 1)
 starters <- scaledTrain[startMixture, 1:3]
 index <- maxDissim(starters, scaledTrain, 10)
```

```
  startPoints <- c(startMixture, index)


  starters <- subTrain[startPoints,1:4]
  startingValues <- starters
  ### For each starting mixture, optimize the Cubist model using
  ### α simplex search routine


  # optimize_val_by_model <- function(intialValues=startingValues,MODEL = svmRFit_Z,model_name = 'SVM-Reg'){
  cbResults <- startingValues
  cbResults$y <- NA


  #  optimx::optimx(unlist(cbResults[i,1:4]),Function_to_Optimize, lower = 0, upper = 6.212, method = 'Nelder-Mead')
  for(i in 1:nrow(cbResults)){
    # i = 1
    # cat('\n',glue('\n=============== ROW#{i} ==================='),'\n')
    results <- optim(unlist(cbResults[i,1:4]),fn = Function_to_Optimize,
                     method = "Nelder-Mead",
                     control=list(maxit=5000,
                                  # trace = 20,
                                  abstol = 0.01),mod = svmRFit_y)


    cbResults$y[i] <- -results$value
    cbResults[i,1:4] <- rbind(results$par %>% unlist %>% as.vector())
  }
```

```
Opt_svmReg = cbResults %>%
  mutate(UI_pred = predict(svmRFit_UI,cbResults[,-5]),
         DR_pred = predict(svmRFit_DR,cbResults[,-5])
  ) %>%
  mutate_all(.funs = \(x) round(x,3)) %>%
  mutate_at(vars(temp, pressure),.funs = \(x) round(x,0)) %>%
  mutate_at(vars(flow_rate),.funs = \(x) round(x,2)) %>%
  select(temp,pressure, flow_rate, mole_frac, DR_pred, UI_pred, y_pred = y) %>%
  arrange(-y_pred) |> print()
  writexl::write_xlsx(Opt_svmReg,paste0('Opt_svmReg_',α,'_',β,'.xlsx'))
}
```

Appendix C

Validation of the SVM model and Nelder-Mead Algorithm with a well-defined problem

Problem Formulation

The problem consists of a two-dimensional optimisation variable and two objective functions.

Minimize

$$f_1 = x_1^4 + x_2^4 + x_1 x_2 - x_1^2 x_2^2 - 8x_1^2$$

$$f_2 = x_1^4 + x_2^4 + x_1 x_2 - x_1^2 x_2^2 - 3x_1^3$$

Subject to

$$-50 \le x_1 \le 50$$

$$-50 \le x_2 \le 50$$

Plot the resulting Pareto front.

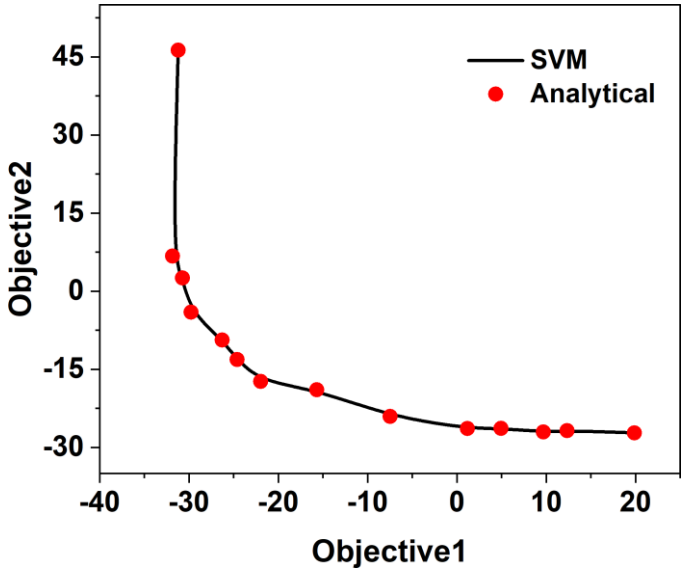

This example shows the plot of a multiobjective optimization problem using the SVM model and Nelder-Mead Algorithm proposed in this thesis.

Appendix D

The effect of thermal diffusion on the velocity profile and concentration of methane is shown in Fig. D1 and D2.

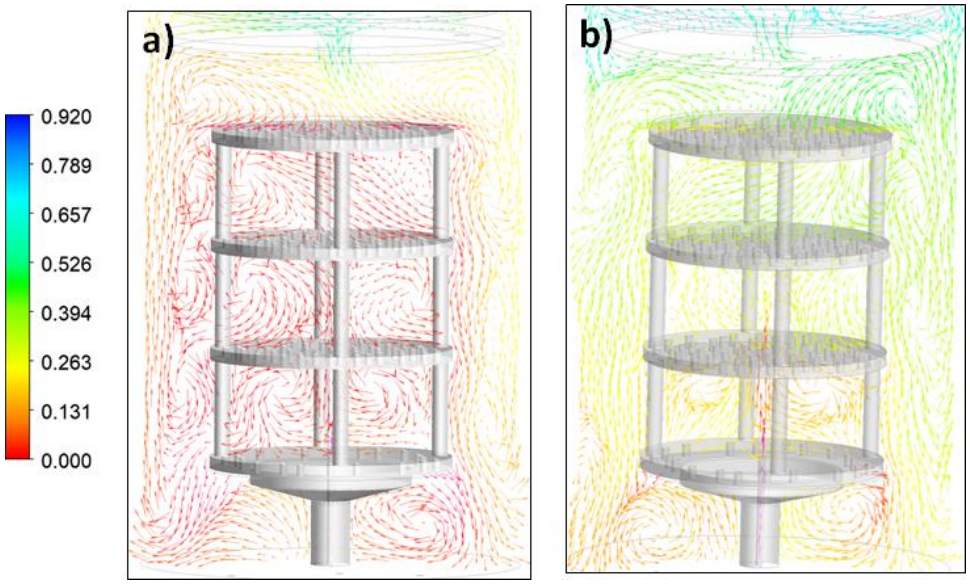

Fig D1: Velocity distribution inside the reactor a) without thermal diffusion and b) with thermal diffusion.

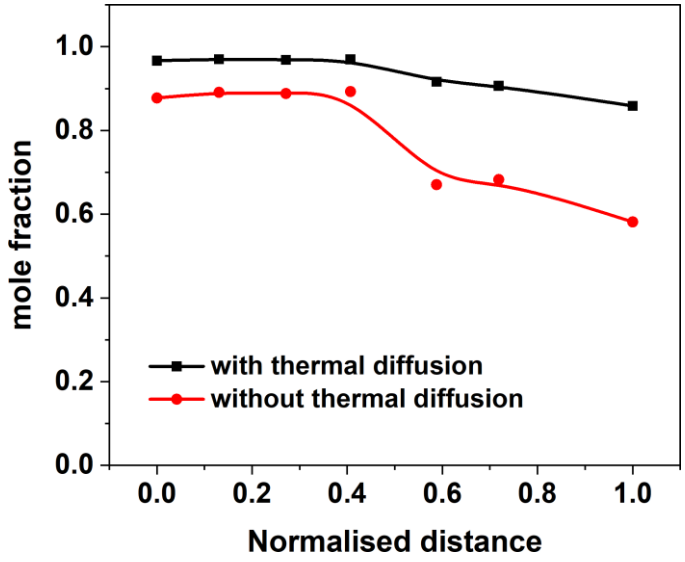

Fig D2: Distribution of mole fraction of methane inside the reactor without thermal diffusion and with thermal diffusion.

Glossary

CFD (Computational Fluid Dynamics): A branch of fluid mechanics that uses numerical analysis and algorithms to solve and analyze fluid flow problems.

CVD (Chemical Vapor Deposition): A chemical process used to produce high-purity, high-performance solid materials, commonly used in semiconductor manufacturing.

Nelder-Mead Algorithm: An optimization algorithm used to minimize an objective function in a multidimensional space without needing derivatives.

Reynolds Number (Re): A dimensionless number used to predict flow patterns in fluid dynamics. It is the ratio of inertial forces to viscous forces.

Grashof Number (Gr): A dimensionless number that estimates the ratio of buoyant to viscous forces in a fluid, important in natural convection processes.

Prandtl Number (Pr): A dimensionless number that characterizes the ratio of momentum diffusivity (viscosity) to thermal diffusivity.

Sherwood Number (Sh): A dimensionless number representing the ratio of convective mass transfer to diffusive mass transfer.

Residuals: The difference between observed and computed values in numerical simulations, used to monitor convergence.

Deposition Rate: The rate at which material accumulates on a substrate during processes like CVD, typically measured in $kg/m^2 \cdot s$.

Uniformity Index: A measure of the consistency or evenness of material deposition across a surface, with values closer to 1 indicating greater uniformity.

Boundary Conditions: Constraints applied to a computational domain in simulations, such as inlet/outlet velocities, temperatures, or heat fluxes.

Implicit Method: A numerical method used in time-dependent simulations where the solution at the next time step depends on unknown future values, often more stable than explicit methods.

Explicit Method: A numerical method where the solution at the next time step is based solely on known values from the current time step.

Time Step (Δt): The increment of time over which numerical calculations are carried out in simulations.

Mesh Independence Study: A study conducted to ensure that the results of a simulation are not dependent on the size or density of the computational mesh.

Convergence Criteria: The conditions under which a numerical solution is considered to have reached a stable and accurate result, often monitored through residuals or flux imbalances.

Kinematic Viscosity: A measure of a fluid's resistance to flow under the influence of gravity, defined as the ratio of dynamic viscosity to fluid density.

Thermal Conductivity: A material's ability to conduct heat, measured in W/m·K.

Mass Diffusivity: A measure of how quickly molecules spread out or diffuse in a given medium, often temperature-dependent.

SLM: Standard liter per minute is a unit of volumetric flow rate, specifically it is commonly used to express the flow rate of gases under standard conditions of temperature and pressure. 1slm= 1.6667×10^{-5} m^3/s.

Finite Volume Method (FVM): A numerical technique used in CFD that discretizes the equations governing fluid flow over small control volumes.

Turbulent Flow: A type of fluid flow characterized by chaotic, irregular motion, typically occurring at high Reynolds numbers.

Laminar Flow: A smooth, orderly flow regime where fluid particles move in parallel layers with little to no mixing, typically occurring at low Reynolds numbers.

Heat Flux: The rate of heat energy transfer through a given surface, measured in W/m^2.

Boundary Layer: A thin region adjacent to a solid surface in fluid flow where viscous forces dominate, affecting heat and mass transfer.

Convective Heat Transfer: The transfer of heat through a fluid (gas or liquid) due to the movement of the fluid itself.

Adiabatic Boundary Condition: A type of boundary condition where no heat transfer occurs through the surface, meaning the surface is perfectly insulated.

Thermal Expansion Coefficient (β): A property of materials that describes how their volume changes with temperature, crucial in buoyancy-driven flows.

Multiphysics Simulation: Simulations that involve solving multiple types of physical processes, such as heat transfer, fluid flow, and chemical reactions, simultaneously.

Steady-State: A condition where the variables of a system (such as temperature, velocity, and pressure) remain constant over time.

Transient Simulation: A time-dependent simulation where the variables change with time, used to study systems that are not in a steady state.

Isothermal Process: A process in which the temperature remains constant throughout, often used as a simplification in simulations.

Species Transport: The process of tracking the movement and concentration of different chemical species in a fluid, often crucial in chemical reaction modeling.

Kinematic Boundary Condition: Boundary conditions applied to velocity fields in fluid simulations, determining how the fluid interacts with the boundary (e.g., no-slip condition).

No-Slip Condition: A boundary condition where the velocity of the fluid at the boundary (e.g., a solid surface) is equal to the velocity of the surface, typically zero.

Enthalpy: A measure of the total energy of a system, including internal energy and the energy required to displace its environment, often used in heat transfer calculations.

Chemical Reaction Rate: The speed at which a chemical reaction occurs, often influenced by temperature, pressure, and concentration of reactants.

Knudsen Number: A dimensionless number used to determine the regime of gas flow, defined as the ratio of the molecular mean free path length to a characteristic physical length scale.

Diffusive Transport: The movement of particles from a region of high concentration to a region of low concentration due to random molecular motion.

Peclet Number (Pe): A dimensionless number that characterizes the relative importance of advective to diffusive transport processes.

Activation Energy (Ea): The minimum energy required for a chemical reaction to occur, an important parameter in reaction kinetics.

Surface Reaction Mechanism: The set of elementary steps describing how molecules interact and react on the surface of a material, often used in catalytic processes like CVD.

Equilibrium State: A state where all forces and reactions in a system are balanced, and there are no net changes in the system's properties over time.

Timestep Convergence: A criterion used in transient simulations to ensure that the chosen timestep size is small enough to accurately capture the system's behavior over time.

Computational Grid (Mesh): The discretized representation of the physical domain over which CFD simulations are performed, with finer meshes leading to higher accuracy at the cost of computational effort.

Residual Error: The difference between the computed and exact values in a numerical simulation, used to evaluate convergence.

Machine Learning (ML): A subset of artificial intelligence (AI) that involves the development of algorithms that enable computers to learn from and make predictions or decisions based on data.

Support Vector Machine (SVM): A supervised machine learning model used for classification and regression tasks. It works by finding the optimal hyperplane that best separates data into different classes.

Training Data: A subset of data used to teach a machine learning model how to recognize patterns and make predictions. The model is adjusted based on the data during training.

Validation Data: A set of data used to tune the parameters of a machine learning model. It helps to prevent overfitting and ensures the model generalizes well to new data.

Test Data: A separate dataset used to evaluate the performance of the machine learning model after it has been trained and validated.

Hyperparameter: Parameters whose values are set before the learning process begins, and they control the behavior of the machine learning model, such as the learning rate or regularization strength.

Regression: A type of machine learning task where the goal is to predict continuous values based on input data, such as predicting deposition rates in a CVD reactor.

Overfitting: A modeling error that occurs when a machine learning model is too complex and learns the noise in the training data rather than the actual pattern, leading to poor performance on new data.

Underfitting: A situation where a machine learning model is too simple to capture the underlying patterns in the data, resulting in poor performance on both training and new data.

Kernel Function: A function used in SVMs and other algorithms to transform data into a higher-dimensional space, making it easier to find a separating hyperplane in complex datasets.

Nelder-Mead Algorithm: An optimization algorithm used to find the minimum or maximum of an objective function in a multidimensional space, often used in conjunction with machine learning models for optimization.

PUBLICATIONS

- **Anand Gupta**, Abhisek Mudgal, Vijay M. Shinde, Harish Kumar, N. Eswara Prasad, *Optimal design of CH_4 pyrolysis in a commercial CVD reactor using support vector machines and Nelder-Mead algorithm*. **Chemical Engineering Research and Design**, 2022;178:124-135.

- **Anand Gupta,** Shikhar Nigam, Vijay M. Shinde, *Gas-phase kinetic of boron carbide chemical vapour deposition using BCl_3+CH_4+H_2 mixture*. **Journal of the American Ceramic Society**, 2022; 105:3885-3895.